University of Bath

PHD

Characterization and evaluation of novel nano/meso-particulate formulations for application to the skin

Wu, Xiao

Award date:
2008

Awarding institution:
University of Bath

Link to publication

Alternative formats
If you require this document in an alternative format, please contact:
openaccess@bath.ac.uk

Copyright of this thesis rests with the author. Access is subject to the above licence, if given. If no licence is specified above, original content in this thesis is licensed under the terms of the Creative Commons Attribution-NonCommercial 4.0 International (CC BY-NC-ND 4.0) Licence (https://creativecommons.org/licenses/by-nc-nd/4.0/). Any third-party copyright material present remains the property of its respective owner(s) and is licensed under its existing terms.

Take down policy
If you consider content within Bath's Research Portal to be in breach of UK law, please contact: openaccess@bath.ac.uk with the details. Your claim will be investigated and, where appropriate, the item will be removed from public view as soon as possible.

Download date: 05. May. 2023

CHARACTERIZATION AND EVALUATION OF NOVEL NANO/MESO-PARTICULATE FORMULATIONS FOR APPLICATION TO THE SKIN

XIAO WU

A thesis submitted for the degree of Doctor of Philosophy

University of Bath

Department of Pharmacy and Pharmacology

November 2008

COPYRIGHT

Attention is drawn to the fact that copyright of this thesis rests with its author. A copy of this thesis has been supplied on condition that anyone who consults it is understood to recognize that its copyright rests with the author and they must not copy it or use material from it except as permitted by law or with the consent of the author.

This thesis may be made available for consultation within the University Library and may be photocopied or lent to other libraries for the purpose of consultation.

Acknowledgements

I would like to thank everyone who has helped and supported me over the past three years. In the first place, I would very much like to express my gratitude to my supervisor, Professor **Richard, H. Guy**, for giving me the opportunity to work in his research group in Bath, for his supervision, advice, and guidance from the very early stage of this research, for his numerous stimulating discussions and motivating support throughout my study, and for his crucial contribution in writing this thesis.

I would also like to thank those people who helped with my experiments: Dr. **Gareth J. Price**, Dr. **Colette Cazeneuve**, Dr. **Bruno Biatry**, Dr. **Alexander F. Routh**, Dr. **Huai Nyin Yow**, Dr. **Katharina Landfester** and Dr. **Anna Musyanovych**, our collaborators, for their constructive advice on nanoparticle preparation and generous provision of nanoparticle formulations; Mrs. **Ursula Potter**, Mr. **Adrian Rogers**, Mr. **Hugh Perrott**, Dr. **Timothy J. Woodman** and Dr. **John Lowe**, for their important technical comments on my transmission electron microscopy, laser scanning confocal microscopy and NMR experiments; Professor **Robert Price** and Professor **Elias Fattal**, for accepting to evaluate this work; All my **friends and colleagues** from the University of Bath, for their personal and technical support. Especially, I would like to thank Dr. **Begona Delgado-Charro** and Miss **Sarah Cordery**, for their support in the arrangement and organization of lab, and Dr. **Sandra Wiedersberg**, for being an important person who taught me how to work on high performance liquid chromatography, diffusion cell, tape-stripping technique, stratum corneum thickness measurement and experimental data fitting. Thanks also to University of Bath for funding my PhD study.

Finally, I want to express my appreciation to my **parents**, for their love, and persistent confidence in me all the time, and my dear **husband**, for his dedication, encouragement and help.

Declaration

I have collaborated with Dr. **Colette Cazeneuve** and Dr. **Bruno Biatr**y (L'Oreal, France) for provision of nanoparticle formulations (in chapter 2).

I have collaborated with Dr. **Huai Nyin Yow** and Dr. **Alexander F. Routh** (University of Cambridge, UK) for provision of nanoparticles and establishing mathematic model to predict diffusion into the stratum corneum (in chapter 3).

I have collaborated with Dr. **Gareth J. Price** (University of Bath, UK) in synthesizing dual-fluorescently labeled nanoparticles (in chapter 4).

I have collaborated with Dr. **Gareth J. Price** and **Mr. Peter Griffin** (University of Bath, UK) for synthesis of polystyrene-poly-2-hydroxyl methacrylate nanoparticles (in chapter 5).

I have collaborated with Dr. **Katharina Landfester** and Dr. **Anna Musyanovych** (University of Ulm, Germany) for provision of nanoparticle formulations (in chapter 6).

Abstract

The use of nano/meso-particles (NP/MP) as constituent of topical formulations of drug and cosmetics has been a topic of considerable interest for the past 20 years. However, the transport mechanism of nanoparticle-associated drug/active following topical application on the skin is still unclear. No general answers have been obtained to such questions as the depth of intact NP penetration into the skin, the skin distribution of active substances, and the fate of the vehicles on/in the skin.

The main objective of this thesis, therefore, was to observe the in vitro penetration of fluorescently-labeled nanoparticle vehicle and “active” on/within the skin by using laser scanning confocal microscopy (LSCM). Furthermore, the concentration profile of the “active” in the outermost skin layer, stratum corneum, has been assessed by using tape stripping technique combined with HPLC analysis. The factors, including particle size, hydrophobicity, shell thickness of nanocapsules and surface charge, have been investigated with regard to their abilities to influence the penetration of “active” into the skin. The methods for NP preparation and characterization have also been developed.

The results demonstrated that the delivery of “active” into the stratum corneum from NP/MP were influenced by a number a factors, including particle size, hydrophobicity, surface charge and shell thickness of capsules. The “active” delivery (i) is greater from larger vectors; (ii) increases as the hydrophobicity of NP/MP increases; (iii) is favoured by cationic NP; (iv) is favoured from capsules with a smaller shell thickness. NP vehicle and “active” mainly co-localize in skin “furrows” and around hair follicles after topical application. No evidence shows NP penetrate beyond the superficial layer of the skin. In the stratum corneum, the “active” remains in part associated with NP, but the release f the “active” clearly occurs to some extent followed by its penetration into deep layers of the stratum corneum. Overall, through this work, the fate of nanoparticle vehicle and the “active” has been distinguished and the physicochemical properties of the nanoparticles that determine their behaviour once applied to the skin, and the kinetics with which an “active” is released, has also been understood.

Table of Contents

List of Figures

List of Tables

CHAPTER 1

APPLICATIONS OF NANOPARTICLES IN TOPICAL DRUG DELIVERY AND IN COSMETICS

Applications of nanoparticles in topical drug delivery and in cosmetics

Xiao Wu[1] and Richard H. Guy[1]

[1]Department of Pharmacy and Pharmacology, University of Bath, Claverton Down, BA2 7AY, Bath, UK

Abstract

The delivery of drugs and active agents to the skin by formulations containing nanoparticles is a topic of considerable current interest. A number of studies have shown important advantages of these nanostructure-based delivery systems over conventional formulations. This review describes the composition, preparation, and characteristics of a wide range of novel vectors, including nanoemulsions, liposomes, transfersomes, solid lipid nanoparticles, polymeric nanoparticles, ethosomes and niosomes.

Keywords: Nanoparticles, skin, stratum corneum, cosmetics, pharmaceutics

1.1 Introduction

The skin is the largest organ in the human body by weight, contributing about 10% of total weight, and covering an average area of 1.7 m^2. It regulates water and heat loss, and prevents the invasion of noxious chemicals and microorganisms. Because skin is an easily accessible organ, its potential as an alternative route for administering drugs for both systemic and local effect has attracted considerable interest [1]. Equally, a large segment of the cosmetic industry is focused on the delivery of “actives” to and into the skin. However, molecules do not easily penetrate the skin because of its excellent barrier function. As a result, various nano-carriers have been developed in an attempt to reversibly modulate the skin barrier and/or to provide novel delivery systems for the active of interest. These particulate carriers include nanoemulsions, liposomes, transfersomes, solid lipid nanoparticles, polymeric nanoparticles,

ethosomes and niosomes. A schematic representation of their structures is shown in Figure 1.1.

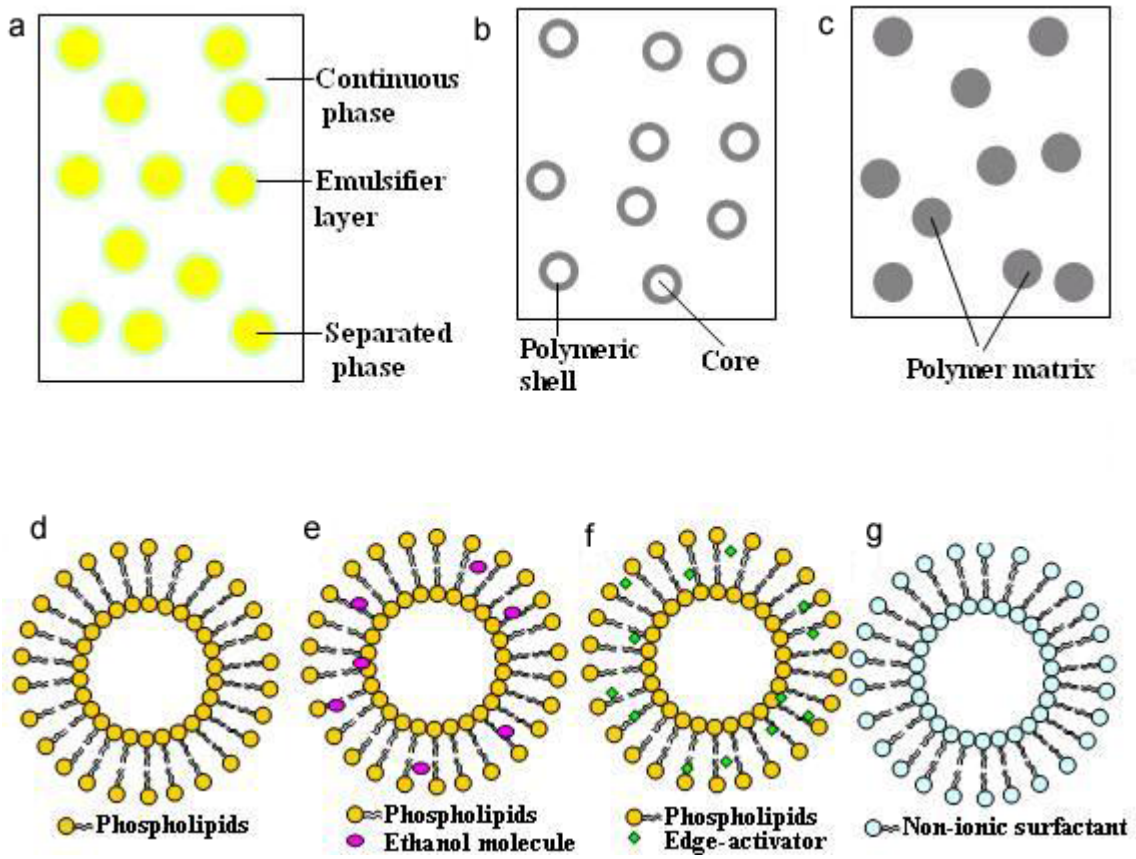

Figure 1.1: Schematic representation of (a) a nanoemulsion, (b) polymeric nanocapsules, (c) polymeric nanospheres, (d) individual liposomes, (e) an ethosome, (f) a transfersome, and (g) a niosome.

1.2 The structure of the skin

The skin consists of the epidermis and the dermis, which sits on a layer of subcutaneous fat.

The epidermis contains four histologically distinct layers, from the innermost stratum basale via the stratum spinosum and stratum granulosum (SG) to the superficial stratum corneum (SC). The SC has been represented as a "brick and mortar" structure [2] in which the corneocytes are embedded in an intercellular lipid matrix. The corneocytes comprise insoluble keratins enveloped by cross-linked proteins, and are arranged in parallel, overlapping, multicellular stacks perpendicular to the skin surface [1]. The inter-corneocyte space is filled

with lipids, usually present in the crystalline phase [3]. Most SC lipids are synthesized in the viable epidermis during differentiation [4], they are released into the intercellular spaces at the SG-SC interface from lamellar bodies. The major SC lipids are ceramides, fatty acids and cholesterol. Eight classes of ceramides have been identified. The lipids are arranged in multiple bilayers with a periodicity of about 13 nm. Unlike almost all other membranes in the body, the SC does not contain phospholipid [2]. This "brick and mortar" structure is now accepted as the location of the skin's excellent permeability barrier, and the SC is the rate-limiting barrier to the transcutaneous penetration and absorption of most chemicals following topical administration [5].

There are three possible pathways of molecular penetration across the SC: (i) intercellular via the lipids between the corneocytes; (ii) transcellular crossing through the corneocytes and the surrounding lipids; (iii) appendagal via follicles and sweat ducts (Figure 1.2) [6]. The principal route is generally believed to be intercellular. Some permeation enhancers (e.g., oleic acid) and vesicular carriers are thought to disorder the SC lipids and facilitate transport across the skin [7-9].

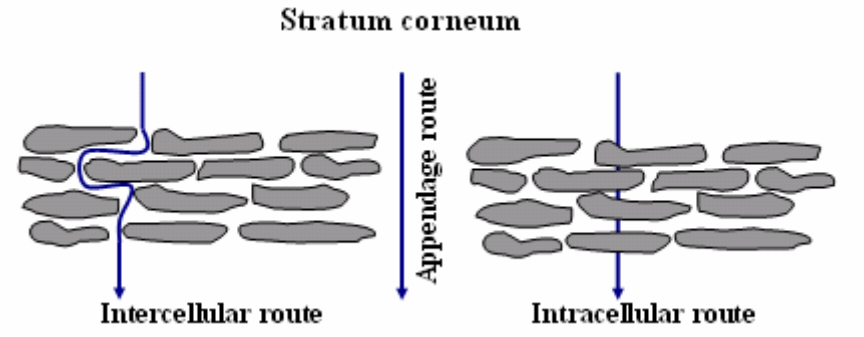

Figure 1.2: Skin permeation pathways.

Underlying the SC is the viable epidermis, the thickness of which is typically ~100 μm, ranging from as little as 50 μm to around 800 μm on the load-bearing palms and soles of the feet [1]. The principal cells of the viable epidermis are keratinocytes, but there are also melanocytes, Langerhans cells, migrant macrophages and lymphocytes [10]. However, there are no blood vessels in the epidermis.

The dermis is typically 3–5 mm thick and is the major component of human skin. It is rich

in blood vessels, lymphatic vessels and nerve endings. The skin appendages, which include hair follicles, sebaceous glands and sweat glands, also originate in the dermis. This layer resembles an aqueous gel and is a minimal barrier to drug transport. As mentioned above, the hair follicles and associated sebaceous glands are considered to play a role with respect to transport across the skin; given that sebum consists mostly of neutral, non-polar lipids, it may be anticipated that this route favours more lipophilic permeants.

The subcutaneous fat layer bridges between the dermis to the underlying tissue, and plays a negligible role in the percutaneous absorption of topically applied substances.

1.3 Nanoemulsions

1.3.1 Composition and preparation

Nanoemulsions are stable dispersions with mean droplet diameters of a few hundred nanometers, and are sometimes called sub-micron or mini-emulsions. These systems are composed of oil, water, and one or more surface-active agents, and may be oil-in-water (o/w) or water-in-oil (w/o) dispersions [11]. In some circumstances, nanoemulsions may be formed using phospholipids as one of the surface-active constituents; if the level of lipid is high, the concurrent formulation of liposomes is possible [12]. The aqueous phase may contain hydrophilic, pharmaceutical or cosmetic active ingredients and preservatives, while the oil phase is typically composed of mineral oil, silicone oil, vegetable oil, esters of fatty acids, and/or lipophilic active ingredients. Surfactants, such as disodium stearoyl glutamate, sucrose alkyl ester, sorbitan alkyl ester and dimethicone copolyol, are added to the formulation to allow formation of a stable dispersion and guarantee an appropriate shelf life of the product.

Both o/w and w/o nanoemulsions can be used in pharmaceutical preparations for topical administration. In the former case, the common oil core constituents are triglycerides, propylene glycol mono caprylic ester, cholesteryl esters and cholesterol [13]. Most nanoemulsions in cosmetics are oil-in-water and contain 10-20% oil stabilized with 0.5-2%

emulsifying agent. Popular oils are triglycerides, silicones, isopropyl myristate, isocetyl isostearate and isododecane. As well as conventional surfactants, polymeric emulsifiers, such as carbomers and hydroxypropyl methylcellulose (HPMC), are also being used to produce stable products with a pleasant appearance [14]. Carbomers are crosslinked polyacrylic acid polymers; and represent the most widely used gelling agents in skincare products [15]. Once introduced into a nanoemulsion, irregular structures on the order of a micron in size are observed (Figure 1.3), in proportion to the amount of carbomer employed. Carbomers can form a thick protective gel layer around each oil droplet and increase the viscosity of the external phase. Following contact with the skin, electrolytes from the skin surface cause the protective gel layer to deswell instantly. The oil phase is released and a thin film is deposited on the skin. This mechanism permits the convenient formulation of sun-care products which are ultimately waterproof despite their predominantly hydrophilic properties prior to application. The emulsification mechanism of HPMC is similar to that of carbomer, although the former is less sensitive to the presence of electrolytes. It is believed that the mechanical stress, imparted on application of these emulsions, causes a partial breakdown of their structures such that a thin film of oil spreads over the skin surface, reducing its wettability. After the water has evaporated, a flexible film remains consisting of oil droplets embedded into the polymer matrix [14].

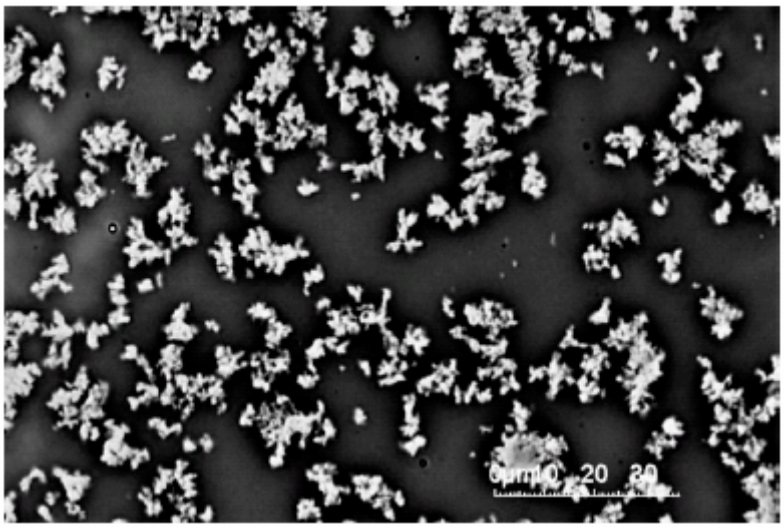

Figure 1.3: Image of a nanoemulsion (15% oil) stabilized with 0.2% carbomer at pH = 7. Adapted from reference [15].

Nanoemulsions are easily produced in large quantities by mixing a water-immiscible oil phase into an aqueous phase using a high-stress, mechanical extrusion process [16, 17].

1.3.2 Applications of nanoemulsions in pharmaceutics

An o/w nanoemulsion containing 10% (m/m) oil (propylene glycol mono-caprylic ester and glycerol triacetate), 50% (m/m) surfactant (diethylene glycol monoethyl ether and Tween-80) and 40% (m/m) water has been suggested as a vehicle for the improved transdermal delivery of celecoxib [18]. *In vitro* skin permeation studies showed enhanced percutaneous uptake of the drug from the nanoemulsion relative to a simple gel [18]. *In vivo*, inhibition of carrageenan-induced paw edema in rats was observed when celecoxib nanoemulsion was used. The ability of nanoemulsion formulations to enhance topical drug delivery has also been shown for ketoprofen [19]. It was claimed that the drug permeation rate could be manipulated by changing the relative amounts of oil, surfactants and co-surfactants. Similarly, another study with an aceclofenac nanoemulsion showed improved permeation of the drug into rat abdominal skin, and significantly increased anti-inflammatory effect on carrageenan-induced paw edema in rats *in vivo*, when compared with a gel formulation [20].

As well as acting as a drug carrier, nanoemulsions themselves have extensive antimicrobial activity against bacteria (e.g., E. coli, Salmonella, S. aureus), viruses (e.g., HIV, Herpes simplex), fungi (e.g., Candida, Dermatophytes), protozoa and spores (e.g., anthrax) due to their ability to fuse with and lyse these different organisms. Fusion is primarily driven by the electrostatic attraction between the typically cationic charge of the emulsion and the anionic charge on the pathogen. There is one example of the antimicrobial effects of surfactant nanoemulsions. A w/o nanoemulsion ($X8W_{60}PC$), containing oil (64%), detergents (9.7%), solvent (8%) and water (18.3%), at a low concentration of 1%, significantly reduced the number of colony forming units (CFU) of *Candida. albicans* by more than four logs within 15 minutes of treatment, and by six logs in a two-hour exposure. Because some of the ingredients of $X8W_{60}PC$ are biocidal, the anti-fungal activity of the individual ingredients was also evaluated at concentrations equivalent to those in $X8W_{60}PC$. However, none of the constituents

was as effective a fungicidal as the nanoemulsion (Figure 1.4), suggesting that the activity of $X8W_{60}PC$ depends upon its nanoemulsion structure [21].

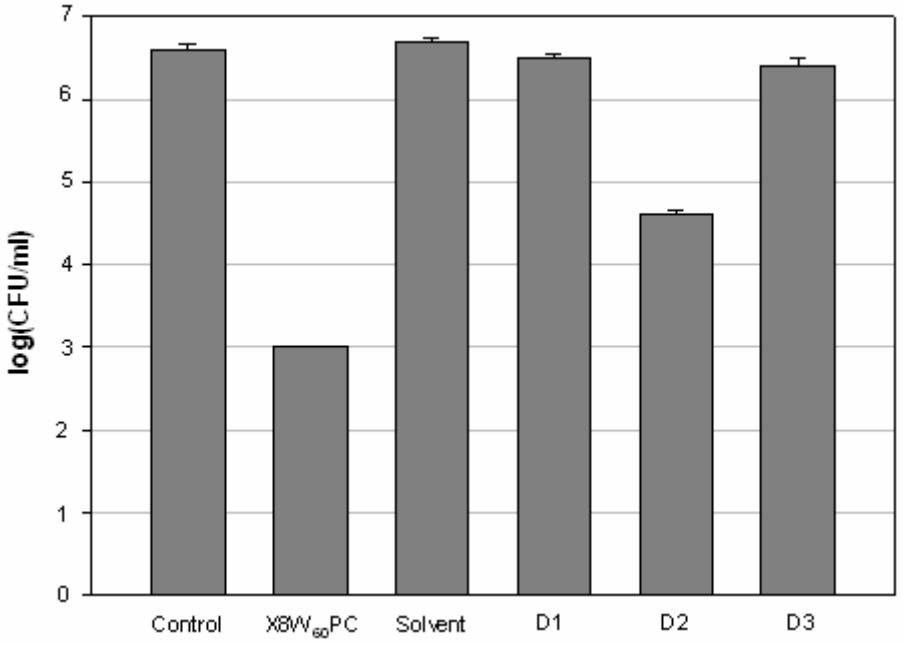

Figure 1.4: The susceptibility of Candida albicans to a $X8W_{60}PC$ nanoemulsion and to its individual ingredients. Cells were treated with either 0.1% $X8W_{60}PC$ nanoemulsion or with individual ingredients at the equivalent concentrations for 15 minutes at 37°C. After treatment, cells were washed and plated on BH1 plates to assess the number of CFU. The bars represent standard error. D1, D2, and D3 depict three detergents used to prepare $X8W_{60}PC$. Redrawn from reference [21].

A special type of topical nanoemulsion has been developed for the instillation of an adrenergic β-blocking agent, adaprolol maleate, into the eye, to treat glaucoma without inducing systemic side-effects. However, the drug has an important clinical disadvantage of irritation to the eye, causing an immediate burning sensation and local discomfort. A nanoemulsion formulation, on the other hand, maintains the therapeutic efficacy of the drug while reducing the level of ocular irritation [13].

1.3.3 Applications of nanoemulsions in cosmetics

The aesthetic properties of nanoemulsions, i.e., low viscosity and transparence with small droplet size, make them attractive for use in cosmetics products such as bath oils, body creams, anti-wrinkle and anti-aging preparations, and numerous patents reflect the active development of these formulations. For example, nanoemulsions containing fluid, non-ionic, amphiphilic lipids, such as diglyceryl isostearate, sorbitan oleate, and α-butylglucoside caprate, were stable on storage between 0°C and 45°C [22], were able to contain significant amounts of fragrance, and promoted the penetration of "actives" into the surface layers of the skin. Nanoemulsions made with anionic, amphiphilic lipids of phosphoric acid fatty esters and oxyethylenated derivatives also retained transparency and good cosmetic properties even when large amounts of oil were added to the formulations [23]. Another o/w nanoemulsion based on one or more nonionic and/or anionic amphiphilic lipids, and one or more water-soluble neutral polymers (e.g. poly-(ethylene oxide), polyvinyl alcohols; polyvinylcaprolactam), allowed the viscosity of the composition to be increased without influencing its transparency or increasing the level of the oil phase [24]. A stable and translucent nanoemulsion for cosmetic, dermatological and/or ophthalmological applications comprised a ternary surfactant system of ethoxylated fatty ester polymer, fatty acid ester of sorbitan and alkali metal salts of cetyl phosphate or palmitoyl sarcosinate, did not require gelling agents for stabilization [25], making it suitable for use on sensitive skin. Several other nanoemulsion technologies have been developed for diverse properties, including sun-protection, anti-wrinkling, anti-aging of the skin and other cosmetic targets [26-29].

1.3.4 Summary

Nanoemulsions consist of fine o/w or w/o dispersions. They are used in dermatology to improve drug delivery to and through the stratum corneum. In addition, nanoemulsions themselves are biocidal towards bacteria, viruses, fungi, protozoa and spores. In cosmetics, nanoemulsions have found use in many cosmetic products for their transparent visual aspect, hydrating power and good skin feel.

1.4 Liposomes

1.4.1 Composition and preparation

Liposomes are spherical vesicles consisting of one or more membrane-like phospholipid bilayers enclosing an aqueous core. Vesicle diameter ranges from 50 to several hundred nanometers. The principal lipid component of liposomes is typically phosphatidylcholine (PC) derived from egg or soybean lecithin [30]. Cholesterol is usually included in the composition to stabilize the structure thereby generating more rigid liposomes [31]. Depending on the processing conditions and the chemical composition, small unilamellar vesicles (SUV), large unilamellar vesicles (LUV), large multilamellar vesicles (MLV) and multivesicular vesicles (MVV) may be formed with one or several concentric bilayers (Figure 1.5). Unlike emulsions, liposomes are thermodynamically stable lamellar structures which form spontaneously when lipid is brought into contact with an aqueous phase [32].

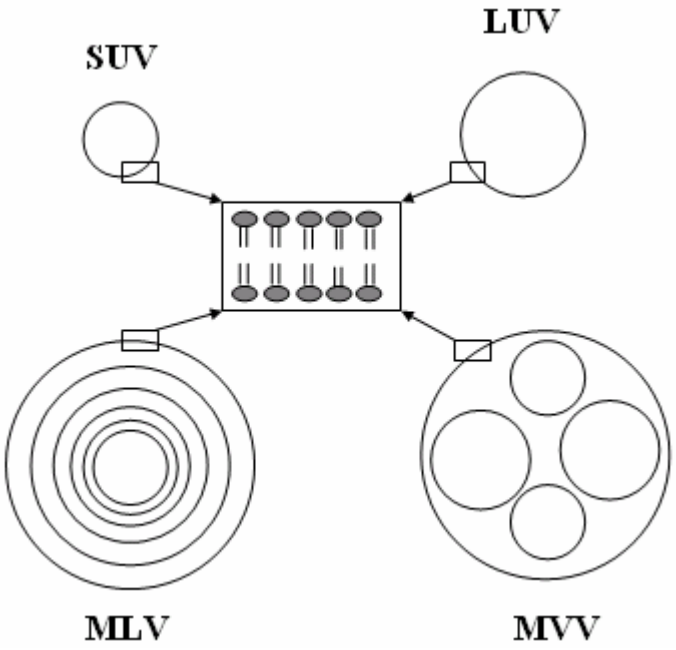

Figure 1.5: Schematic illustration of liposomes of different size and number of lamellae. Redrawn from reference [14].

Liposomes can be prepared by a number of methods. The major techniques are lipid film

hydration, emulsification, reverse phase evaporation, freeze-thaw processes, and solvent injection. Large liposomes form spontaneously when phospholipids are dispersed in water above their phase transition temperature. To prepare small vesicles, an appropriate technique, such as high-pressure homogenization, sonication, or extrusion, is required to reduce particle size. It should be stated that most of the methods for preparing liposomes have at least one of the following drawbacks: use of large quantities of solvent, need for special equipment, and low "active" encapsulation efficacy.

Due to their biphasic character, liposomes can act as carriers for lipophilic, amphiphilic and hydrophilic substances. The entrapped compound's solubility and partitioning characteristics will determine its location in the liposomal bilayer, its level of association with the liposome and its release rate. In general, lipophilic and amphiphilic substances, e.g., oil-soluble UV filters, are located in the lipid bilayer of the liposome. As such compounds are very poorly water-soluble, loss of entrapped drug on storage is minimal. Hydrophilic drugs are entrapped inside the aqueous core of liposomes, but may also be in the external water phase. The percentage of encapsulated hydrophilic drug depends on the liposome bilayer composition and the preparation procedure.

1.4.2 Applications of liposomes in pharmaceutics

The first report of the use of liposomes in topical drug delivery involved delivery of triamcinolone acetonide. It was claimed that the liposomal formulation significantly increased the concentration of steroid achieved in the epidermis and dermis [33]. In a further study, it was reported that application of triamcinolone acetonide-loaded liposomes resulted in ~5-fold more drug accumulation within the epidermis in comparison to a more conventional gel formulation [34]. A number of other studies have implied the efficiency of liposome formulations to deliver enhanced drug amounts to the upper skin layers. For example, a liposome formulation of betamethasone dipropionate out-performed a commercial conventional formulation containing a higher concentration of drug in a clinical trial considering the treatment of atopic eczema [35]. The liposome formulation was less efficient in

treating psoriasis for which deeper penetration of the drug is needed. Econazole, topical antifungal drug, can be irritant to the skin when topically applied in conventional vehicles. The application of liposome formulation has been shown to be a good strategy to minimize this irritation and enhance patient compliance. In biodisposition studies with a econazole in a liposomal gel dosage form, an ~7-fold increase in drug concentration in the epidermis was achieved, relative to a control cream [36]. It was possible, therefore, to reduce the applied drug dose yet maintain an equivalent therapeutic efficacy, thereby minimizing skin irritation. Similar results have been obtained with minoxidil, a drug to combat hair loss, and several liposomal products have been shown to be more efficient in delivering the drug to hair follicles than conventional dosage forms [36, 37]. Likewise, the local anesthetic agents, tetracaine and lidocaine, showed enhanced activity over conventional dermatological preparations when liposomal products were used [38, 39].

Of course, the efficiency of topical drug delivery from liposomal vehicles depends on the physicochemical properties of drug involved [40]. For example, the release of progesterone from Intralipid® emulsion was substantial, whereas egg-phosphatidylcholine and dipalmitoylphosphatidylcholine liposomal formulations delivered only 1% of the drug "payload" over a similar period [41]. The release of progesterone from liposomes followed zero-order kinetics, controlled by slow interfacial transport of the drug from the bilayer into the surrounding aqueous medium.

When caffeine (3% w/v) was delivered from (i) an aqueous solution, (ii) a PEG solution, (iii) an aqueous solution containing the enhancers, transcutol and oleic acid, (iv) a PEG-water solution with the same enhancers, and (v) a phosphatidylcholine/cholesterol liposomal (SV) formulation, the results in Figure 1.6 were obtained [42]. Notably, the enhancers were effective, and interestingly the vesicles significantly retarded the delivery of caffeine. This resulted, after 24 hours, in a much higher retention of the active in the epidermis following SV application. The same improved accumulation of drug in the skin has also been reported for a liposome formulation containing unfractionated heparin [43].

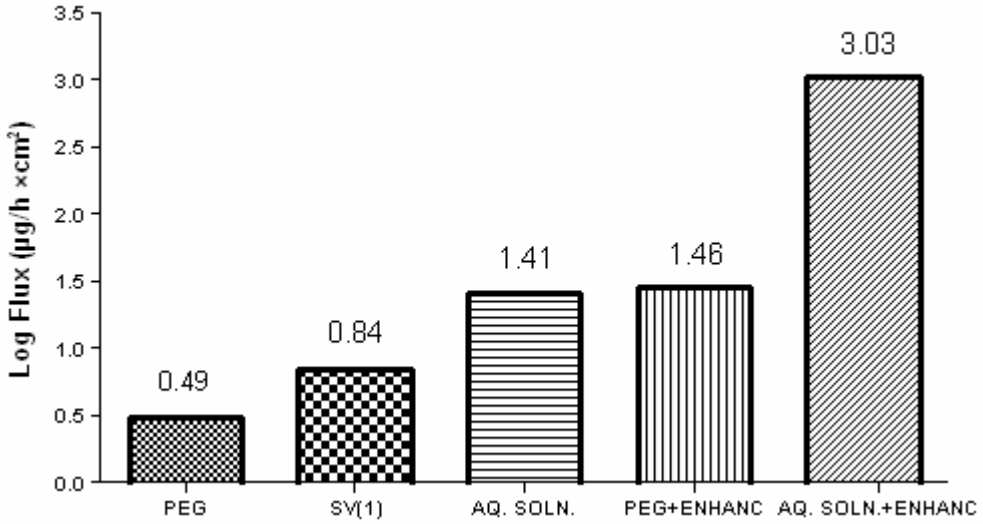

Figure 1.6: Effect of different formulations on the flux of caffeine through hairless mouse skin (3% caffeine in each system). Adapted from reference [42].

The exact manner in which topical liposomes interact with the SC, and the lipids therein, is not fully characterized, especially when this occurs in the presence of an organic solvent, such as ethanol. Enhanced mixing with the intercellular lipids of the SC and/or the sebaceous lipid on the surface and within the hair follicles seems likely and logical. Microscopic observations have confirmed the fusion of liposomes on the SC surface resulting in stacks of lamellae and other, irregular structures [44]. It must be also remembered that the amount of lipid in the SC intercellular spaces may be small, relative to that applied in the form of liposomes. A square centimeter of SC of thickness of 10 µm has a volume of 1µl; given the "brick-and-mortar" structure of the SC, ~20% may be assumed to be associated with intercellular (and surface) lipid, which is 0.2 µl of lipid. Taking lipid density as about 1 g/ml (1 mg/µl), then the lipid content of 1 cm^2 of SC is approximately 0.2 mg, an amount comparable to or smaller than the levels of lipid typically used when assessing the impact of formulations. It is perhaps not surprising, therefore, that enhanced deposition of drug into the SC is found when these preparations are used.

1.4.3 Applications of liposomes in cosmetics

Liposomes are found in numerous products designed to deliver active cosmetic substances into the epidermis. The aim is to concentrate the active ingredients in the outermost skin layers. For example, liposome-encapsulated UV filters incorporated into aqueous-based sunscreens products have good substantivity on the skin surface, thereby preventing them from being easily washed off. Liposomes themselves, when formulated into cosmetics, can replenish/augment the endogenous SC lipids, increase moisturization and reduce skin dryness [45].

There are many marketed liposomal cosmetics. Capture® was the first product incorporating liposomes and was introduced by C. Dior in 1986. It contains 5% thymus extract, 1% collagen and elastin peptides, and 0.1% hyaluronic acid in liposomes (100 nm diameter) made from soya lecithin [46]. Estée Lauder's "Advanced Night Repair Protective Recovery Complex®" contains a liposome delivery system which is claimed to neutralize and repair 90% the damage caused by free radicals generated by UV, pollutants and oxidants. The formulation contains hyaluronic acid and is an effective moisturizer too. L'Oréal has pioneered the development of nanosomes (i.e., very small liposomes) in an anti-wrinkle product, "Revitalift® Double Lifting", containing pro-retinol A [47]. Jafra Cosmetics International's "Royal Jelly Lift Concentrate®" includes liposomes and a complex mixture of amino acids, vitamins and minerals, to stimulate cell renewal and prevent wrinkles [48]. Overall, cosmetic preparations containing liposomes range from simple creams and gels to complex formulations containing various extracts, moisturizers, antibiotics, and recombinant proteins for wound or sunburn healing. The commercial products are available as anti-aging skin creams, sunscreens, long-lasting perfumes, hair conditioners and so on.

1.4.4 Summary

The use of liposomes for the topical delivery of drugs and cosmetic actives represents a huge area of activity. The lipids comprising the vesicles clearly mix with endogenous SC lipids and transfer their encapsulated "payload" into the skin, sometimes undermining barrier function, at others providing reinforcement and improving hydration. Retention of an active at

the SC surface can also be achieved as a positive benefit (e.g., for a sunscreen). Many cosmetic products based on liposomes have reached the market.

1.5 Transfersomes

1.5.1 Composition and characteristics

Transfersomes® (IDEA AG), are highly deformable mixed lipid aggregates, regarded as "elastic liposomes". They differ from liposomes because of the presence of so-called edge-activators [49], and comprise phospholipids as the main ingredient with 10-25% surfactant (e.g. sodium cholate) and 3-10% ethanol. The surfactants are the "edge activators", which confer ultradeformability on the transfersomes [50]. The elasticity of the vesicle is correlated with the quantity and the structure of the incorporated surfactant [51]. In comparison with liposomes, it has been claimed that transfersomes are able to deliver their "payload" deeper into the skin [35, 52].

1.5.2 Interaction of transfersomes with the skin

The proposed driving force for the putative penetration of transfersomes across the skin is the water activity gradient between the relatively dehydrated skin surface and the aqueous viable epidermis [53]. Hence, when a transfersome formulation is applied on the skin under non-occlusive conditions, the evaporation of water from the vehicle drives the penetration of vesicles towards the viable epidermis to avoid their dehydration [54]. It has been reported that transfersomes penetrate into the SC via two different hydrophilic pathways [55, 56]: (i) An intercluster route via the "gorge" between corneocytes clusters (formed by 3 to 10 individual corneocytes) which has a uniform width (≤ 4-6 μm) and depth (≤ 3-5 μm) (Figure 1.7); this pathway has a relatively low penetration resistance and corresponds to ≤ 1% of the total skin surface area. (ii) The intercorneocyte pathway travels between the individual corneocytes in the cell clusters, and occupies an area greater than 3% of the total skin surface area.

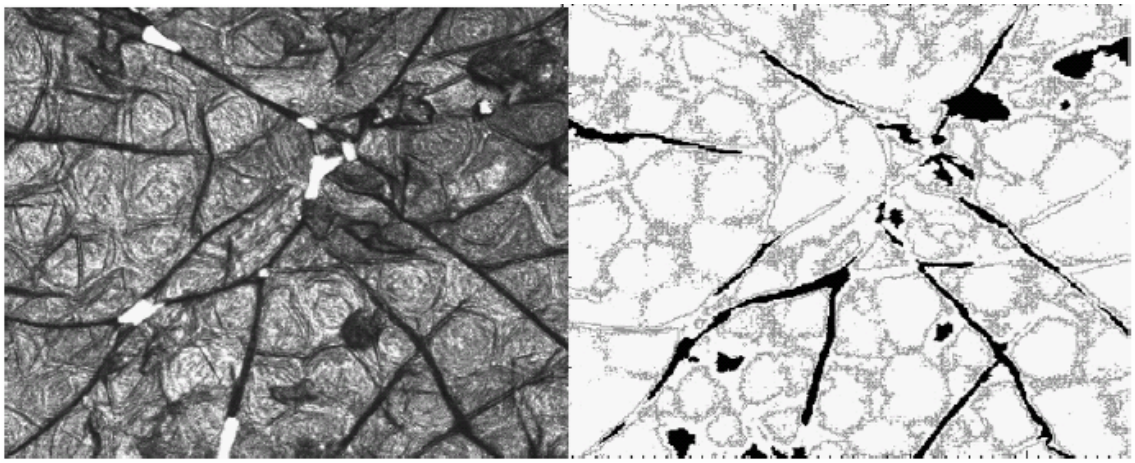

Figure 1.7: Left panel: laser scanning confocal microscopy image of nude mouse skin *in vivo* (~200 μm^2 area). Right panel: Distribution of a fluorescent penetrant in the so-called intercluster (black) and intercorneocyte (grey) regions of the skin. Reprinted from reference [56].

1.5.3 Applications of transfersomes in pharmaceutics

The anti-inflammatory action of topical triamcinolone acetonide delivered from transfersomes was significantly greater than that induced by marketed products [57]. Moreover, the biological activity of the drug was maintained at doses at least one order of magnitude lower than that commonly used in commercial topical lotions or creams. As a result, it may be anticipated that any systemic side effects would be greatly reduced.

It has also been reported that diclofenac associated with ultradeformable transfersomes is a good alternative for the combined oral and topical administration of the drug for rheumatoid disease [58]. Delivery from transfersomes sustained a prolonged therapeutic effect and resulted in a higher drug concentration in the skin than that from a commercial hydrogel.

The topical administration of oestradiol from transfersomes and from rigid liposomes has been compared [59], and the deformable vesicles were shown to be significantly superior. This enhanced delivery was maintained for different “edge activators” [60]. Similarly, phosphatidylcholine vesicles containing sodium cholate, Span-80 or oleic acid significantly enhanced oestradiol transport across human skin *in vitro* relative to control formulations in

which the transfersome constituents were present, but had not been assembled into the ultradeformable particles [61]. Similarly, flexible liposomes containing cyclosporin A delivered more drug into the skin than conventional vesicles [62].

Finally, and remarkably, transfersomes have also been claimed as a technology for the non-invasive delivery of insulin across the skin [63, 64], although the ultimate practicality of the approach remains to be established.

1.5.4 Summary

Transfersomes have been claimed to enhance significantly the local and systemic delivery of a wide range of compounds. The osmotic gradient across nonoccluded skin has been proposed as the driving force for this improved delivery when ultradeformable vesicles are used. Initial applications are focused upon non-steroidal anti-inflammatory drugs with a site of action beneath the skin in the subcutaneous tissue.

1.6 Polymeric nanoparticles

1.6.1 Nanocapsules

1.6.1.1 Composition and preparation

Polymeric nanocapsules are submicron colloidal particles with a core surrounded by a polymeric shell. In general, the core of nanocapsules is an organic (oil) solvent. Some of the most widely used polymers for the nanocapsule shell are poly-(ε-caprolactone) (PCL) [65], poly-L-lactide (PLA) [66], poly-(glycolic acid) (PGA), poly-(lactide-co-glycolide) (PLGA) [67], poly-(butylcyanoacrylates) [68-71], poly-(ethylcyanoacrylates) [72], poly-(alkylene adipate) [73], polyvinyl acetate (PVA) [74], cellulose acetate phthalate [75], poly-(ε-caprolactone)-block-poly-(ethylene glycol) [76], poly-(methyl methacrylate) [70], and polystyrene.

Methods for preparing nanocapsules can be classified into two categories. The first involves in situ interfacial polymerization around a droplet [77]; the second requires interfacial nanodeposition of a preformed polymers [78]. In interfacial polymerization, either a monomer, or an amphiphilic polymer with a cross-linkable group, is used and polymerization is induced at the surface of a droplet. A w/o or o/w emulsion is usually formed first before the shell is polymerized at the interface of two phases [79, 80]. This technique allows the polymeric shell to follow the contour of the inner phase. The drawback is that the polymerization process may provoke side-reactions involving the drug or active ingredient and reduce thereby their ultimate availability from the formulation. In preparing nanocapsules from preformed polymers, the deposition of the polymer at the surface of an oil droplet can be achieved by mixing the organic phase containing the polymer with an aqueous phase containing a hydrophilic surfactant. As the nanometer-sized droplets of oil form, the polymer precipitates at the interface with the aqueous phase and the nanocapsules are stabilized by the surfactant [81]. This technique avoids some of drawbacks of the interfacial polymerization process, such as lack of control of molecular weight, the presence of residual monomer in the preparation, and the possibility of side-reactions.

1.6.1.2 Applications of nanocapsules

Nanocapsules have been proposed as topical formulation constituents for several active compounds, including diclofenac, lidocaine, caffeine, retinoids, vitamin E, beta-carotene, amino acids, plant extracts, fragrances, antioxidants and UV protectants. The nanocapsule core has the advantage of providing a high loading capacity, with a relatively low polymer content. Compared to liposomes, polymeric nanocapsules are more robust as the shell is a covalently linked structure.

1.6.1.2.1 Applications of nanocapsules in pharmaceutics

The first polymeric particle system used for transdermal drug delivery comprised PLA microcapsules containing the contraceptive steroid, levonorgestrel [66]. Subsequently, indomethacin was encapsulated in poly-n-butylcyanoacrylate nanocapsules and improved the

transdermal delivery of the drug compared with a conventional gel [71]. Nanoencapsulation of flufenamic acid using PLGA nanocapsules also resulted in significantly increased drug accumulation in the viable skin layers when assessed *in vitro* using different experimental models [67]. Delivery of chlorhexidine from PCL nanocapsules synthesized by interfacial polymerization has been assessed on eight bacteria strains. Sustained drug release was achieved and a prolonged *ex vivo* topical antimicrobial activity on porcine ear skin against Staphylococcus epidermis was reported [82]. The improved efficacy was explained by a more direct and sustained contact between the particles, bacteria, skin surface and hair follicles.

1.6.1.2.2 Applications of nanocapsules in cosmetics

Generally, nanocapsules are used in cosmetics to protect sensitive actives, reduce undesirable odours and avoid incompatibility between formulation ingredients. One of the first nanocapsule-based products was an anti-wrinkle cream encapsulating vitamin A; the particles acted as reservoirs, slowly releasing the active over time [83]. Recently, L'Oréal marketed two products, Primordiale Intense and Hydra Zen Serum, which use nanocapsules to encapsulate several active ingredients.

Nanocapsules have also been intensively investigated as sunscreen vehicles for octyl methoxycinnamate (OMC), octyl salicylate and benzophenone-3. It is believed that the nanocapsules form a protective film on the skin surface and retard any penetration of the active sunscreen into the viable tissue. For example, PCL has been used to prepare OMC-loaded nanocapsules which were more effective in protecting against UVB radiation than a conventional gel [65]. OMC was also encapsulated in cellulose acetate phthalate nanocapsules and its accumulation in the SC was compared to that from a nanoemulsion [75]. In this case, the nanocapsules were less efficient in delivering OMC. The encapsulation of benzophenone-3 (oxybenzone) in a series of nanoparticles made from PVA-fatty acid (Figure 1.8) with different molecular weights has been reported [74]. The nanocapsules significantly decreased the transport of oxybenzone through porcine ear skin *in vitro* by more than an order of magnitude (Figure 1.9)

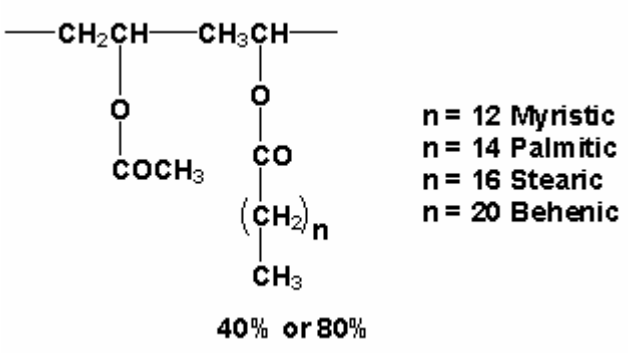

Figure 1.8: Chemical structure of PVA-FA derivatives. Redrawn from reference [74].

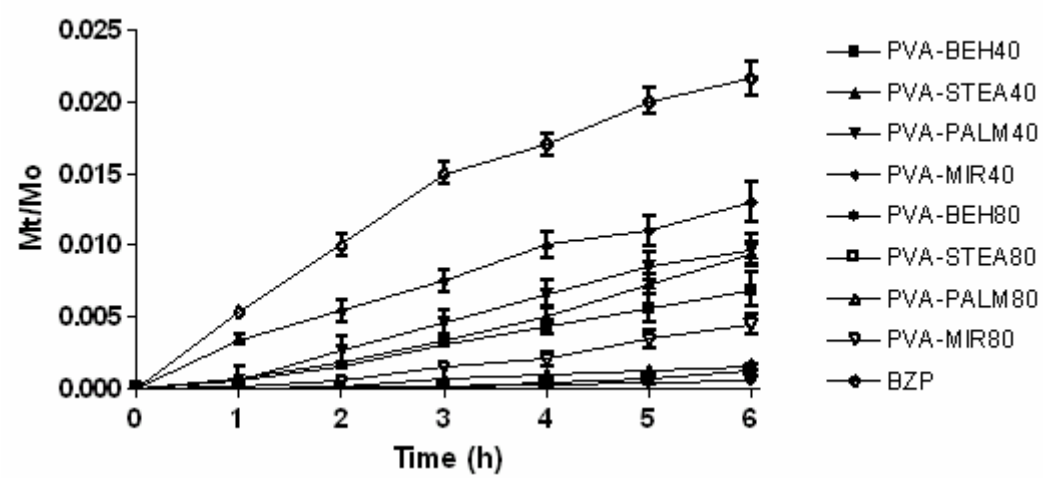

Figure 1.9: Amount of benzophenone-3 absorbed across porcine ear skin *in vitro* (Mt), relative to the applied quantity (Mo), as a function of time following administration of various PVA-fatty acid nanocapsule-containing suspensions. The highest degree of transport occurred when the sunscreen was applied in solution in the absence of nanocapsules. Redrawn from reference [74].

1.6.2 Nanospheres

Nanospheres comprise a homogeneous matrix of polymer in which the drug or active ingredient is dispersed throughout. Generally, methods used to prepare nanospheres can also be adapted to the manufacture of nanospheres [77], i.e., interfacial polymerization, emulsion polymerization and solvent evaporation [11].

For example, the controlled release of captopril from poly-butylcyanoacrylate nanoparticles has been achieved, but improved skin transport was not observed [69]. Somewhat improved delivery of minoxidil from poly-(caprolactone)-block-poly-(ethylene glycol) nanoparticles was reported, with a better result achieved from that of smaller diameter (40 versus 130 nm) [76]. Further, cyclosporine A loaded into chitosan nanospheres better maintained an effective drug concentration on the ocular surface (for up to 48 hours) while avoiding systemic exposure, rapid clearance, eye irritation and blurred version [84].

1.6.3 Summary

Polymeric nanoparticles are unable to cross intact SC. Drugs incorporated into nanoparticles may be slowly released onto the skin surface and into the superficial skin strata. Nanoparticles incorporated in cosmetic preparations can protect unstable active ingredients, avoid incompatibility between different ingredients, and ensure that the absorption of sunscreens, for example, is avoided by forming a film on the skin surface. However, the number of products on the market that are based on polymeric nanoparticles is limited. This is due to a number of factors including the cytotoxicity of some polymers, and problems of scaling up the complex preparation methods involved.

1.7 Solid lipid nanoparticles (SLN)

1.7.1 Composition and preparation

SLN are sub-micrometer in size [85, 86]. The lipids employed include triglycerides, partial glycerides, fatty acids, steroids and wax. Different emulsifiers have been utilized to stabilize SLN dispersions, including Poloxamer 188, Polysorbate 80, lecithin, polyglycerol methylglucose distearate, sodium cocoamphoacetate and saccharose fatty acid esters [87].

The two principal SLN preparation methods are high pressure homogenization and via microemulsion formation. The former is subdivided into hot and cold techniques [86, 88-91].

Hot homogenization is the most frequently used. In this method, the lipid melt is dispersed in a hot surfactant solution at the same temperature by high-speed stirring. The resulting pre-emulsion is passed through a high pressure homogenizer to produce a hot o/w nanoemulsion. The lipid recrystallizes to SLN as the hot nanoemulsion is cooled to room temperature. It is noteworthy that for lipids (e.g., glycerides) with a low melting point close to room temperature, the nanoemulsion needs to be cooled to even lower temperatures to initiate recrystallization. The hot homogenization method may be suitable for temperature-sensitive compounds, because the time of exposure to an elevated temperature is relatively short [86].

The cold homogenization technique is recommended for preparing SLN containing either highly temperature-sensitive compounds or hydrophilic compounds which can partition from the melted lipid phase to the water during a hot homogenization process [88]. In the cold homogenization technique, the melted lipid containing the drug is cooled, and then ground to microparticles which are subsequently dissolved in a cold surfactant solution to form a pre-emulsion. This is then homogenized into SLN at or below room temperature. As homogenization can cause an increase in temperature, the difference between the lipid melting point and the homogenization temperature should be large enough to avoid melting of lipid in the homogenizer.

When SLN are produced by the microemulsion technique, the melted lipid and the aqueous surfactant solution must be at the same temperature. Surfactants and co-surfactants used include lecithin, bile salts and alcohols such as butanol. The two phases are mixed in the correct ratio to form a microemulsion, which is then dispersed in a cold aqueous medium (2-3°C) under gentle mechanical mixing, to ensure that small particles are formed by precipitation [92].

SLN can be also produced by a precipitation method [93]. The lipid is dissolved in an organic solvent and an aqueous phase is added provoking emulsification [94]. The solvent is then evaporated and the lipid precipitates forming nanoparticles. A disadvantage of this method is the use of organic solvent.

1.7.2 Applications of SLN in pharmaceutics

SLN have been used to enhance the topical delivery of several drugs. For example, SLN containing tristearin glyceride, soybean lecithin and polyethylene glycol 400 stearate increased the transport of triptolide *in vitro* by 3 to 4-fold over that from a simple solution of the drug [95]. In eczema patients, SLN loaded with clobetasol propionate showed improved efficacy over a conventional cream [96]. Prednicarbate associated with SLN (again for eczema treatment) was better delivered to the viable epidermis, with less exposure to (and atrophy of) the underlying dermis [90, 97], suggesting a possible targeting effect. Antiandrogens for acne treatment have also been shown to have better efficacy when topically applied in SLN formulations [98]. Once again, drug was concentrated in the outer skin layer and deeper penetration to underlying tissues and to the systemic circulation would be expected to be minimal. It was also shown that the lipophilic fluorescent marker, Nile Red, was delivered from the SLN to the hair follicle infundibulum, once more implying an ability to target a specific skin structure.

1.7.3 Applications of SLN in cosmetics

After topical application, SLN can form an occlusive adhesive film on the skin surface [99-103]. For example, an SLN formulation containing tocopherol acetate was twice as occlusive as an emulsion with identical lipid content (Figure 1.10) [100]. Scanning electron microscopy was used to visualize the SLN on a single tape, and showed complete film formation without distinguishing individual particles (Figure 1.11).

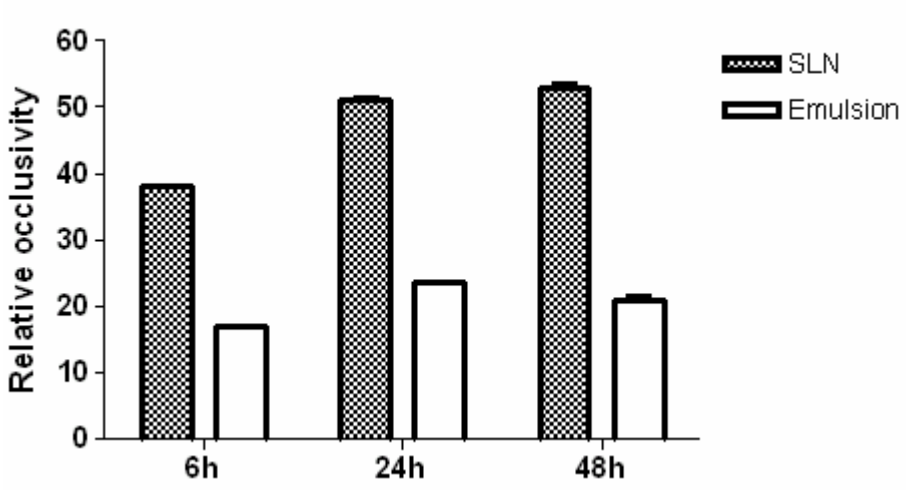

Figure 1.10: Relative occlusivity of tocopherol acetate-based SLN and a reference emulsion after 6, 24 and 40 h post-application. Redrawn from reference [100].

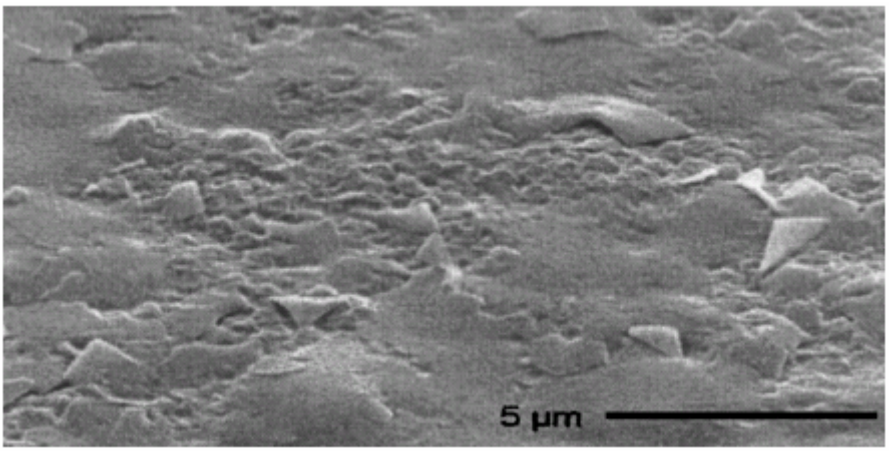

Figure 1.11: Scanning electron micrograph of a dried SLN film on a single tape. Reprinted from reference [100].

SLN appear quite attractive as components for sunscreen products. Not only does the lipid matrix at the skin surface retard the penetration of the active, molecular UV absorbers themselves (thereby reducing potential toxicity relative to conventional formulations) [88, 100, 104-107], the SLN on their own have a sun-protective effect by efficiently scattering the radiation falling on the skin (similar to titanium dioxide particles [108]). Cetyl palmitate SLN containing molecular sunscreens have been shown to have this synergistic photoprotection

effect [88, 100, 105, 108].

Moreover, incorporation of chemically labile active ingredients (e.g., coenzyme Q10, retinol, and tocopherol) into SLN offers protection against decomposition [109-114] and, finally, it should be mentioned that the controlled release of an active ingredient is possible from SLN either to provide a burst release or a more sustained delivery profile [104]. This feature has been exploited for the controlled release of retinol and oxybenzone from SLN incorporated into creams and hydrogels [105, 112].

1.7.4 Summary

SLN have formed a wide range of applications and have useful properties for maintaining "actives" on the SC surface or within the upper skin layers. Their ability to form adhesive, occlusive films is particularly useful for sunscreen applications and for maintaining the stability of labile chemicals.

1.8 Ethosomes

1.8.1 Composition and characteristics

Ethosome are primarily composed of phospholipids, relatively high concentrations of ethanol, and water [115-118]. Their average diameter ranges from tens of nanometers to microns, and depends upon the relative amounts of phospholipids and ethanol [115]. Similar to liposomes, ethosomes can be unilamellar [119, 120] or multilamellar [115, 116, 121].

A number of methods have been used to prepare stable ethosomal formulations depending on the drug characteristics and on the drug delivery target [117, 118]. The manufacturing processes are easily scaled-up. The presence of ethanol allows for efficient entrapment of hydrophilic, lipophilic and amphiphilic molecules. This feature is illustrated by research in which three fluorescent probes of distinct physicochemical properties were encapsulated in ethosomes and liposomes, and their behaviour was then examined by laser scanning confocal

microscopy (LSCM) [115]. The three dyes were the lipophilic Rhodamine Red, dihexadecanoyl glycerophosphoethanolamine (RR), the amphiphilic 4-(4-diethylamino) styryl-N-methylpyridinium iodide (D-289), and the hydrophilic calcein. Figure 1.12 shows that the lipophilic and amphiphilic drugs were clearly associated with the liposomal bilayer, while calcein was concentrated in the aqueous core. In contrast, all the dyes were found throughout the entire volume of the ethosomes at high apparent loading.

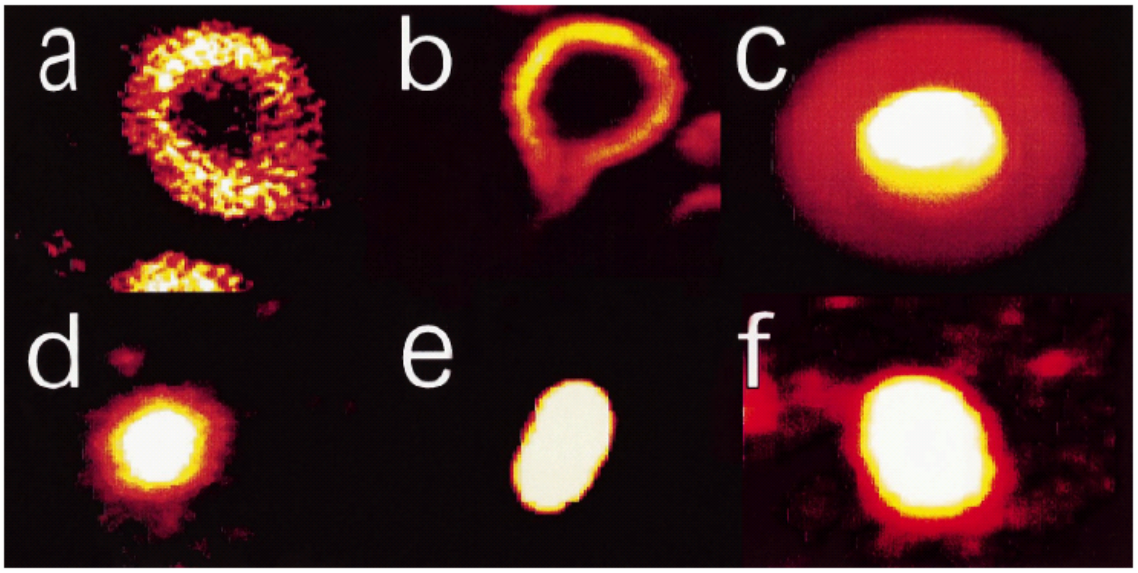

Figure 1.12: Entrapment of three fluorescent probes by liposomes (a-c) and ethosomes (d-f). The fluorescent probes were rhodamine red (a, d), D-289 (b, e) and calcein (e, f). White represents the highest concentration of probe, with yellow and red signifying progressively lower levels. Reprinted from reference [115].

1.8.2 Enhanced transdermal drug delivery from ethosomes

It is claimed that ethosomes significantly enhance drug delivery across the skin by two principal mechanisms: (a) a fluidizing effect of ethanol on phospholipid bilayers creating a "soft", deformable vesicle [115, 119-121], and (b) SC lipid disruption by ethanol thereby permitting entry of ethosomes and their associated "payload" into the deeper skin layers (Figure 1.13) [115].

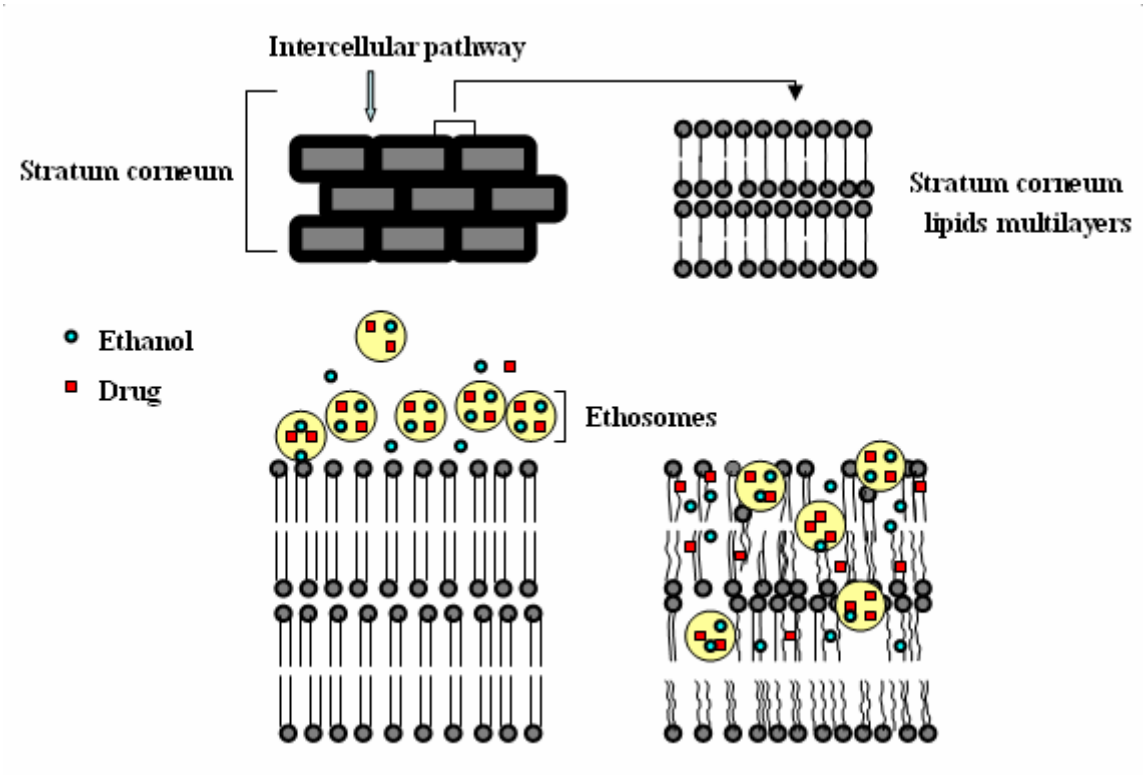

Figure 1.13: Proposed mechanisms for enhanced drug delivery across the skin from ethosomal vehicles. Adapted from reference [115].

Delivery of the three aforementioned fluorescent probes into nude mouse skin from ethosomes, liposomes and a hydroalcoholic solution was assessed by LSCM. For both rhodamine red and D-289, optical sectioning of the skin after an 8-hour application clearly demonstrated that ethosomes were the superior delivery system (Figures 1.14 and 1.15). Uptake from the hydroalcoholic solution was greater than that from the liposomes employed. Quantitative analysis of the fluorescence intensity as a function of the depth again revealed the superiority of the ethosomal formulation, in this instance, for calcein and rhodamine red (Figure 1.16).

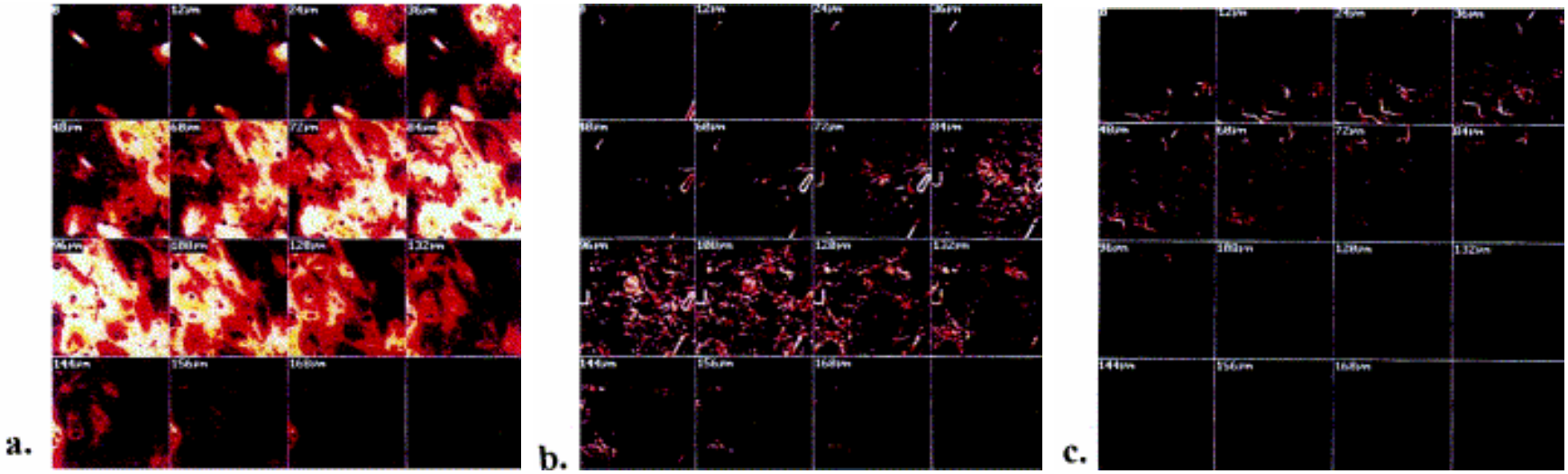

Figure 1.14: LSCM images of rhodamine red penetration into nude mouse skin following an 8 hour application of (a) ethosomes, (b) a hydroalcoholic solution of the dye, and (c) liposomes. Reprinted from reference [115].

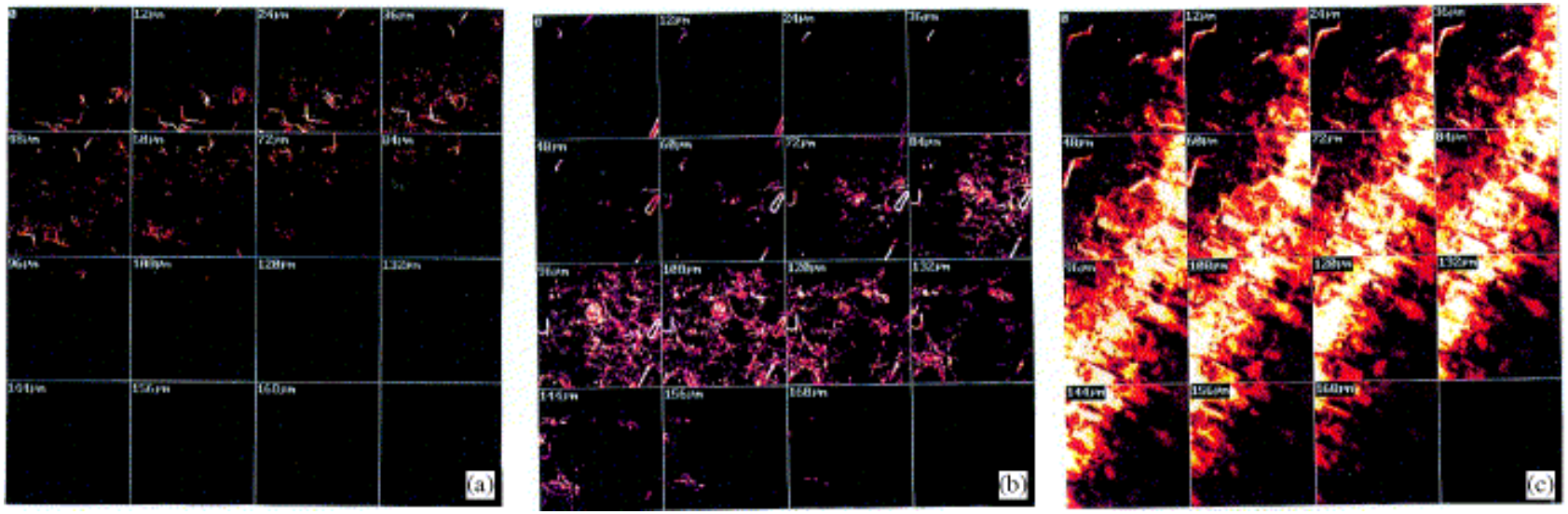

Figure 1.15: LSCM images of D-289 penetration into nude mouse skin following an 8-hour application of (a) liposomes, (b) a hydroalcoholic solution of the dye, and (c) ethosomes. Reprinted from reference [119].

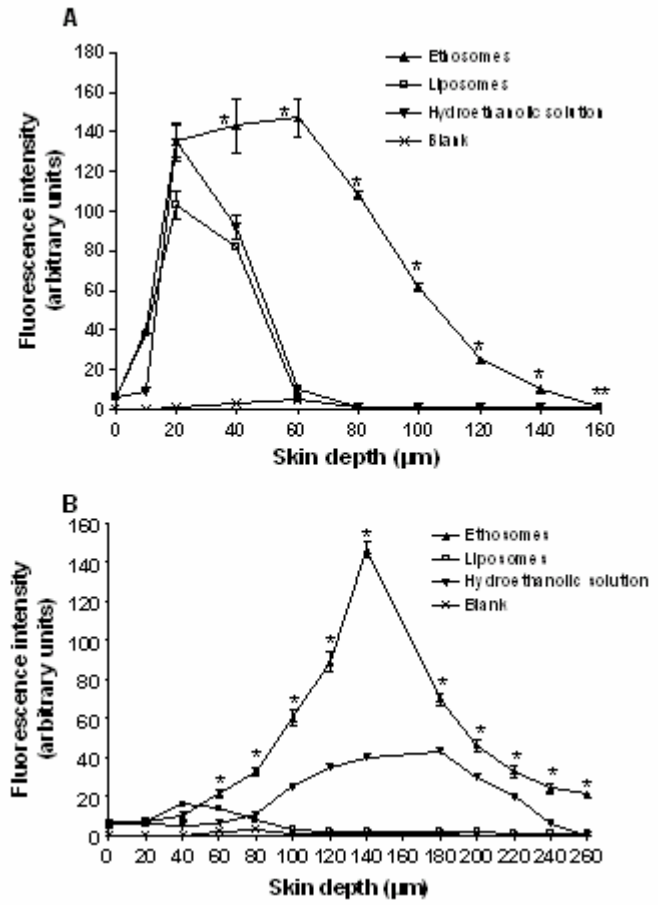

Figure 1.16: Skin penetration profiles of (A) calcein, and (B) rhodamine red, following their application to hairless mouse skin from either ethosomes, liposomes or a hydroethanolic solution for 8 hours. Depth of skin penetration and fluorescence intensity were determined by LSCM. Significantly different values (*$p<0.001$, **$p<0.05$; ethosomes versus other systems) are highlighted. Redrawn from reference [122].

Anti-infective drugs when associated with ethosomes appear to be much more efficient delivery systems than classic liposomes. For instance, fluorescently-labeled bacitracin, a polypeptide antibiotic, was delivered from ethosomes to a depth of 200 µm in dermatomed human cadaver skin, whereas its delivery from classic liposomes was negligible [121]. Another study with ethosomal erythromycin demonstrated an improved antibacterial action in comparison to a hydroethanolic solution of the drug. Moreover, an infected skin site treated with the topically applied ethosomal formulation healed as well as that achieved when the drug was systemically injected [123].

Other examples of the efficacy of ethosomal vehicles can be mentioned. Pretreatment of the skin with a formulation containing ammonium glycyrrhizinate (AG), a natural anti-inflammatory agent effective in acute and chronic dermatitis, significantly reduced the intensity and duration of methyl nicotinate-induced erythema in healthy human volunteers, compared to hydroalcoholic solutions of the drug [124].

Ethosomes have also been reported to enhance the percutaneous delivery of ionized drugs, very lipophilic compounds and large hydrophilic molecules. For example, the flux of trihexylphenidyl hydrochloride, an anti-Parkinsonian agent, from an ethosomal vehicle was substantially higher than that from liposomes [119]. Similar results have been reported for propranolol hydrochloride and sodium diclofenac [117]. Ethosomal formulations of testosterone have been compared with marketed transdermal patches, and shown to achieve significantly higher AUC and C_{max} values [115, 125]. Finally, when acyclovir (an effective antiviral drug for the treatment of recurrent herpes labialis infection) was formulated in ethosomes, its delivery resulted in a marked improvement in therapeutic efficiency, compared to the normal treatment (Zovirax® cream), presumably as a result of the improved penetration of the active from the lipid-ethanol vehicle [126].

1.8.3 Summary

Ethosomes have recorded some notable improvements in topical and even transdermal drug delivery. While the precise mechanisms of action remain less than fully clear, the combination of a relatively high “dose” of exogenous lipid and ethanol can cause perturbation of SC barrier function. Whether this approach will ultimately make a significant impact in the clinic requires considerable further work.

1.9 Niosomes

1.9.1 Composition and preparation

Niosomes are vesicles prepared from non-ionic surfactants, such as polyoxyethylene alkyl ethers, sorbitan esters, polysorbate-cholesterol mixtures, crown ethers, perfluoroalkyl surfactants, alkyl glycerol ethers, and others [127-131]. The surfactants combine one or more hydrophobic components (e.g., alkyls (C_{12}-C_{18}) or perfluoroalkyls (C_{10}) or a steroidal group) with a hydrophilic head group (e.g., ethylene oxide, glycerol, crown ether, polyhydroxyls, and sugars). The hydrophilic and hydrophobic moieties are linked by ether, ester, or amide bonds.

Niosomes are prepared by similar methods to those used for liposomes, such as hydration of a deposited surfactant/lipid film. This process is usually followed by homogenization, sonication, or extrusion to reduce vesicle size, and then separation of the un-entrapped drug [127, 128, 130]. The stability of niosomal formulations is influenced by factors such as storage temperature, preparation technique, and composition [127, 130]. Vesicle aggregation may be prevented by co-formulation with surfactants. Like liposomes, niosomes can form unilamellar or multilamellar structures, and have the further advantages of improved stability, high purity and low cost.

1.9.2 Interaction of niosomes with the skin

The interactions of niosomes with the SC have been studied using microscopic techniques. The presence of vesicular structures on or near the surface are clearly seen, but this concentration is quickly attenuated as one examines (e.g., with sequential tape-stripping) the deeper SC layer [132]. The implication is that the niosomes have fused and mixed with the endogenous SC lipids at this point [133, 134]. Although some images of vesicular structures at even deeper regions of the SC have been published, it is impossible to say whether these really represent intact niosomes which have transported down from the skin surface, or whether there has been spontaneous regeneration of a vesicle as the degree of hydration of the SC increases.

1.9.3 Applications of niosomes in pharmaceutics and cosmetics

Drugs encapsulated in niosomes, when these vesicles fuse with the SC, may be subjected to enhanced skin penetration due to an altered thermodynamic activity gradient [133, 134], or to the action of the "released" nonionic surfactants on SC barrier function [134, 135]. Enoxacin, for example, was much better delivered from niosomes than either liposomes or when applied as a simple drug solution [133]. If niosomes are used on skin for which the barrier function is significantly less than that typical of intact skin, then even rather large compounds can be delivered. Thus, β-galactosidase and luciferase reporter genes have been successfully transported across rat pup skin from niosome formulations [136]. In addition, and similar to other vesicular carriers, niosomes have been shown capable of drug delivery to hair follicles, with successful results reported for the polypeptides, interferon-α and cyclosporine [137], as well as for minoxidil [138]. From a transdermal standpoint, estradiol has been examined and the nature of the surfactant used to prepare the niosomes clearly has an important effect [139, 140]. Finally, niosomes have been incorporated into cosmetics for several years, and used in a manner not particularly different from liposomes [141].

1.9.4 Summary

The behaviour and applications of niosomes parallel, in large part, those described for liposomes, although the level of activity, overall, is rather less.

1.10 Conclusions

Research into nano-sized delivery systems for topical "actives" has been the focus of considerable effort in the pharmaceutical and cosmetic industries for more than twenty years. The composition of different nanoparticles and their methods of preparation show some diversity. However, a size-reduction step with high pressure homogenization, sonication or extrusion is usually required to break some sort of microemulsion into nanoparticles. Depending on their intended use, the resulting carriers can be designed to facilitate or to retard the penetration of drugs and active ingredients into the epidermis or deep dermis and beyond. Rigid nanoparticles, such as liposomes, polymeric nanocapsules and SLN, improve

localization of the “active” in the upper skin layers, and may have an ability to form a skin surface film after topical application, thereby preventing water evaporation and increasing skin hydration. Transfersomes and ethosomes are variations of liposomes which incorporate “edge activators” or ethanol to confer the property of ultradeformability. It is claimed that this allows significantly enhanced transport of associated active species into the deeper skin layers via a variety of (not unambiguously proven) mechanisms, including an action as true “carriers”, SC lipid disruption, osmotic gradients, and so on.

There is also a general perception that just about all nano-carriers can “target” appendagal structures, like hair follicles. However, it seems likely that this is a non-specific, physical phenomenon and it remains to be seen whether these observations can be translated into a real, observable benefit.

In conclusion, despite a large and growing scientific and patent literature on the development and evaluation of nanoparticles for the delivery of topical agents, only a few commercial products containing such structures have appeared on the market. While the cosmetic industry has been quick to seize on these novel nanostructures, and to exploit their marketing and sensorial attributes, the pharmaceutical sector has been more reticent and has (currently) demanded quantifiable evidence that these inevitably more expensive products in terms of both materials and manufacture out-perform significantly more conventional formulations. For the moment, at least, this challenge has rarely been met.

References

1. A.C. Williams, *Structure and function of human skin*, in *Transdermal and topical drug delivery*, A.C. Williams, Editor. 2003, Pharmaceutical Press: London and Chicago. p. 1-25.
2. P.W. Wertz and D.T. Downing, *Stratum corneum: biological and biochemical considerations*, in *Transdermal drug delivery*, J. Hadgraft and R.H. Guy, Editors. 1989, Marcel Dekker, Inc.: New York. p. 1-22.
3. D.T. Downing, M.E. Stewart, P.W. Wertz, S.W. Colton, W. Abraham, and J.S. Strauss, *Skin lipids: an update.* J Invest Dermatol, 1987. **88**(3 Suppl): p. 2s-6s.
4. P.M. Elias, *Epidermal lipids, barrier function, and desquamation.* J Invest Dermatol, 1983. **80 Suppl**: p. 44s-49s.
5. R.O. Potts and R.H. Guy, *Predicting skin permeability.* Pharm Res, 1992. **9**(5): p. 663-9.
6. R.J. Scheuplein and I.H. Blank, *Permeability of the skin.* Physiol Rev, 1971. **51**(4): p. 702-47.
7. K.A. Walters, *Penetration enhancers and their use in transdermal therapeutic systems*, in *Transdermal drug delivery: developmental issues and research initiatives*, J. Hadgraft and R.H. Guy, Editors. 1989, Marcel Dekker: New York. p. 197-246.
8. A.C. Williams and B.W. Barry, *Penetration enhancers.* Adv Drug Deliv Rev, 2004. **56**(5): p. 603-18.
9. B.W. Barry, *Mode of action of penetration enhancers in human skin.* J Control Release, 1987. **6**(1): p. 85-97.
10. A.S. Breathnach, *Branched cells in the epidermis: an overview.* J Invest Dermatol, 1980. **75**(1): p. 6-11.
11. S. Benita, M.C. Martini, and M. Seiller, *Cosmetic applications of vesicular delivery systems*, in *Microencapsulation: methods and industrial applications*, S. Benita, Editor. 1996, Marcel Dekker Inc. : New York. p. 587-631
12. J. Gareiß, E. Hoff, and M. Ghyczy, *Phospholipide - Liposomen - Nanoemulsionen.* Parfümerie und Kosmetik, 1994. **75**(10): p. 652-659.
13. S. Amselem and D. Friedman, *Solid fat nanoemulsions as drug delivery vehicles*. United States Patent: 5576016. (1996)
14. R. Daniels. *Galenic principles of modern skin care products*. 2001 [cited; Available from: http://www.scf-online.com/english/25_e/galenic_25_e.htm.
15. O. Sonneville-Aubrun, J.T. Simonnet, and F. L'Alloret, *Nanoemulsions: a new vehicle for skincare products.* Adv Colloid Interface Sci, 2004. **108-109**: p. 145-9.
16. A. Forgiarini, J. Esquena, C. González, and C. Solans, *Formation of nano-emulsions by low-energy emulsification methods at constant temperature* Langmuir, 2001. **17**(7): p. 2076-2083.

17. M. Porras, C. Solans, C. González, A. Martinez, A. Guinart, and J.M. Gutierrez, *Studies of formation of W/O nano-emulsions.* Colloids and Surfaces A: Physicochem Eng Aspects, 2004. **249**(1-3): p. 115-118.

18. S. Baboota, F. Shakeel, A. Ahuja, J. Ali, and S. Shafiq, *Design, development and evaluation of novel nanoemulsion formulations for transdermal potential of celecoxib.* Acta Pharm, 2007. **57**(3): p. 315-32.

19. B.S. Kim, M. Won, K.M. Lee, and C.S. Kim, *In vitro permeation studies of nanoemulsions containing ketoprofen as a model drug.* Drug Deliv, 2008. **15**(7): p. 465-9.

20. F. Shakeel, S. Baboota, A. Ahuja, J. Ali, M. Aqil, and S. Shafiq, *Nanoemulsions as vehicles for transdermal delivery of aceclofenac.* AAPS PharmSciTech, 2007. **8**(4): p. E104.

21. A. Myc, T. Vanhecke, J.J. Landers, T. Hamouda, and J.R. Baker, Jr., *The fungicidal activity of novel nanoemulsion (X8W60PC) against clinically important yeast and filamentous fungi.* Mycopathologia, 2002. **155**(4): p. 195-201.

22. A. Ribier Deceased., J.T. Simonnet, and S. Legret, *Transparent nanoemulsion less than 100 NM based on fluid non-ionic amphiphilic lipids and use in cosmetic or in dermopharmaceuticals*. United States Patent: 5753241. (1998)

23. J.T. Simonnet, O. Sonneville, and S. Legret, *Nanoemulsion based on phosphoric acid fatty acid esters and its uses in the cosmetics, dermatological, pharmaceutical, and/or ophthalmological fields*. United States Patent: 6274150. (2001)

24. F. L'alloret, O. Aubrun-sonneville, and J.T. Simonnet, *Nanoemulsion containing nonionic polymers, and its uses*. United States Patent: 6998426. (2006)

25. E. Quemin, *Translucent nanoemulsion, production method, and uses thereof in the cosmetic, dermatological and/or ophthalmological fields*. United States Patent: 6902737. (2005)

26. C. Guiramand, *Oil-in-water emulsion containing fillers*. United States Patent: 20060057170. (2006)

27. B.H. Yoo, B.Y. Kang, M.H. Yeom, D.S. Sung, S.H. Han, H.K. Kim, and H.K. Ju, *Nanoemulsion comprising metabolites of ginseng saponin as an active component and a method for preparing the same, and a skin-care composition for anti-aging containing the same*. United States Patent: 20060216261. (2006)

28. D. Huglin, J.F. Roding, A.W. Supersaxo, and H.G. Weder, *Use of nanodispersions in cosmetic end formulations*. United States Patent: 20050191330. (2005)

29. H.G. Weder and M.A. Weder, *Cosmetic preparations*. United States Patent: 5997888. (1999)

30. E. Touitou, H.E. Junginger, N.D. Weiner, T. Nagai, and M. Mezei, *Liposomes as carriers for topical and transdermal delivery.* J Pharm Sci, 1994. **83**(9): p. 1189-203.

31. M. Brandl, *Liposomes as drug carriers: a technological approach.* Biotechnol Annu Rev, 2001. **7**: p. 59-85.

32. J.Y. Fang, *Nano- or submicron-sized liposomes as carriers for drug delivery.* Chang Gung Med

J, 2006. **29**(4): p. 358-62.

33. M. Mezei and V. Gulasekharam, *Liposomes--a selective drug delivery system for the topical route of administration. Lotion dosage form.* Life Sci, 1980. **26**(18): p. 1473-7.
34. M. Mezei and V. Gulasekharam, *Liposomes--a selective drug delivery system for the topical route of administration: gel dosage form.* J Pharm Pharmacol, 1982. **34**(7): p. 473-4.
35. M.H. Schmid and H.C. Korting, *Liposomes: a drug carrier system for topical treatment in dermatology.* Crit Rev Ther Drug Carrier Syst, 1994. **11**(2-3): p. 97-118.
36. M. Mezei, *Multiphase liposomal drug delivery system*. United States Patent: 4761288. (1988)
37. M. Mezei, *Administration of drugs with multiphase liposomal delivery system*. United States Patent: 4897269. (1990)
38. M. Mezei and A. Gesztes, *Liposomal local anesthetic and analgesic products*. United States Patent: 4937078. (1990)
39. A. Gesztes and M. Mezei, *Topical anesthesia of the skin by liposome-encapsulated tetracaine.* Anesth Analg, 1988. **67**(11): p. 1079-81.
40. M.J. Choi and H.I. Maibach, *Liposomes and niosomes as topical drug delivery systems.* Skin Pharmacol Physiol, 2005. **18**(5): p. 209-19.
41. V.M. Knepp, R.S. Hinz, F.C.J. Szoka, and R.H. Guy, *Controlled drug release from a novel liposomal delivery system. I. Investigation of transdermal potential.* J Control Release, 1988. **5**(3): p. 211-221.
42. E. Touitou, F. Levi-Schaffer, N. Dayan, F. Alhaique, and F. Riccieri, *Modulation of caffeine skin delivery by carrier design: liposomes versus permeation enhancers.* Int J Pharm, 1994. **103**(2): p. 131-136.
43. G. Betz, P. Nowbakht, R. Imboden, and G. Imanidis, *Heparin penetration into and permeation through human skin from aqueous and liposomal formulations in vitro.* Int J Pharm, 2001. **228**(1-2): p. 147-59.
44. W. Abraham and D.T. Downing, *Interaction between corneocytes and stratum corneum lipid liposomes in vitro.* Biochim Biophys Acta, 1990. **1021**(2): p. 119-25.
45. D.D. Lasic, *Applications of liposomes*, in *Handbook of Biological Physics: Structure and Dynamics of Membranes*, R. Lipowsky and E. Sackmann, Editors. 1995, Elsevier Science B. V. : Amsterdam. p. 491-519.
46. U. Gross, J. Roding, K. Stanzl, and L. Zastrow, *Phospholipid-and fluorocarbon-containing cosmetic*. United States Patent: 5643601. (1997)
47. http://www.nanotechproject.org/inventories/consumer/browse/products/5145/. 2008 [cited 2008/09/28].
48. http://www.jafra.com/en/Prod_RoyalJelly_en.html. 2008 [cited 2008/09/28].
49. G. Cevc, *Transfersomes, liposomes and other lipid suspensions on the skin: permeation enhancement, vesicle penetration, and transdermal drug delivery.* Crit Rev Ther Drug Carrier

Syst, 1996. **13**(3-4): p. 257-388.

50. H.A. Benson, *Transdermal drug delivery: penetration enhancement techniques.* Curr Drug Deliv, 2005. **2**(1): p. 23-33.
51. B.A. van den Bergh, P.W. Wertz, H.E. Junginger, and J.A. Bouwstra, *Elasticity of vesicles assessed by electron spin resonance, electron microscopy and extrusion measurements.* Int J Pharm, 2001. **217**(1-2): p. 13-24.
52. H.C. Korting, H. Zienicki, M. Schaefer-Korting, and O. Braun-Falco, *Liposome encapsulation improves efficacy of betamethasone diproprionate in atopic eczema but not in psoriasis vulgaris.* Eur J Clin Pharmacol, 1990. **39**: p. 349-351.
53. G. Cevc and G. Blume, *Lipid vesicles penetrate into intact skin owing to the transdermal osmotic gradients and hydration force.* Biochim Biophys Acta, 1992. **1104**(1): p. 226-32.
54. G. Cevc, *Material transport across permeability barriers by means of lipid vesicles*, in *Handbook of Biological Physics*, R. Lipowsky and E. Sackmann, Editors. 1995, Elsevier: Amsterdam. p. 465-490.
55. A. Schatzlein and G. Cevc, *Non-uniform cellular packing of the stratum corneum and permeability barrier function of intact skin: a high-resolution confocal laser scanning microscopy study using highly deformable vesicles (Transfersomes).* Br J Dermatol, 1998. **138**(4): p. 583-92.
56. G. Cevc, *Lipid vesicles and other colloids as drug carriers on the skin.* Adv Drug Deliv Rev, 2004. **56**(5): p. 675-711.
57. G. Cevc and G. Blume, *Biological activity and characteristics of triamcinolone-acetonide formulated with the self-regulating drug carriers, Transfersomes.* Biochim Biophys Acta, 2003. **1614**(2): p. 156-64.
58. G. Cevc and G. Blume, *New, highly efficient formulation of diclofenac for the topical, transdermal administration in ultradeformable drug carriers, Transfersomes.* Biochim Biophys Acta, 2001. **1514**(2): p. 191-205.
59. G.M. El Maghraby, A.C. Williams, and B.W. Barry, *Skin delivery of oestradiol from deformable and traditional liposomes: mechanistic studies.* J Pharm Pharmacol, 1999. **51**(10): p. 1123-34.
60. G.M. El Maghraby, A.C. Williams, and B.W. Barry, *Oestradiol skin delivery from ultradeformable liposomes: refinement of surfactant concentration.* Int J Pharm, 2000. **196**(1): p. 63-74.
61. G.M. El Maghraby, A.C. Williams, and B.W. Barry, *Skin delivery of oestradiol from lipid vesicles: importance of liposome structure.* Int J Pharm, 2000. **204**(1-2): p. 159-69.
62. J. Guo, Q. Ping, G. Sun, and C. Jiao, *Lecithin vesicular carriers for transdermal delivery of cyclosporin A.* Int J Pharm, 2000. **194**(2): p. 201-7.
63. G. Cevc, D. Gebauer, J. Stieber, A. Schatzlein, and G. Blume, *Ultraflexible vesicles, Transfersomes, have an extremely low pore penetration resistance and transport therapeutic*

amounts of insulin across the intact mammalian skin. Biochim Biophys Acta, 1998. **1368**(2): p. 201-15.

64. G. Cevc, A. Schatzlein, and G. Blume, *Transdermal drug carriers: Basic properties, optimization and transfer efficiency in the case of epicutaneously applied peptides.* J Control Release, 1995. **36**(1-2): p. 3-16.
65. R. Alvarez-Roman, G. Barre, R.H. Guy, and H. Fessi, *Biodegradable polymer nanocapsules containing a sunscreen agent: preparation and photoprotection.* Eur J Pharm Biopharm, 2001. **52**(2): p. 191-5.
66. E.S. Nuwayser, *Method of transdermal drug delivery*. United States Patent: 4624665. (1986)
67. J. Luengo, B. Weiss, M. Schneider, A. Ehlers, F. Stracke, K. Konig, K.H. Kostka, C.M. Lehr, and U.F. Schaefer, *Influence of nanoencapsulation on human skin transport of flufenamic acid.* Skin Pharmacol Physiol, 2006. **19**(4): p. 190-7.
68. M. Simeonova, R. Velichkova, G. Ivanova, V. Enchev, and I. Abrahams, *Poly(butylcyanoacrylate) nanoparticles for topical delivery of 5-fluorouracil.* Int J Pharm, 2003. **263**(1-2): p. 133-40.
69. B. Muller and J. Kreuter, *Enhanced transport of nanoparticle associated drugs through natural and artificial membranes--a general phenomenon?* Int J Pharm, 1999. **178**(1): p. 23-32.
70. M.J. Cappel and J. Kreuter, *Effect of nanoparticles on transdermal drug delivery.* J Microencapsul, 1991. **8**(3): p. 369-74.
71. S. Miyazaki, A. Takahashi, W. Kubo, J. Bachynsky, and R. Loebenberg, *Poly n-butylcyanoacrylate (PNBCA) nanocapsules as a carrier for NSAIDs: in vitro release and in vivo skin penetration.* J Pharm Pharm Sci, 2003. **6**(2): p. 238-45.
72. R. Diaz-Torres, V.M. Castano, A. Ganem-Quintanar, D. Quintanar-Guerrero, and S. Rodriguez-Romo, *Oscillations in the kinetics of ethylcyanoacrylate nanoparticles intended as skin drug carriers.* Nanotechnology, 2005. **16**(11): p. 2612-2618.
73. J.T. Simonnet, P. Richart, and B. Biatry, *Nanocapsules based on poly(alkylene adipate), process for their preparation and cosmetic or dermatological compositions containing them*. United States Patent: 6565886. (2003)
74. B. Luppi, T. Cerchiara, F. Bigucci, R. Basile, and V. Zecchi, *Polymeric nanoparticles composed of fatty acids and polyvinylalcohol for topical application of sunscreens.* J Pharm Pharmacol, 2004. **56**(3): p. 407-11.
75. B.I. Olvera-Martinez, J. Cazares-Delgadillo, S.B. Calderilla-Fajardo, R. Villalobos-Garcia, A. Ganem-Quintanar, and D. Quintanar-Guerrero, *Preparation of polymeric nanocapsules containing octyl methoxycinnamate by the emulsification-diffusion technique: penetration across the stratum corneum.* J Pharm Sci, 2005. **94**(7): p. 1552-9.
76. J. Shim, H. Seok Kang, W.S. Park, S.H. Han, J. Kim, and I.S. Chang, *Transdermal delivery of mixnoxidil with block copolymer nanoparticles.* J Control Release, 2004. **97**(3): p. 477-84.

77. P. Couvreur, G. Barratt, E. Fattal, P. Legrand, and C. Vauthier, *Nanocapsule technology: a review.* Crit Rev Ther Drug Carrier Syst, 2002. **19**(2): p. 99-134.

78. H. Fessi, F. Puisieux, J.P. Devissaguet, N. Ammoury, and S. Benita, *Nanocapsule formation by interfacial polymer deposition following solvent displacement.* Int J Pharm, 1989. **55**(1): p. R1-R4.

79. F. Tiarks, K. Landfester, and M. Antonietti, *Preparation of polymeric nanocapsules by miniemulsion polymerization.* Langmuir, 2001. **17**(3): p. 908-918.

80. G. Lambert, E. Fattal, H. Pinto-Alphandary, A. Gulik, and P. Couvreur, *Polyisobutylcyanoacrylate nanocapsules containing an aqueous core as a novel colloidal carrier for the delivery of oligonucleotides.* Pharm Res, 2000. **17**(6): p. 707-14.

81. R.S. Underhill, *Oil-filled nanocapsules*, in *Dekker Encyclopedia of Nanoscience and Nanotechnology*, J.A. Schwarz, C.I. Contescu, and K. Putyera, Editors. 2004, Marcel Dekker, Inc. : New York. p. 2739 - 2747.

82. H. Lboutounne, J.F. Chaulet, C. Ploton, F. Falson, and F. Pirot, *Sustained ex vivo skin antiseptic activity of chlorhexidine in poly(epsilon-caprolactone) nanocapsule encapsulated form and as a digluconate.* J Control Release, 2002. **82**(2-3): p. 319-34.

83. I.P. Kaur and R. Agrawal, *Nanotechnology: a new paradigm in cosmeceuticals.* Recent Pat. Drug Delivery Formulation, 2007. **1**(2): p. 171-182.

84. A.M. De Campos, A. Sanchez, and M.J. Alonso, *Chitosan nanoparticles: a new vehicle for the improvement of the delivery of drugs to the ocular surface. Application to cyclosporin A.* Int J Pharm, 2001. **224**(1-2): p. 159-68.

85. C. Schwarz, W. Mehnert, J.S. Lucks, and R.H. Müller, *Solid lipid nanoparticles (SLN) for controlled drug delivery. I. Production, characterization and sterilization.* J Control Release, 1994. **30**(1): p. 83-96.

86. R.H. Muller, K. Mader, and S. Gohla, *Solid lipid nanoparticles (SLN) for controlled drug delivery - a review of the state of the art.* Eur J Pharm Biopharm, 2000. **50**(1): p. 161-77.

87. M. Schafer-Korting, W. Mehnert, and H.C. Korting, *Lipid nanoparticles for improved topical application of drugs for skin diseases.* Adv Drug Deliv Rev, 2007. **59**(6): p. 427-43.

88. R.H. Muller, M. Radtke, and S.A. Wissing, *Solid lipid nanoparticles (SLN) and nanostructured lipid carriers (NLC) in cosmetic and dermatological preparations.* Adv Drug Deliv Rev, 2002. **54 Suppl 1**: p. S131-55.

89. W. Mehnert and K. Mader, *Solid lipid nanoparticles: production, characterization and applications.* Adv Drug Deliv Rev, 2001. **47**(2-3): p. 165-96.

90. C. Santos Maia, W. Mehnert, M. Schaller, H.C. Korting, A. Gysler, A. Haberland, and M. Schafer-Korting, *Drug targeting by solid lipid nanoparticles for dermal use.* J Drug Target, 2002. **10**(6): p. 489-95.

91. H. Bunjes and M.H. Koch, *Saturated phospholipids promote crystallization but slow down*

polymorphic transitions in triglyceride nanoparticles. J Control Release, 2005. **107**(2): p. 229-43.

92. M.R. Gasco, *Solid lipid nanospheres from warm micro-emulsions.* Pharm Technol Eur, 1997. **9**(11): p. 52-58.
93. B. Sjöström and B. Bergenståhl, *Preparation of submicron drug particles in lecithin-stabilized o/w emulsions. I. Model studies of the precipitation of cholesteryl acetate.* Int J Pharm, 1993. **88**(1-3): p. 53-62.
94. B. Siekmann and K. Westesen, *Investigations on solid lipid nanoparticles prepared by precipitation in o/w emulsions.* Eur J Pharm Biopharm, 1996. **43**(2): p. 104-109.
95. Z. Mei, H. Chen, T. Weng, Y. Yang, and X. Yang, *Solid lipid nanoparticle and microemulsion for topical delivery of triptolide.* Eur J Pharm Biopharm, 2003. **56**(2): p. 189-96.
96. M. Kalariya, B.K. Padhi, M. Chougule, and A. Misra, *Clobetasol propionate solid lipid nanoparticles cream for effective treatment of eczema: formulation and clinical implications.* Indian J Exp Biol, 2005. **43**(3): p. 233-40.
97. C.S. Maia, W. Mehnert, and M. Schafer-Korting, *Solid lipid nanoparticles as drug carriers for topical glucocorticoids.* Int J Pharm, 2000. **196**(2): p. 165-7.
98. U. Munster, C. Nakamura, A. Haberland, K. Jores, W. Mehnert, S. Rummel, M. Schaller, H.C. Korting, C. Zouboulis Ch, U. Blume-Peytavi, and M. Schafer-Korting, *RU 58841-myristate--prodrug development for topical treatment of acne and androgenetic alopecia.* Pharmazie, 2005. **60**(1): p. 8-12.
99. R.H. Muller and A. Dingler, *The next generation after the liposomes: solid lipid nano particles (SLN^{TM}, Lipopearls^{TM}) as dermal carrier in cosmetics.* Eurocosmetics, 1998. **7/8**: p. 19-26.
100. S.A. Wissing and R.H. Muller, *A novel sunscreen system based on tocopherol acetate incorporated into solid lipid nanoparticles.* Int J Cosmet Sci, 2001. **23**(4): p. 233-43.
101. T. de Vringer and H.A.G. de Ronde, *Preparation and structure of a water-in-oil cream containing lipid nanoparticles.* J Pharm Sci, 1995. **84**(4): p. 466-472.
102. H. Zhai and H.I. Maibach, *Effects of skin occlusion on percutaneous absorption: an overview.* Skin Pharmacol Appl Skin Physiol, 2001. **14**(1): p. 1-10.
103. S.A. Wissing and R.H. Muller, *The influence of solid lipid nanoparticles on skin hydration and viscoelasticity--in vivo study.* Eur J Pharm Biopharm, 2003. **56**(1): p. 67-72.
104. S.A. Wissing and R.H. Muller, *Cosmetic applications for solid lipid nanoparticles (SLN).* Int J Pharm, 2003. **254**(1): p. 65-8.
105. S.A. Wissing and R.H. Muller, *Solid lipid nanoparticles as carrier for sunscreens: in vitro release and in vivo skin penetration.* J Control Release, 2002. **81**(3): p. 225-33.
106. S. Wissing and R. Muller, *The influence of the crystallinity of lipid nanoparticles on their occlusive properties.* Int J Pharm, 2002. **242**(1-2): p. 377-9.
107. C. Song and S. Liu, *A new healthy sunscreen system for human: Solid lipid nannoparticles as*

carrier for 3,4,5-trimethoxybenzoylchitin and the improvement by adding Vitamin E. Int J Biol Macromol, 2005. **36**(1-2): p. 116-119.

108. S.A. Wissing and R.H. Muller, *Solid lipid nanoparticles (SLN)--a novel carrier for UV blockers.* Pharmazie, 2001. **56**(10): p. 783-6.

109. V. Jenning and S.H. Gohla, *Encapsulation of retinoids in solid lipid nanoparticles (SLN).* J Microencapsul, 2001. **18**(2): p. 149-58.

110. V. Jenning, A. Gysler, M. Schafer-Korting, and S.H. Gohla, *Vitamin A loaded solid lipid nanoparticles for topical use: occlusive properties and drug targeting to the upper skin.* Eur J Pharm Biopharm, 2000. **49**(3): p. 211-8.

111. P.V. Pople and K.K. Singh, *Development and evaluation of topical formulation containing solid lipid nanoparticles of vitamin A.* AAPS PharmSciTech, 2006. **7**(4): p. 91.

112. V. Jenning, M. Schafer-Korting, and S. Gohla, *Vitamin A-loaded solid lipid nanoparticles for topical use: drug release properties.* J Control Release, 2000. **66**(2-3): p. 115-26.

113. R.H. Muller and A. Dingler, *Feste Lipid-Nanopartikel (Lipopearls™) als neuartiger Carrier für kosmetische und dermatologische Wirkstoffe.* PZ Wiss, 1998. **49**: p. 11-15.

114. A. Dingler, R.P. Blum, H. Niehus, R.H. Muller, and S. Gohla, *Solid lipid nanoparticles (SLN^{TM}/Lipopearls^{TM}) a pharmaceutical and cosmetic carrier for the application of vitamin E in dermal products.* J Microencapsul, 1999. **16**(6): p. 751-767.

115. E. Touitou, N. Dayan, L. Bergelson, B. Godin, and M. Eliaz, *Ethosomes - novel vesicular carriers for enhanced delivery: characterization and skin penetration properties.* J Control Release, 2000. **65**(3): p. 403-18.

116. B. Godin and E. Touitou, *Ethosomes: new prospects in transdermal delivery.* Crit Rev Ther Drug Carrier Syst, 2003. **20**(1): p. 63-102.

117. E. Touitou, *Compositions for applying active substances to or through the skin*. United States Patent: 5540934. (1996)

118. E. Touitou, *Composition for applying active substances to or through the skin*. United States Patent: 5716638. (1998)

119. N. Dayan and E. Touitou, *Carriers for skin delivery of trihexyphenidyl HCl: ethosomes vs. liposomes.* Biomaterials, 2000. **21**(18): p. 1879-85.

120. B. Godin and E. Touitou, *Erythromycin ethosomal systems: physicochemical characterization and enhanced antibacterial activity.* Curr Drug Deliv, 2005. **2**(3): p. 269-75.

121. B. Godin and E. Touitou, *Mechanism of bacitracin permeation enhancement through the skin and cellular membranes from an ethosomal carrier.* J Control Release, 2004. **94**(2-3): p. 365-79.

122. E. Touitou, B. Godin, N. Dayan, C. Weiss, A. Piliponsky, and F. Levi-Schaffer, *Intracellular delivery mediated by an ethosomal carrier.* Biomaterials, 2001. **22**(22): p. 3053-9.

123. B. Godin, E. Touitou, E. Rubinstein, A. Athamna, and M. Athamna, *A new approach for*

treatment of deep skin infections by an ethosomal antibiotic preparation: an in vivo study. J Antimicrob Chemother, 2005. **55**(6): p. 989-94.

124. D. Paolino, G. Lucania, D. Mardente, F. Alhaique, and M. Fresta, *Ethosomes for skin delivery of ammonium glycyrrhizinate: in vitro percutaneous permeation through human skin and in vivo anti-inflammatory activity on human volunteers.* J Control Release, 2005. **106**(1-2): p. 99-110.
125. D. Ainbinder and E. Touitou, *Testosterone ethosomes for enhanced transdermal delivery.* Drug Deliv, 2005. **12**(5): p. 297-303.
126. E. Horwitz, S. Pisanty, R. Czerninski, M. Helser, E. Eliav, and E. Touitou, *A clinical evaluation of a novel liposomal carrier for acyclovir in the topical treatment of recurrent herpes labialis.* Oral Surg Oral Med Oral Pathol Oral Radiol Endod, 1999. **87**(6): p. 700-5.
127. I.F. Uchegbu and S.P. Vyas, *Non-ionic surfactant based vesicles (niosomes) in drug delivery* Int J Pharm, 1998. **172**(1-2): p. 33-70.
128. T. Yoshioka, B. Sternberg, and A.T. Florence, *Preparation and properties of vesicles (niosomes) of sorbitan monoesters (Span 20, 40, 60 and 80) and a sorbitan triester (Span 85).* Int J Pharm, 1994. **105**(1): p. 1-6.
129. P. Arunothayanun, M.S. Bernard, D.Q. Craig, I.F. Uchegbu, and A.T. Florence, *The effect of processing variables on the physical characteristics of non-ionic surfactant vesicles (niosomes) formed from a hexadecyl diglycerol ether.* Int J Pharm, 2000. **201**(1): p. 7-14.
130. I.F. Uchegbu and A.T. Florence, *Non-ionic surfactant vesicles (niosomes): Physical and pharmaceutical chemistry.* Adv Colloid Interface Sci, 1995. **58**(1): p. 1-55.
131. T.P. Assadullahi, R.C. Hider, and A.J. McAuley, *Liposome formation from synthetic polyhydroxyl lipids.* Biochim Biophys Acta, 1991. **1083**(3): p. 271-6.
132. B.A. van den Bergh, J. Vroom, H. Gerritsen, H.E. Junginger, and J.A. Bouwstra, *Interactions of elastic and rigid vesicles with human skin in vitro: electron microscopy and two-photon excitation microscopy.* Biochim Biophys Acta, 1999. **1461**(1): p. 155-73.
133. J.Y. Fang, C.T. Hong, W.T. Chiu, and Y.Y. Wang, *Effect of liposomes and niosomes on skin permeation of enoxacin.* Int J Pharm, 2001. **219**(1-2): p. 61-72.
134. H. Schreier and J.A. Bouwstra, *Liposomes and niosomes as topical drug carriers: dermal and transdermal drug delivery.* J Control Release, 1994. **30**(1): p. 1-15.
135. S.C. Jayaraman, C. Ramachandran, and N. Weiner, *Topical delivery of erythromycin from various formulations: an in vivo hairless mouse study.* J Pharm Sci, 1996. **85**(10): p. 1082-4.
136. N. Raghavachari and W.E. Fahl, *Targeted gene delivery to skin cells in vivo: a comparative study of liposomes and polymers as delivery vehicles.* J Pharm Sci, 2002. **91**(3): p. 615-22.
137. S.M. Niemiec, C. Ramachandran, and N. Weiner, *Influence of nonionic liposomal composition on topical delivery of peptide drugs into pilosebaceous units: an in vivo study using the hamster ear model.* Pharm Res, 1995. **12**(8): p. 1184-8.
138. S.N. Ciotti and N. Weiner, *Follicular liposomal delivery systems.* J Liposome Res, 2002.

12(1-2): p. 143-8.

139. J.Y. Fang, S.Y. Yu, P.C. Wu, Y.B. Huang, and Y.H. Tsai, *In vitro skin permeation of estradiol from various proniosome formulations.* Int J Pharm, 2001. **215**(1-2): p. 91-9.

140. D. Vanhal, A. Vanrensen, T. Devringer, H.E. Junginger, and J.A. Bouwstra, *Diffusion of estradiol from non-ionic surfactant vesicles through human stratum corneum in vitro.* STP Pharm Sci, 1996. **6**(1): p. 72-78.

141. S. Nacht, *Encapsulation and other topical delivery systems.* Cosmet Toilet, 1995. **110**(9): p. 25-30.

CHAPTER 2

DRUG DELIVERY TO THE SKIN FROM POLYMETRIC NANOPARTICLE AND MESOPARTICLE FORMULATIONS: INFLUENCE OF POLYMER HYDROPHOBICITY AND PARTICLE SIZE

Drug delivery to the skin from polymeric nanoparticle and mesoparticle formulations: influence of polymer hydrophobicity and particle size

Xiao Wu[1], Bruno Biatry[2], Colette Cazeneuve[2], and Richard H. Guy[1]

[1]Department of Pharmacy and Pharmacology, University of Bath, Claverton Down, Bath, BA2 7AY, U.K.

[2]L'Oréal Research, France

Abstract

The influence of particle size and polymer properties on the topical delivery of a lipophilic "active" species from polymeric nanoparticles and mesoparticles was investigated. The formulations were prepared using a mini-emulsion/solvent evaporation technique and the fluorophore, Nile Red (NR), acting as a model for a lipophilic drug, was associated with the polymeric vectors. Three poly-(ε-caprolactone) (CAPA) formulations, with mean diameters of 90 nm, 260 nm and 630 nm, were examined to assess the impact of particle size. Three other NP formulations (diameter ~100 nm), based on cellulose acetate butyrate (CAB), CAPA and polystyrene (PS) were studied to address the role of polymer hydrophobicity. The association of NR with the different particles was measured by ultracentrifugation. *In vitro* skin permeation experiments were performed for 6 hours, and confocal microscopy and tape-stripping of the stratum corneum (SC) were used to evaluate the disposition of NR in the skin. The SC concentration profiles of NR were influenced by nanoparticle size, with delivery being greater from the larger vectors, probably due to the overall smaller surface area of these particles enhancing the "leaving tendency" of the lipophilic "active". The skin uptake of NR from PS, CAPA and CAB nanoparticles decreased, in absolute terms, with decreasing polymer hydrophobicity (PS>CAPA>CAB). However, given the degree to which NR was associated with the different particles, the relative "%payload released" actually increased as the polymer

hydrophobicity decreased (in a manner exactly as expected for a lipophilic moiety like NR). Confocal microscopy revealed that NR released from nanoparticles accumulated in, and penetrated via, the lipid domains between the corneocytes of the SC; furthermore, there was evidence that the particles themselves showed affinity for, and concentration at, the openings of hair follicles.

Keywords: skin; stratum corneum; nanoparticle; Nile Red; particle size; tape-stripping; laser scanning confocal microscopy (LSCM).

2.1 Introduction

The development of nanotechnology, and the increasing presence of nanoparticles (and other nano-structures) in pharmaceutical and cosmetic formulations designed for application to the skin [1-7], makes it essential to develop techniques to assess the local disposition of these materials. Although the principal function of the skin is to provide a protective barrier (a job that it performs remarkably well) [8-10], it is nevertheless important to determine whether nanostructures can find their way into and/or across this tissue, or whether they show a particular affinity, for example, to specific skin components such as hairs and the follicles from which hairs emerge.

A number of fundamental questions must therefore be addressed. For example, what happens to nanoparticles when they contact the skin? What is the disposition of the nanoparticles, and what is their residence time? It is necessary, therefore, to visualize nanoparticle disposition on and within the skin, to explore whether penetration pathways exist, and to examine the "substantivity" of the nanostructures to the membrane. Further, is there evidence that nanoparticles can cross the skin's barrier, the stratum corneum (SC)? Do nanoparticles show affinity for specific skin structures, e.g., hair follicles? Microscopic techniques and adhesive tape-stripping procedures can be used to address these issues qualitatively and quantitatively. Finally, to what extent does nanoparticle disposition depend on the properties of the particles (such as size and composition)? What happens to "active" species (e.g., drugs, cosmetic actives) which are associated with nanoparticles?

This paper addresses these latter issues, and explores the manner in which nanoparticle size and

polymer hydrophobicity influence the cutaneous disposition of a model, lipophilic compound associated with various "vectors". Uptake into the skin's outermost layer, the SC, has been determined by a validated and quantitative adhesive tape-stripping methodology and has been visualised by confocal microscopy.

2.2 Materials and methods

2.2.1 Materials

2.2.1.1 Chemicals

Poly-(ε-caprolactone) (CAPA 6100, Solvay, Paris, France), cellulose acetate butyrate (CAB-551-0.01, Eastman, Capelle aan den IJssel, the Netherlands), polystyrene (18544, PolySciences, Eppelheim, Germany), phenonip (Nipa, Clariant, Charlotte, NC, USA), pluronic F127 (Sigma-Aldrich, CHEMIE GmbH, Steinhelm, Germany), Nile Red (Analytical grade, Sigma-Aldrich, St. Louis, MO, USA), dichloromethane (99% Acros Organics, Loughborough, UK), acetonitrile (HPLC grade, Fisher Scientific Corporation, Loughborough, UK), ruthenium tetroxide (Taab Laboratories, Aldermaston, England), uranyl acetate (Agar Scientific Ltd. Stansted, UK).

2.2.1.2 Skin tissues

Full thickness porcine skin was obtained from a local slaughterhouse. The skin was cleaned under cold running water. The subcutaneous fat was removed from the skin with a scalpel. The remaining tissue was then dermatomed to a thickness of ~750 μm and was stored frozen at -20°C for up to a maximum of one month before use.

2.2.2 Methods

2.2.2.1 Nano/mesoparticle preparation

Nano/mesoparticles were prepared in the presence of the model "active", Nile Red (NR), a lipophilic fluorophore, by a mini-emulsion/solvent evaporation method [11]. 1.25 g polymer, 0.3 g dimethicone copolyol and 1.25 mg Nile Red were dissolved in 17 ml dichloromethane, to form the organic phase. 0.125 g Pluronic F127 was dissolved in 25 ml water by vigorously stirring the mixture at 40°C for 30 minutes to provide the aqueous phase. The phases were then quickly mixed and dispersed under ultrasound (Ultra turrax® T25), 4°C. The resulting nanosphere pre-emulsion had a milky appearance with pink opalescence. Ultrasound at maximal power intensity for 5 minutes was then used to break the pre-emulsion into fine nanoparticles. Finally, the organic solvent (dichloromethane) and some of the water present were removed by rotary evaporation. Phenonip was added into the emulsion as a preservative.

2.2.2.2 Size distribution measurement

The mean size and polydispersity (index from 0 to 1) of the NP were measured with dynamic light scattering (DLS BI90Plus, Brookhaven Instruments Corporation, NY, USA). Measurements were made in triplicate for all prepared batches. DLS is an instrument which determines the size distribution of particles by measuring dynamic fluctuations of light scattering intensity caused by the Brownian motion of the particle. This technique yields a hydrodynamic diameter that is calculated via the Stokes-Einstein equation from the aforementioned measurements. The DLS measures the average hydrodynamic diameter of the particles, the peak values in the hydrodynamic diameter distribution and the polydispersity index (PI) that describes the width of the particle size distribution. The PI scale ranges from 0 to 1, with 0 meaning that the size approaches a monoparticle size distribution and 1 indicating large variations in the particle size distribution.

2.2.2.3 Assessment of Nile Red incorporation and HPLC assay

To determine the degree of Nile Red incorporation into the nanoparticles, the formulations were filtered (0.45 μm nylon filters, Whatman, Japan) and then subjected to ultracentrifugation

at 17000 g for 3 h at 20°C. The supernatant was kept for analysis of NR. The sediment was washed with distilled water to remove surfactant and again centrifuged 17000 g for 3 h. The resulting pellet was freeze-dried, and then dissolved in dichloromethane. Finally, Nile Red in this organic solvent was measured by HPLC (Dionex, Sunnyvale, CA, USA) with fluorescence detection at 559 nm and 630 nm for excitation and emission wavelengths, respectively. A Hypersil BDS C18 (5 μm) 250×4.6 mm column, was used and the mobile phase was dichloromethane pumped at a flow rate of 1 ml/min at 25°C. Each injection was 200 μl of solution. The Nile Red retention time was 5.6 minutes. Nile Red in the supernatant was also measured by HPLC using a mobile phase comprising acetonitrile-water (80:20). The column, injection volume, temperature were as above. The retention time in this case was 12.1 minutes.

2.2.2.4 *In vitro* skin permeation

Each skin sample used in these experiments represented one-half of a larger piece of tissue. The other portion was reserved for a determination of the SC thickness as described below.

Visible hairs on the skin were trimmed as closely as possible to the surface. Skin permeation experiments were performed in vertical Franz diffusion cells thermostatted at 37°C. The excised tissue was clamped between the donor and receptor compartments exposing a diffusion area of 3.8 cm^2. The receptor phase was physiological buffer (pH = 7.4); the donor compartment held 1 ml of the NP formulation and was covered with Parafilm. After an application lasting 6 hrs, the cell was dismantled, and the skin was immediately either examined by confocal microscopy or tape-stripped to determine the NR concentration profile across the SC.

2.2.2.5 SC tape-stripping

A validated tape-stripping procedure was used to assess the depth of NR penetration into the SC and recover NR from the treated skin. About 20 pieces of 2.7×2.7 cm square tapes were prepared using transparent Scotch® No.845 Book Tapes (3M Media, Broken, Germany). To

delimit a fixed area for tape stripping, a 5×5 cm square mask was prepared with a cut central aperture of 2 cm in diameter. A strip of adhesive tape was pressed firmly onto the skin surface, and then removed in a single movement. The direction of stripping was changed with each tape to ensure a more uniform removal of the SC with fewer tape-strips. Before and after each tape-strip, transepidermal water loss (TEWL) across the skin was measured with an Aquaflux device (Biox Systems Ltd., London, UK) to provide an idea of when most of the SC had been removed and to the end of the tape-stripping process. This was considered appropriate when TEWL reached 80 $g^{-1}m^{-2}h$. The tapes were weighed before and after stripping to determine the mass of SC removed. As the density of the tissue is ~1 g/cm^3 [12, 13], the volume of SC removed by each strip is known assuming uniform coverage of SC on the tape-strip [12]. Then, given that the area stripped is kept at known, constant value, the thickness of SC removed as tape-stripping proceeds can be found.

NR was extracted from the SC on the adhesive tapes by immersion in acetonitrile and shaking for at least 12 hrs. The extract was filtered (Whatman PTFE filter 0.45μm) into HPLC vials and analysed. The mobile phase was 80:20 v/v acetonitrile and water. All other HPLC conditions were as stated above. The limits of detection and quantification were 0.34 ng/ml and 1.16 ng/ml, respectively.

2.2.2.6 SC thickness determination

To calculate the total thickness of the SC, the same tape-stripping procedure was performed on the second of the skin sample with measurements of TEWL after each tape-strip [12]. The amount of SC removed on each tape was again determined gravimetrically and converted into a SC thickness removed on each strip. It was then possible to calculate the total thickness of the SC from the x-intercept of a graph of $TEWL^{-1}$ versus the cumulative thickness of SC removed [12]. Knowing the SC thickness of each skin used in the NR uptake experiments made it possible to express all concentration profiles of the “active” as a common function of the relative position (depth) into the SC, greatly facilitating objective comparison of the results [14, 15].

2.2.2.7 Laser scanning confocal microscopy (LSCM)

The treated skin was cleaned carefully with physiological buffer and dried with tissue. The skin was examined using a LSM 510 Invert Laser Scanning Microscope (Carl Zeiss, Jena, Germany). The system was equipped with both an argon laser (excitation line at 488 nm) and a HeNe laser (excitation line at 543 nm). A Plan-Neofluar 10×/0.3 objective, an EC Plan-Neofluar 40×/1.30 oil DIC M27 objective and a Plan-Apochromat 63×/1.40 oil DIC M27 objective were used. Confocal images were obtained in the plane parallel to the sample surface (xy-mode), or in the plane perpendicular (optical sectioning z-stack mode).

2.3 Results and discussion

2.3.1 Nile Red association with nano/mesoparticles

The quantities of NR incorporated into the particles, together with information on their size and polydispersities are summarized in Table 2.1. Uptake into the nano/mesoparticles made from CAPA was quite constant (46-49%). More NR was taken up into the hydrophobic PS particles (~77%), less into the more hydrophilic CAB formulation (~24%). A relatively constant amount of Nile Red was recovered in the supernatant for all nanoparticles, and it is inferred that the remaining fraction of the dye was associated with surfactant micelles.

Table 2.1: Properties of nano/mesoparticle formulations examined.

Nanoparticle formulation	Average diameter (nm)	Polydispersity Index	% Nile Red associated	% Nile Red in supernatant
CAPA NP I	90	0.172	46.3 ± 1.1	5.8 ± 0.2
CAPA NP II	260	0.108	48.0 ± 1.6	5.8 ± 0.4
CAPA NP III	630	0.116	48.6 ± 0.8	5.8 ± 0.3
PS	156	0.098	76.9 ± 2.0	5.8 ± 0.4
CAPA	148	0.133	48.6 ± 0.5	5.8 ± 0.3
CAB	93	0.125	23.9 ± 1.5	5.8 ± 0.4

2.3.2 SC thickness determination

Figure 2.1 shows typical results from the experiments conducted to determine SC thickness of the skin samples used in the NR uptake measurements. The variability between different skins is clear, and it was generally observed that SC on the abdomen of the pig was thinner than that on the dorsal surface (6.9 ± 0.8 μm versus 10.2 ± 1.7 μm, respectively, for the examples in Figure 2.1 (mean ± SD, n=3)). These results emphasize the value of the determination of SC thickness when the disposition of an "active" across the barrier is to be evaluated, as it means that all concentrations can be expressed on a common scale of SC penetration depth normalized by the total membrane width (see below).

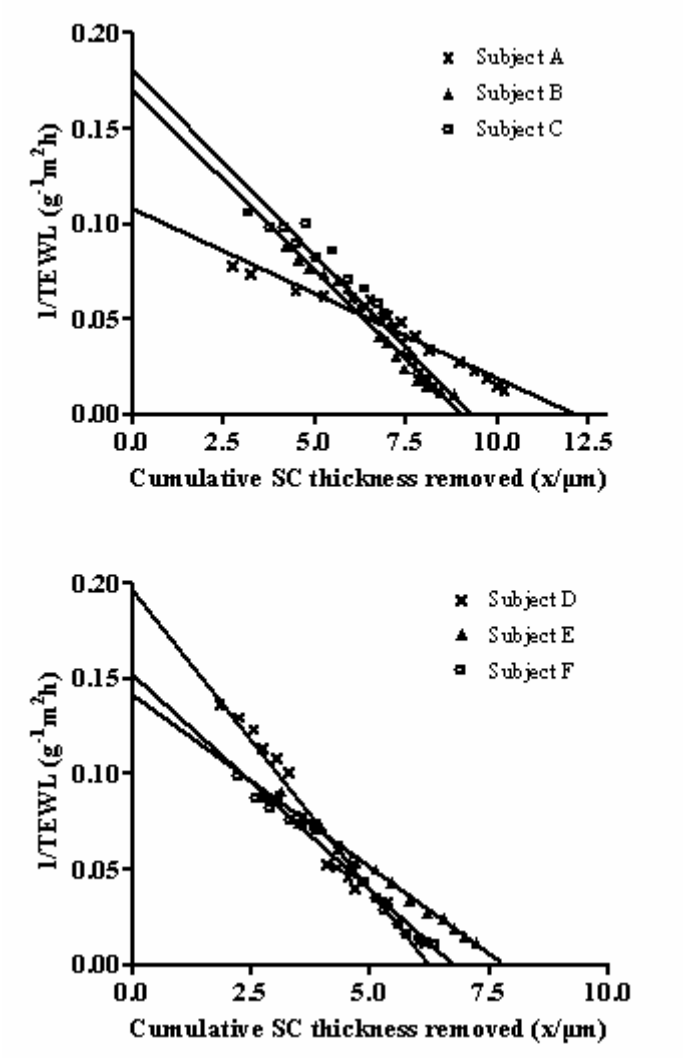

Figure 2.1: Illustrative experimental data for the determination of SC thickness (obtained from the x-axis intercepts of the above plots). Results in panel (a) were from dorsal skin samples, those in panel (b) from the abdomen.

2.3.3 NR concentration profiles across the SC

In all experiments, independent of the formulation used, no fluorescence from NR was ever detected in the receptor phase, an observation consistent with earlier work [16, 17].

The SC concentration profiles of Nile Red delivered from the CAPA nano/mesoparticles of different average diameters are in Figure 2.2. From the measurements of TEWL and of the SC mass removed on each tape, the concentrations could be expressed as a function of relative position within the SC (as reported before [15]), thereby correcting for differences in absolute SC thickness from one porcine skin sample to another. The effectiveness of this strategy is reflected in the excellent reproducibility in the results obtained.

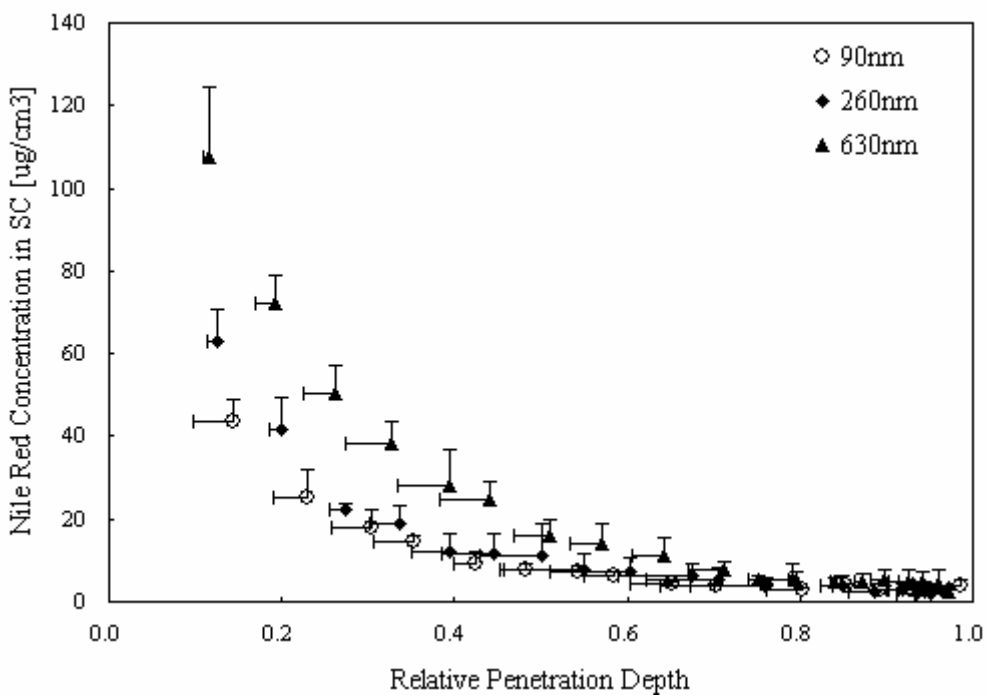

Figure 2.2: SC concentration profiles of NR following a 6-hour application of CAPA nano/mesoparticles having mean diameters of 90 nm, 260 nm and 630 nm (n = 5; mean ± SD). Note that, on the x-axis, 0 indicates the SC surface, 1 reflects the SC-stratum granulosum interface.

NR was more efficiently transferred into the SC from the nano/meso-carriers as the particle size increased. The total amounts of NR delivered into the SC from the 90 nm, 260 nm, and 630 nm formulations were 0.023, 0.033, and 0.058 μg, respectively. As the precise localization of NR in the CAPA nano/mesoparticles is not known, an unambiguous explanation for the observations is not possible. However, if, as suspected, NR is predominantly absorbed onto the particle surface, then the larger carriers obviously offer a smaller surface area and the "leaving tendency" of NR from the vehicle would be enhanced. Furthermore, the larger particles have bigger contact areas with the surface of SC than the smaller particles, which could be also facilitate the partition of NR from their vehicles into the SC (Figure 2.3).

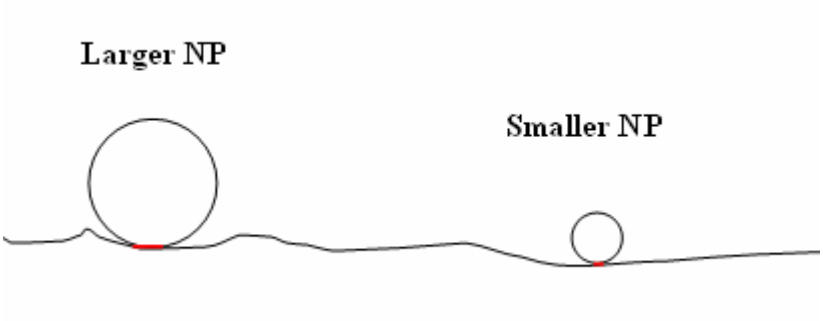

Figure 2.3: Illustration of the contact area between nanoparticles and the surface of stratum corneum. Larger particles might have a bigger contact area than smaller particles, considering the skin surface is not even.

Figure 2.4 shows the concentration profiles of NR in porcine SC following delivery of the active from PS, CAPA and CAB nanoparticles. Uptake of the lipophilic "active" was greatest (0.053 μg) from the most hydrophobic polymer (PS) and least (0.029 μg) from the most hydrophilic (CAB), with that from CAPA (of intermediate properties) falling in between (0.038 μg). These differences are influenced, of course, by the different loadings of NR achieved into the different nanoparticles (Table 2.1): the "payloads" for PS, CAPA and CAB were 77%, 49% and 24%, respectively. If the SC uptake levels are normalized by these different fractional loadings (i.e., average amounts of the dye taken up into the SC are divided by the fraction of the active eventually associated with the particles), the resulting ratios are 0.69 for PS, 0.78 for CAPA and 1.20 for CAB indicating, as would be expected, that NR release from the least hydrophobic nanoparticle (into the lipophilic SC) is favored relative to that from the more

hydrophobic polymers.

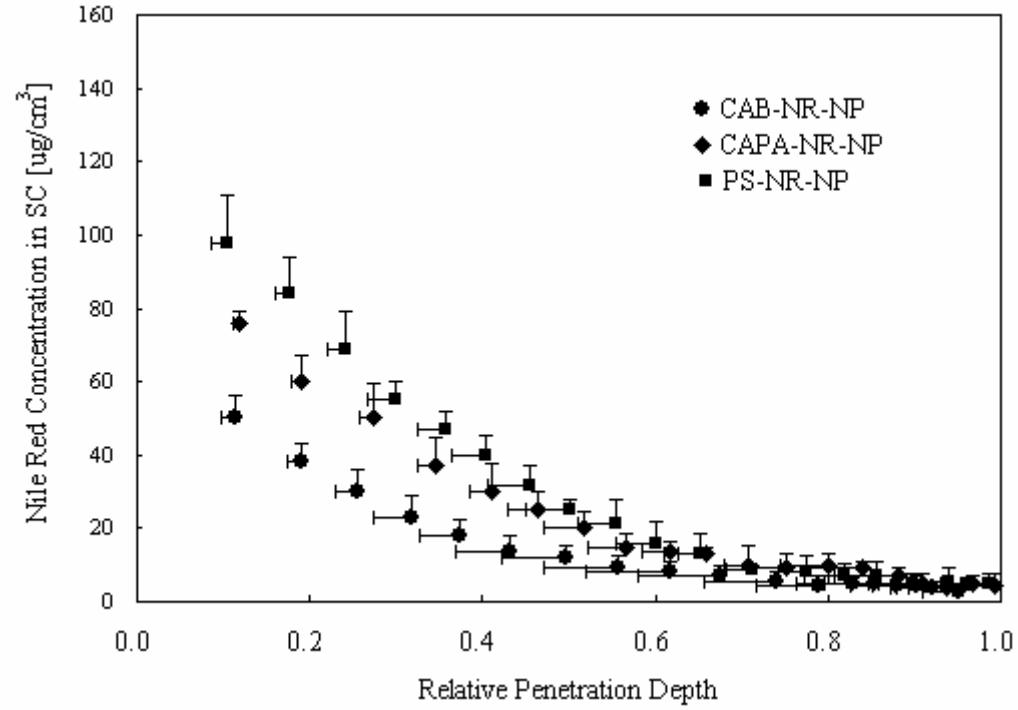

Figure 2.4: SC concentration profiles of NR following a 6-hour application of PS, CAPA and CAB nanoparticles (n = 5; mean ± SD).

2.3.4 Visualization of NR disposition in the SC by confocal microscopy

To visualize fluorescently-labeled biological samples, laser scanning confocal microscopy (LSCM) is a very valuable tool. Its optical sectioning function provides in-depth information of thick specimens without perturbation or destruction of the sample [18]. Confocal images from the surface of skin treated with nano/mesoparticles revealed the disposition of the associated NR post-application. Figure 2.5, for example, shows intense red fluorescence around a clearly imaged hair follicle following application of the CAPA 90 nm diameter nanoparticles. The affinity of polymeric particles for such appendageal structures has been reported previously [17]. Figure 2.6 illustrates NR distribution at the surface of the stratum corneum and nicely outlines the polygonal shapes of the corneocytes [19, 20]. Not surprisingly, therefore, the NR released from (in this case, CAB) nanoparticles enters the SC via the intercellular lipid domains.

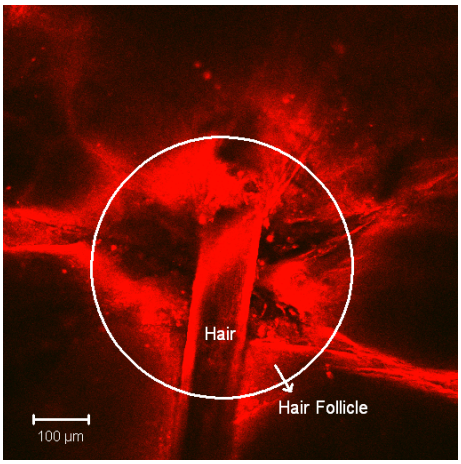

Figure 2.5: Confocal image (×10) of the skin surface following a 6-hour application of CAPA nanoparticles (90 nm diameter) containing NR. Clear localization around a hair follicle is observed.

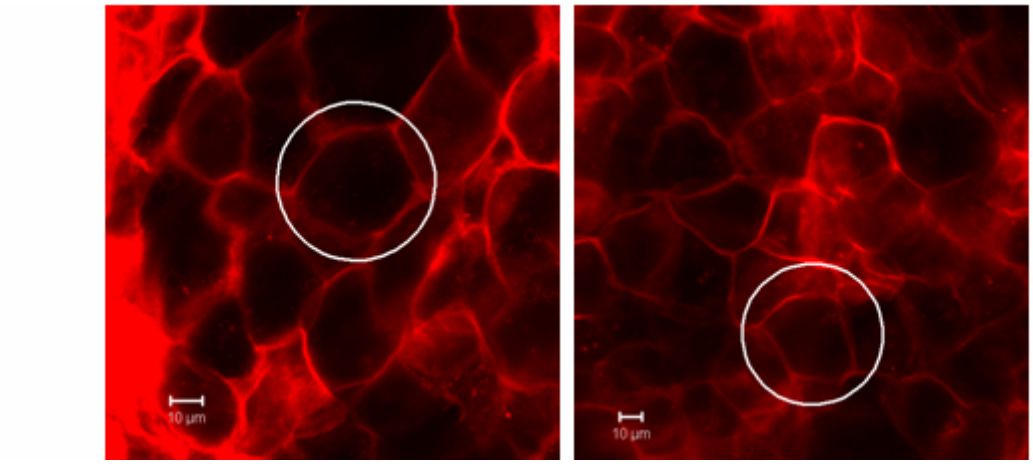

Figure 2.6: Confocal image (×63) of the skin surface following a 6-hour application of CAB nanoparticles containing NR. The release of the fluorophore into the intercellular lipid domains clearly outlines the polygonal shapes of the SC corneocytes.

Figure 2.7 illustrates the use of LSCM to optically section through the skin to produce a z-stack series of images as a function of depth into the SC and upper epidermis. In this example, NR released from CAB nanoparticles is seen to penetrate via the intercellular pathway but that it is effectively constrained to the SC, with little evidence of deeper transport during the 6-hour application period. Figure 2.8 demonstrates how the z-stack images can be

"reconstructed" to provide a cross-sectional image of the skin by sectioning through a specified plane. The NR released from the CAPA 90 nm diameter nanoparticles shown is limited in its disposition to the upper layer (primarily the SC) of the skin. Only in the vicinity of a hair follicle is there evidence for deeper penetration of the fluorescence.

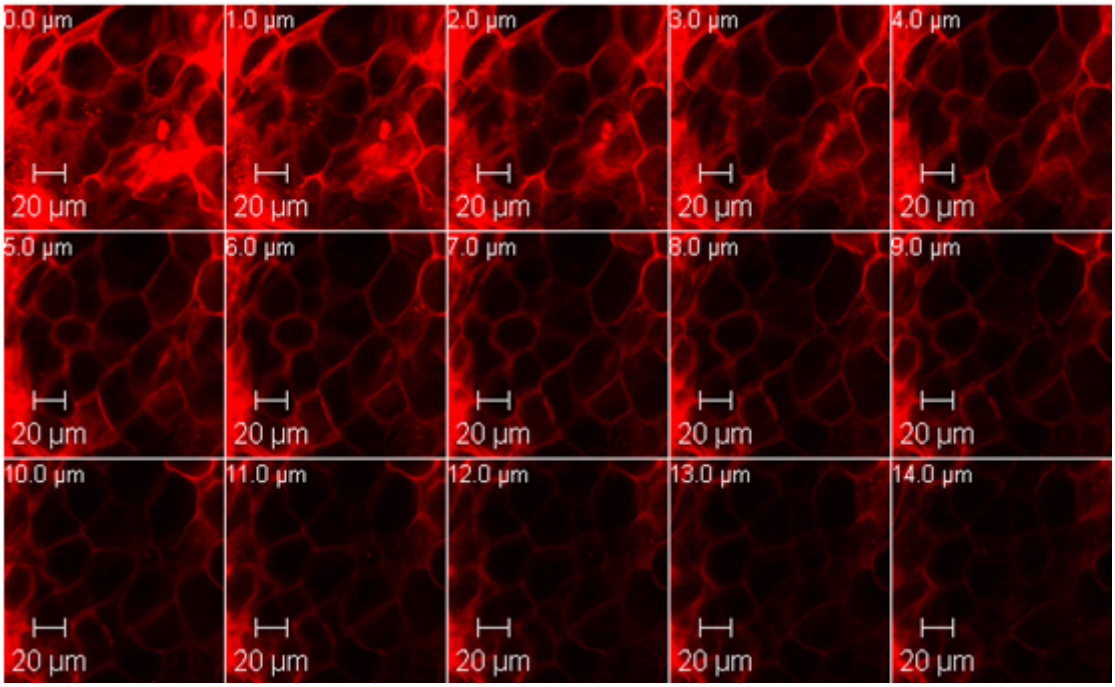

Figure 2.7: Optical sectioning images (×63) of skin after a 6-hour application of CAB nanoparticles containing NR. The sample area was imaged as the focus plane of the LSCM was lowered in steps of 1 µm.

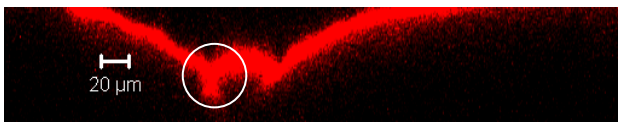

Figure 2.8: Reconstructed, optical cross-sectional image (×10) of skin after a 6-hour application of CAPA (90 nm diameter) nanoparticles containing NR. Penetration of the fluorophore is mostly constrained to the SC to a depth of ~10 µm but is occasionally visualized further into the tissue around hair follicles as highlighted by the white circle above.

Additionally, skin samples may be mechanically sectioned in the normal way and then examined by LSCM at a plane beyond the cut surface (thereby avoiding artifacts associated

with the sectioning procedure). This provides an alternative approach to obtain information about penetration into the deeper skin layers and has the advantage that it overcomes the progressive loss of resolution and signal of confocal microscopy with depth within the tissue, due to scattering and absorption of both the laser excitation and fluorescence emission light [21, 22]. An example of this approach is illustrated in Figure 2.9, which captures a hair follicle leaving the skin and demonstrates once more that NR uptake is limited to the SC.

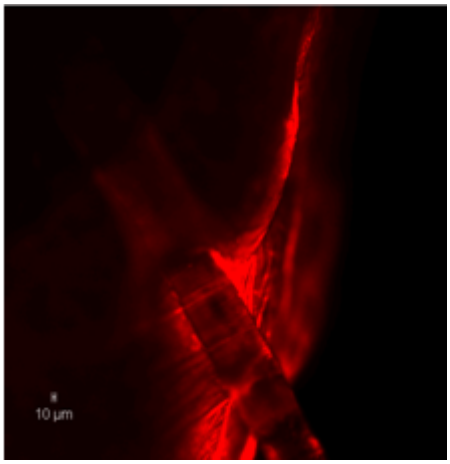

Figure 2.9: CLSM image of a mechanical cross-section of skin following a 6-hour application of CAB nanoparticles containing NR. The fluorophore was visualized in the SC and around a hair follicle but did not penetrate into deeper regions of skin.

2.4 Conclusions

The size and the hydrophobicity of nano/mesoparticles clearly influence the local disposition of an associated, lipophilic "active" species when applied to the skin. Larger particles, with a relatively smaller total surface area encourage the "active" to enter the lipophilic stratum corneum more efficiently. Nanoparticles made with more hydrophobic polymers are able to bring a greater "payload" of the lipophilic active to the skin surface and the absolute uptake into the SC is higher than that from less hydrophobic carriers. However, when delivery is more appropriately viewed as the fraction of the payload transferred from particle to skin, the expected, improved release from the least hydrophobic polymer (i.e., that least sympathetic to the lipophilic "active") is observed.

Confocal microscopy reveals that the released “active” is constrained to the SC and that it diffuses into the barrier via the intercellular lipids. Affinity of the formulations for appendageal structures, such as hair follicles, is clear, but the present study is unable to distinguish whether the red fluorescence seen is free “active”, or “active” still associated with the nanoparticles. Resolution of this key question forms the basis of future work.

Acknowledgements

Supported by the European Commission 6th Research and Technological Development Framework Programme (NAPOLEON: NAnostructured waterborne POLymEr films with OutstaNding properties) and a University Research Scholarship for Xiao Wu.

References

1. S. Magdassi, *Delivery systems in cosmetics.* Colloids Surface A: Physicochem. Eng. Aspects, 1997. **123-124**: p. 671-679.
2. B. Luppi, T. Cerchiara, F. Bigucci, R. Basile, and V. Zecchi, *Polymeric nanoparticles composed of fatty acids and polyvinylalcohol for topical application of sunscreens.* J Pharm Pharmacol, 2004. **56**(3): p. 407-11.
3. I.P. Kaur and R. Agrawal, *Nanotechnology: a new paradigm in cosmeceuticals.* Recent Pat. Drug Delivery Formulation, 2007. **1**(2): p. 171-182.
4. A.E.B. Shefer, NJ), Shefer, Shmuel David (East Brunswick, NJ), *Controlled delivery system for hair care products*. United States Patent: 6491902. (2002)
5. D.S.P. Soane, CA), Linford, Matthew R. (Orem, UT), *Nanoscopic hair care products*. United States Patent: 6821509. (2004)
6. C.R.N. Quellet, CH-2502 Biel, CH), Hotz, Jutta (Gemsenstrasse 3, Zurich CH-8006, CH), Balmer, Marc (Im Aegelsee 5, Unterengstringen CH-8006, CH), *Polymeric nanoparticles including olfactive components*. United States Patent: 7205340. (2007)
7. R. Alvarez-Roman, G. Barre, R.H. Guy, and H. Fessi, *Biodegradable polymer nanocapsules containing a sunscreen agent: preparation and photoprotection.* Eur J Pharm Biopharm, 2001. **52**(2): p. 191-5.
8. P.W. Wertz and D.T. Downing, *Stratum corneum: biological and biochemical considerations*, in *Transdermal drug delivery*, J. Hadgraft and R.H. Guy, Editors. 1989, Marcel Dekker, Inc.: New York. p. 1-22.
9. D.T. Downing, M.E. Stewart, P.W. Wertz, S.W. Colton, W. Abraham, and J.S. Strauss, *Skin lipids: an update.* J Invest Dermatol, 1987. **88**(3 Suppl): p. 2s-6s.
10. R.O. Potts and R.H. Guy, *Predicting skin permeability.* Pharm Res, 1992. **9**(5): p. 663-9.
11. H. Fessi, F. Puisieux, J.P. Devissaguet, N. Ammoury, and S. Benita, *Nanocapsule formation by interfacial polymer deposition following solvent displacement.* Int J Pharm, 1989. **55**(1): p. R1-R4.
12. Y.N. Kalia, F. Pirot, and R.H. Guy, *Homogeneous transport in a heterogeneous membrane: water diffusion across human stratum corneum in vivo.* Biophys J, 1996. **71**(5): p. 2692-700.
13. R.L. Anderson and J.M. Cassidy, *Variation in physical dimensions and chemical composition of human stratum corneum.* J Invest Dermatol, 1973. **61**(1): p. 30-2.
14. Y.N. Kalia, I. Alberti, N. Sekkat, C. Curdy, A. Naik, and R.H. Guy, *Normalization of stratum corneum barrier function and transepidermal water loss in vivo.* Pharm Res, 2000. **17**(9): p. 1148-50.
15. Y.N. Kalia, I. Alberti, A. Naik, and R.H. Guy, *Assessment of topical bioavailability in vivo: the*

importance of stratum corneum thickness. Skin Pharmacol Appl Skin Physiol, 2001. **14 Suppl 1**: p. 82-6.

16. V. Jenning, A. Gysler, M. Schafer-Korting, and S.H. Gohla, *Vitamin A loaded solid lipid nanoparticles for topical use: occlusive properties and drug targeting to the upper skin.* Eur J Pharm Biopharm, 2000. **49**(3): p. 211-8.
17. R. Alvarez-Roman, A. Naik, Y.N. Kalia, R.H. Guy, and H. Fessi, *Skin penetration and distribution of polymeric nanoparticles.* J Control Release, 2004. **99**(1): p. 53-62.
18. D.M. Shotton, *Confocal scanning optical microscopy and its application for biological specimens.* J Cell Sci, 1989. **94**: p. 175-206.
19. E. Christophers, *Cellular architecture of the stratum corneum.* J Invest Dermatol, 1971. **56**(3): p. 165-9.
20. J.C. Mackenzie, *Ordered structure of the stratum corneum of mammalian skin.* Nature, 1969. **222**(5196): p. 881-2.
21. A.J. Hoogstraate, C. Cullander, J.F. Nagelkerke, F. Spies, J. Verhoef, A.H.G.J. Schrijvers, H.E. Junginger, and H.E. Bodde, *A novel in-situ model for continuous observation of transient drug concentration gradients across buccal epithelium at the microscopical level.* J Control Release, 1996. **39**(1): p. 71-78.
22. M. Laurent, G. Johannin, N. Gillbert, L. Lucas, D. Cassio, P.X. Petit, and A. Fleury, *Power and limits of laser scanning confocal microscopy.* Bio cell, 1994. **80**: p. 229-240.

CHAPTER 3

DYE DIFFUSION FROM MICROCAPSULES WITH DIFFERENT SHELL THICKNESS INTO MAMMALIAN SKIN

Dye diffusion from microcapsules with different shell thickness into mammalian skin*[1]

Huai Nyin Yow[1], Xiao Wu [2], Alexander F. Routh[*1], and Richard H. Guy[2]

[1] Department of Chemical Engineering and BP Institute, University of Cambridge, Cambridge, CB3 0EZ

[2] Department of Pharmacy and Pharmacology, University of Bath, Claverton Down, Bath, BA2 7AY

Abstract

Oil-in-water microcapsules with varying shell thicknesses were fabricated via a coacervation technique, whereby evaporation of volatile solvents induced the shell-forming polymer to precipitate, phase separate and migrate to the oil/water interface to form microcapsules. These microcapsules encapsulated a lipophilic dye within their cores and were applied topically onto porcine skin for 6 hours. Results indicated that the dye preferentially accumulated within the skin furrows and hair follicles, though the dye did not penetrate beyond the stratum corneum. A model estimates the diffusion coefficients of dye through the microcapsule shell and within the skin to be approximately 10^{-18} and 10^{-16} m^2s^{-1}, respectively.

Keywords: Nanocapsules, shell thickness, skin, stratum corneum, Nile Red

3.1 Introduction

In the past 35 years, microcapsules have found broad applications in many drug and vitamin products [1, 2], cosmetics, personal care items [3, 4] and foods and beverages [5]. Release mechanisms of the encapsulated ingredients include rupture by stress/pressure, shell dissolution

[*1] Accepted by *European Journal of Pharmaceutics and Biopharmaceutics* in November 2008. To whom correspondence should be addressed (afr10@cam.ac.uk).

[6], shell permeation [7] and responsive shell swelling [8-11]. This variety provides a range of release profiles: for example, shell breakage and/or dissolution offers immediate release, while permeable and/or swellable shells are more useful for gradual, targeted release.

Despite their widespread use, however, safety concerns remain about the fate of microstructures in the human organism [12], an issue which has achieved even greater prominence with the advent of 'nanotechnology' in recent years. The motivation for this work lies in the investigation of percutaneous transport of an encapsulated ingredient into the skin from permeable microcapsules with varying shell thicknesses. This, coupled to a simple model for the diffusion profiles, crucially allows the understanding of individual control parameters for the 'active' ingredient movement within each environment (polymeric shell and skin). Hence, in this paper, polystyrene microcapsules (700 – 900 nm) had been used to encapsulate a model, 'active' ingredient (Nile Red dye) and then applied topically on porcine skin. Subsequently, the release and penetration of the 'active' was investigated and the results modeled.

Microcapsules were prepared using a previously reported coacervation method [13-15], whereby the shell-forming polymer and oil core are initially premixed in a volatile solvent, in which the polymer is soluble. The oil phase is then emulsified in an aqueous solution and the emulsification intensity determines the size of capsules formed. As the volatile solvent evaporates, the polymer precipitates from the oil phase. Given the right wetting conditions, the polymer will migrate to the water/oil interface and envelope the oil droplet to form a complete spherical shell. The final morphology of the particles is governed by the relative interfacial energies between the various phases [13].

Porcine skin has been used as a substitute for human skin, which it closely resembles in terms of epidermal thickness, lipid composition, permeability to diverse compounds and overall barrier function [16]. The latter is furnished by the stratum corneum, the thin (~10 μm) outermost layer of the skin. It has been described as a "brick and mortar" structure [17], in which corneocytes are embedded in an intercellular lipid matrix composed of ceramides, free fatty acids and cholesterol.

3.2 Theory

3.2.1 Dye diffusion model

The polystyrene shells encapsulated Nile Red dye and hexadecane cores. As the formulation of microcapsules came into contact with the porcine skin, passive diffusion of dye from the oil core into the skin takes place over the duration of the application time. This dye diffusion process is described by Fick's second law of diffusion.

$$\frac{\partial c}{\partial t} = D\frac{\partial^2 c}{\partial x^2} \tag{1}$$

Figure 3.1 presents the system schematically, with the microcapsule encapsulating the active (in this work, the dye, Nile Red) at a concentration C_{NR}. The microcapsules have a shell thickness of L_s and diffusion of dye through the shell is characterized by a diffusion coefficient, D_s. The microcapsules are in contact with the stratum corneum, of thickness L. The Nile Red diffusion coefficient through the skin is D, and its concentration within the stratum corneum is represented by c and is a function of application time (t) and distance (x) into the membrane.

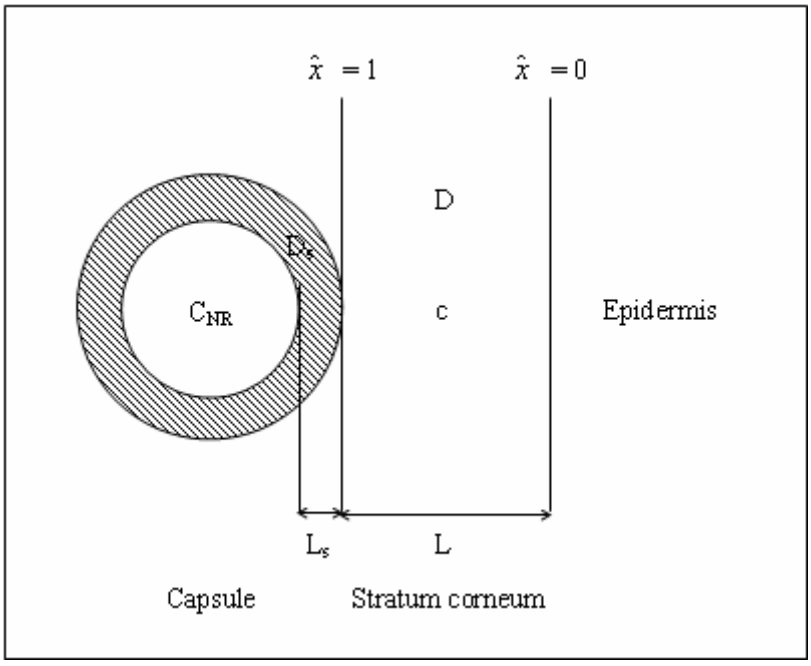

Figure 3.1: Schematic diagram illustrating the basis of the mathematical model developed (not to scale).

The applicable boundary conditions are:

(i) At $x = 0$, $\frac{\partial c}{\partial x} = 0$,

which represents no flux of material at the inner surface of the skin.

(ii) At $x = L$, $\frac{D_s(C_{NR} - c)}{L_s} = D\frac{\partial c}{\partial x}$,

which represents a balance between the amount of dye passing through the shell and that passing through the stratum corneum.

For ease of calculation, the concentration gradient, $(C_{NR} - c)$, is normalized by the Nile Red concentration in the oil core. The thickness of capsule shell is also normalized, in this case, by the thickness of the stratum corneum yielding the dimensionless parameters:

$$\hat{c} = \frac{c}{C_{NR}} - 1 \qquad \text{and} \qquad \hat{x} = \frac{x}{L} \tag{2}$$

and the simplified form of Equation (1):

$$\frac{\partial \hat{c}}{\partial t} = \frac{D}{L^2}\frac{\partial^2 \hat{c}}{\partial \hat{x}^2} \tag{3}$$

with revised boundary conditions:

(i) At $\hat{x} = 0$, $\frac{\partial \hat{c}}{\partial \hat{x}} = 0$.

(ii) At $\hat{x} = 1$, $D\frac{\partial \hat{c}}{\partial \hat{x}} = -\frac{D_s L}{L_s}\hat{c}$.

Solution is obtained by separation of variables, resulting in an Eigenfunction series with the Eigenfunction, λ, given by the solution to:

$$\lambda \tan \lambda = \frac{D_s L}{D L_s} \tag{4}$$

and the solution for concentration as follows:

$$\hat{c} = \sum_{n=1}^{\infty} A_n \exp\left(-\frac{\lambda_n^2 Dt}{L^2}\right) \cos \lambda_n \hat{x} \tag{5}$$

with the values of A_n obtained from:

$$A_n = -\frac{4 \sin \lambda_n}{2\lambda_n + \sin 2\lambda_n} \tag{6}$$

In summary, the diffusion of dye through the microcapsule shell into the stratum corneum is characterized by Equation (5), with λ_n provided in Equation (4) and the corresponding A_n calculated from Equation (6), where n = 1, 2, 3…

3.2.2 Solution when C_{NR} >> c

When the 'active' concentration within the oil core, CNR, is much greater than that within the stratum corneum, c, (i.e., $C_{NR} >> c$), then the concentration difference ($C_{NR} - c$) dominates the passive diffusion process, which is no longer governed by the thickness of the shell.

Using Figure 3.1 with the illustrated symbols and notations, together with Equation (1) and the corresponding boundary conditions given before, and defining:

$$\breve{c} = c \times L_s \qquad \text{and} \qquad \hat{x} = \frac{x}{L} \tag{7}$$

then:

$$\frac{\partial \breve{c}}{\partial t} = \frac{D}{L^2} \frac{\partial^2 \breve{c}}{\partial \hat{x}^2} \tag{8}$$

and:

(i) At $\hat{x} = 0$, $\frac{\partial \breve{c}}{\partial \hat{x}} = 0$.

(ii) At $\hat{x} = 1$, $\frac{D}{L}\frac{\partial \breve{c}}{\partial \hat{x}} = D_s C_{NR}\left(1 - \frac{c}{C_{NR}}\right)$.

However, since $C_{NR} >> c$ or $c/C_{NR} << 1$, then the second boundary condition becomes:

$$\frac{\partial \breve{c}}{\partial \hat{x}} = \frac{D_s L C_{NR}}{D} \tag{9}$$

which is independent of the capsule shell thickness, L_s.

Therefore, the solutions to Equation (8) will be independent of shell thickness, L_s, and the data obtained from different microcapsules should then collapse on to a single profile, providing a simple proof that the dye diffusion through the stratum corneum follows simple Fickian diffusion.

3.3 Materials and methods

3.3.1 Materials

Polystyrene (melt index 14, MW ~ 225,000 g/mol, Aldrich, Dorset UK) was used to form the microcapsule shells. Dichloromethane (99%, Acros Organics, Loughborough UK) was the volatile polymer solvent. n-Hexadecane (99%, Fisher Scientific, Loughborough UK) was employed without purification as the non-volatile, non-solvent oil core. Acetone (>99%, Aldrich) was added to aid the emulsification process. Poly(vinyl alcohol) (96% hydrolysed - average MW 85,000 – 124,000 g/mol, Aldrich) was the external aqueous phase after dilution to 2% w/v solution with MilliQ water (18.2 MΩ•cm). Nile Red (Aldrich), a fluorescent dye, was the encapsulated, lipophilic ‘active’. Acetonitrile (HPLC grade, Aldrich) was the solvent used in the

high performance liquid chromatography (HPLC) assay of Nile Red (see below).

Anhydrous sodium phosphate dibasic (Acros Organics), potassium dihydrogen phosphate monobasic (Acros Organics) and sodium chloride (Acros Organics) were used to make phosphate buffered solutions. Phosphoric acid (85% in solution, Acros Organics) was added for pH adjustment. Porcine skin was obtained from four 1-year old pigs (two female, two male) from a local slaughterhouse. Tissue was dermatomed to a nominal depth of 750 μm, then cut into 4 cm × 6 cm pieces. The skin samples were washed under cold running water, dried and sealed in plastic bags at -20°C until used.

3.3.2 Methods

3.3.2.1 Fabrication of polystyrene microcapsules with encapsulated dye

Polystyrene microcapsules were made using a coacervation technique; the precipitated polymer induced by internal phase separation enveloped the oil core to form a complete shell [13-15, 18]. Nile Red (1.6 mg) was first pre-dissolved in hexadecane (24 g) and acetone (6.2 g). The presence of acetone facilitated dissolution without causing phase separation from hexadecane. This mixture was then separated into four identical batches.

Next, polystyrene (3.2–16 g) was dissolved in dichloromethane (110.2 g) and a batch of the Nile Red containing oil phase was added. Additional acetone (4.65 g) was introduced to aid the subsequent emulsification process. Meanwhile, 2% w/v poly(vinyl alcohol) solution (125 mL) was poured into a 400 ml beaker and thermostatted at 20°C.

With the aqueous phase being stirred at approximately 9,200 rpm, the oil phase was gradually added over ~1 minute to form an oil-in-water emulsion. Stirring was continued for 1 hour. Subsequently, the emulsion was heated, with gentle stirring, from 20°C to 65°C over 20 minutes and was then maintained at this elevated temperature for a further 40 minutes. The temperature

was then reduced to 40°C and held for 4 hours. Finally, the emulsion was left overnight in a fume cupboard at atmospheric conditions, again with gentle stirring. This ensured that all the dichloromethane and acetone had evaporated and allowed for complete polystyrene shell formation. The formed microcapsules were then placed in sealed containers and kept in the dark until use.

3.3.2.2 Characterization of polystyrene microcapsules

The microcapsules were characterized by scanning electron microscopy (SEM). A JEOL-6340F Field Emission Gun Scanning Electron Microscope was used to image the morphology of the microcapsules at an accelerating voltage of 5 kV. A drop of the microcapsule suspension was air-dried on a stainless steel SEM stub overnight. The sample was then platinum-coated using an Emitech K575 sputter coater. This was carried out under argon at 1×10^{-3} millibar and 40 mA for 1 minute.

The microcapsule diameters were measured by dynamic light scattering (Brookhaven ZetaPlus, Brookhaven Instruments Corporation, Holtsville NY, USA). A drop of the microcapsule dispersion (approximately 0.1 ml) was placed in a disposable plastic cell and diluted to 3 ml. The effective diameters deduced were accurate to ±1%, with an average of 10 measurements taken.

3.3.2.3 Dye diffusion study

Before the experiment, the skin was fully defrosted and any visible hairs were trimmed as close as possible to the surface. Each piece of skin was cut in half, one part being used for the Nile Red diffusion experiment, the other reserved for the measurement of stratum corneum thickness (see below).

The former piece of skin was clamped between the donor and receptor compartments of a vertical Franz diffusion cell. The receptor compartment was filled with phosphate buffer solution.

The donor solution was 3 ml of a polystyrene microcapsule formulation and was covered with Parafilm to prevent evaporation. Replicate cells (n = 3) were positioned on a Skin Permeation System (Model LG-1083, Laboratory Glass Apparatus Inc, Berkeley CA, USA), which allowed magnetic stirring of the receptor phases and provided a means to thermostat the cells at 37ºC. Diffusion was allowed to proceed for 6 hours, at which point the experiment was terminated, the skin removed and gently washed three times with phosphate buffer solution, and patted dry with paper towel.

Subsequently, the depth of Nile Red penetration into the stratum corneum of porcine skin was assessed using a validated tape-stripping procedure [19]. Briefly, twenty 2.7 cm × 2.7 cm square tapes were first cut from transparent Scotch adhesive book tape 845. Each tape was weighed pre- and post-skin stripping. A circular template with a 2 cm diameter hole was prepared and secured onto the treated skin. The stratum corneum was then stripped twenty times with the pre-weighed tapes. After, each tape was rolled and placed in 1 mL acetonitrile in a 2 mL glass vial. The vials were capped and shaken overnight. The next day, the samples were filtered (Whatman PTFE filters, 0.45 μm, Florham Park, NJ USA) into HPLC vials. The experimental solutions, together with known concentration standards of Nile Red, were assayed by HPLC.

3.3.2.4 High-performance liquid chromatography assay

Nile Red was quantified by HPLC with fluorescence detection. The chromatographic system (Dionex, Sunnyvale, CA USA) was equipped with a RF 2000 fluorescence detector and a reversed-phase column (25 cm × 4.6 mm internal diameter, KYA Tech, Tokyo Japan). The system was set at 559 nm and 630 nm for excitation and emission wavelengths, respectively. The mobile phase was acetonitrile-water (80:20) with a flow rate of 1 ml/min. Each injection utilized 200 μL of solution maintained at 25°C. The Nile Red retention time was 12.6 minutes. The limits of detection and quantitation were 0.3 ng/ml and 1.1 ng/ml, respectively.

3.3.2.5 Stratum corneum thickness determination

The second half of each skin section was used for measurement of stratum corneum thickness using a previously published method [20]. Stratum corneum removal using pre-weighed tape-strips was again employed, having delimited a 2 cm diameter area of skin with a circular template. Prior to the first strip and following the removal of each layer, the passive transepidermal water loss (TEWL) across the skin was measured with an Aquaflux device (Biox Systems Ltd., London UK) specifically designed for this purpose. Stripping was continued until TEWL reached 80 g m^{-2} h^{-1} [20]. Then, the tapes were reweighed to determine the amount (and, hence, the thickness) of stratum corneum removed on each tape-strip. The reciprocal of TEWL was plotted against the cumulative thickness of stratum corneum removed and the resulting linear regression was extrapolated to $TEWL^{-1} = 0$ to yield the total stratum corneum thickness as the intercept on the x-axis.

3.3.2.6 Laser scanning confocal microscopy

After 6 hours exposure to the Nile Red microcapsule formulation, the skin was cleaned and then examined by laser scanning confocal microscopy (LSM 510 Meta, Carl Zeiss, Jena Germany). A HeNe laser was used to excite Nile Red at 543 nm. The skin was then inspected under 10×, 20× and 63× objectives. Confocal images were recorded and edited with LSM Image Browser software (Carl Zeiss, Release 4.0).

3.4 Results and discussion

3.4.1 Polystyrene microcapsules

Figure 3.2 is a SEM image of polystyrene microcapsules encapsulating Nile Red. The capsules are spherical and range in size from 500 nm to 1 μm. This was confirmed quantitatively by dynamic light scattering, which gave an average effective diameter of 750 nm. Some

microcapsules appeared to have a hole within their shells, and these structures have been termed "colloidal buckets". It is believed that the formation of these structures (which will be discussed in a separate article) is triggered by the presence of excess dye. As most of the particles formed did not display this feature, the analysis of the results assumed a continuous shell. NR is distributed in both the core and the shell.

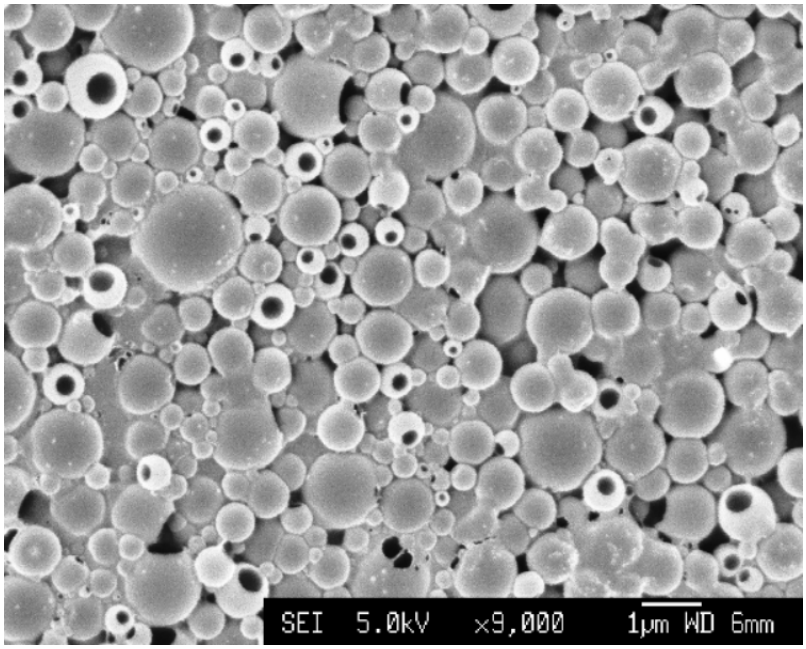

Figure 3.2: Scanning electron microscopy image of polystyrene microparticles.

Five sets of polystyrene microcapsules were fabricated with varying shell thickness. This was achieved either by varying the amount of polystyrene or by decreasing the hexadecane content. The crucial element is the volume ratio of the shell-forming polymer to the non-volatile oil. This ratio governs the total surface area that the polymer must cover to form a complete shell and, in turn, for a given capsule diameter, determines the thickness of the shell that the precipitating polymer can produce.

To calculate the shell thickness, it is assumed that volume is conserved [13]. For a capsule of radius, r, with shell thickness, L_s, the ratio of volume occupied by the shell, V_s, to the total volume of the capsule, V_t, is:

$$\frac{V_s}{V_t} = \frac{r^3 - (r - L_s)^3}{r^3} \tag{10}$$

This ratio equals the volume fraction of polystyrene (ϕ_p) within the non-volatile non-solvent oil. In this study, the oil phase is hexadecane. Hence, equation (10) can be rearranged as:

$$\frac{L_s}{r} = 1 - (1 - \phi_p)^{1/3} \tag{11}$$

Hence, as ϕ_p is known and the radius of the microcapsules is determined by dynamic light scattering, the shell thickness, L_s, can be calculated. The results for the different microcapsules are in Table 3.1. For the first, second and fourth series, the average capsule radius was 431±12 nm and, with a 3-fold increase in polymer content, L_s approximately doubled; for the third and fifth sets, reducing the amount of hexadecane by a factor of 2 resulted in a 1.5-fold increase in L_s. In summary, therefore, it proved possible to obtain a range of microcapsules with varying shell thickness to examine in subsequent experiments.

Table 3.1: Properties of the various polystyrene microcapsules investigated.

Set	Polystyrene content (cm^3)	Hexadecane content (cm^3)	Polymer fraction, ϕ_p (%)	[1] Capsule radius, r (nm)	Shell thickness, L_s (nm)
1	3.1	8.7	26	425	40
2	5.9	8.7	40	445	70
3	11.9	10.3	54	360	82
4	9.0	8.7	51	425	89
5	11.8	5.0	70	360	120

[1] Measured by dynamic light scattering.

3.4.2 Confocal microscope imaging of skin

Figure 3.3 shows that Nile Red had accumulated in the furrows, of the skin (Figure 3.3a) and in and around the hair follicle openings (Figure 3.3b). It is perhaps not surprising that this lipophilic fluorophore showed a predilection for these lipid-rich sites on or near the skin surface, and the data are consistent with earlier observations [21]. However, these skin appendages only

cover 0.1% of the total skin surface; hence the contribution of this to percutaneous transport is considered minimal [22]. It is generally the intercellular lipid matrix that is the main barrier to percutaneous transport.

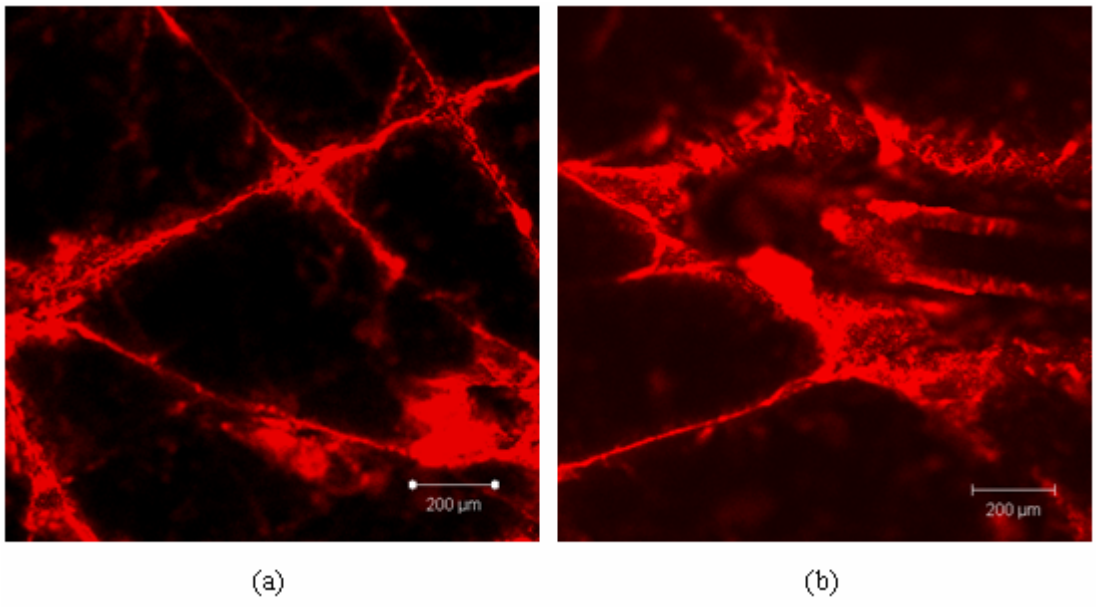

Figure 3.3: Laser scanning confocal microscopy image showing Nile Red disposition (a) in skin furrows and (b) in and around a hair follicle.

3.4.3 Skin penetration of Nile Red

The thickness of the stratum corneum of ten pieces of porcine skin was determined via measurements of TEWL. Examples of the data obtained are shown in Figure 3.4. The x-axis intercept gives the total thickness of the stratum corneum. Therefore, the average (±SD) stratum corneum thickness is 10 ± 2 µm. With this information, it was possible to display all Nile Red concentration profiles across the barrier as a function of normalized position (from 0 at the skin surface to 1 at the interface with the underlying viable tissue). The Nile Red concentrations were obtained by dividing the Nile Red amount, as detected by HPLC, by the volume of stratum corneum, assuming a density of 1 g cm^{-3} [23].

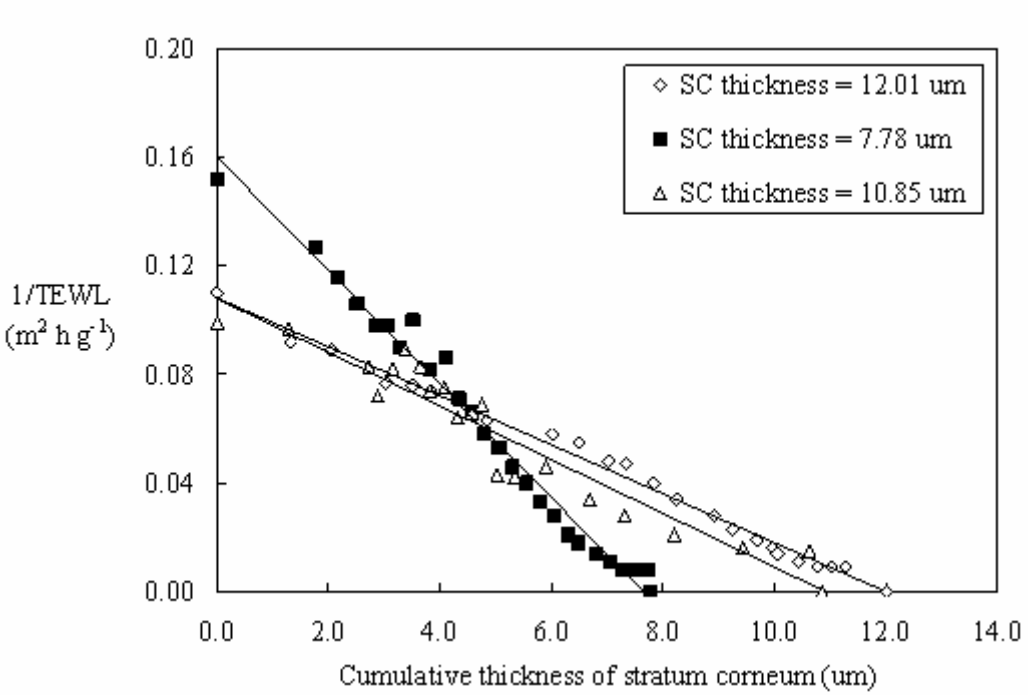

Figure 3.4: Example TEWL results enabling stratum corneum thickness determination.

The Nile Red concentration profiles observed as a function of microcapsule shell thickness are illustrated in Figure 3.5. The diffusion of dye into the deeper regions of the stratum corneum indicates that it has been released from the microparticles, the size of which are clearly too large to cross an intact cutaneous barrier [24]. Apparent from the data, however, is that a gradual increase in the microcapsule shell thickness resulted in a decrease in the amount of Nile Red taken up into the stratum corneum. This has been confirmed quantitatively by integration of the area under the concentration profiles to give the calculated total amount of Nile Red uptake as a function of microcapsule thickness (Table 3.2). These results suggest a means whereby the uptake of an 'active' ingredient into the skin may be manipulated by judicious design of the formulation employed. As NR is in both the core and the shell of the microcapsules, it may exhibit a "burst release" from the carriers at the initial stage of application, a sign of NR released from the shell, and then the rate of release reduces until it becomes constant, indicating NR is released from the core [14, 15].

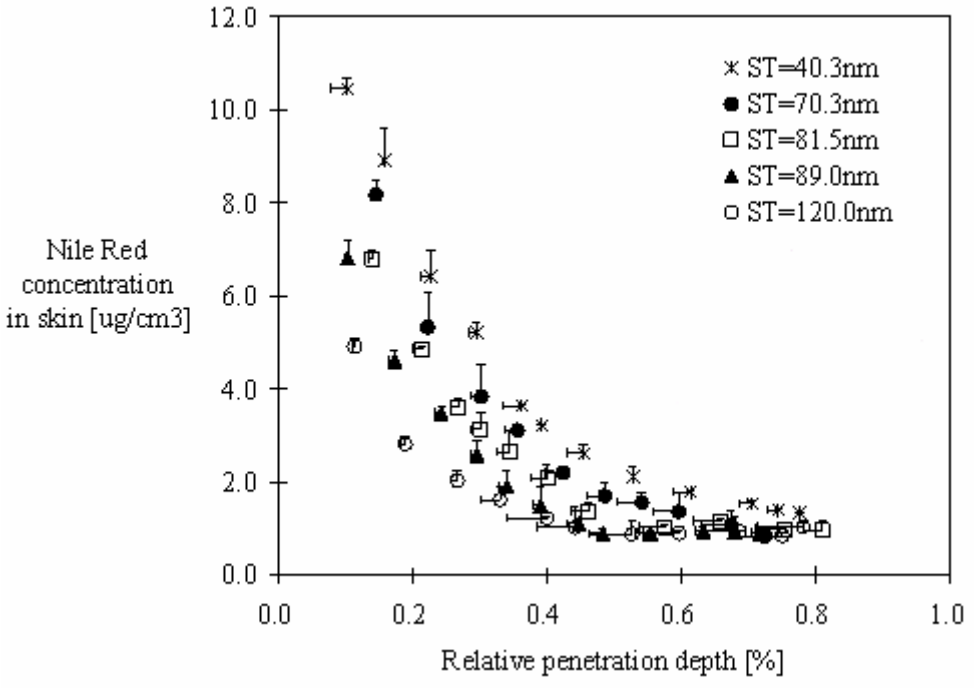

Figure 3.5: Nile Red concentration profiles across the stratum corneum (mean ± SD; n = 3) as a function of the relative depth of penetration into the barrier following a 6-hour application of five formulations of microcapsules of different shell thickness (ST).

Table 3.2: Total amount of Nile Red taken into the stratum corneum, determined by integration of the area under the curves in Figure 3.5.

Capsule ST (nm)	Total Nile Red taken into the SC (μg/ml)
40	3.3 ± 0.2
70	2.6 ± 0.2
82	2.2 ± 0.2
89	1.8 ± 0.1
120	1.4 ± 0.1

3.4.4 Model fitting of of NR concentration profiles across SC

The Nile Red concentration profiles across the stratum corneum were fitted to the theoretical model, using ten terms in the Eigenfunction expansion to ensure convergence. The best fits to the data (Figure 3.6a) were obtained with D = 5 x 10^{-16} m^2 s^{-1} and D_s = 1.5 x 10^{-18} m^2 s^{-1}. To the authors' best knowledge, no coefficient data had been quoted for diffusion of Nile Red dye in pig

skin or polystyrene shell. Comparing with similar release studies, the proposed coefficients were comparable to literature; 10^{-15}–10^{-16} m^2 s^{-1} for D [25, 26] and 10^{-16}–10^{-21} m^2 s^{-1} for D_s [7, 27]. The diffusion of an active is generally governed by its size, solubility in the diffusion medium and nature of the diffusion medium. The sensitivity of the fitting to the values of the proposed diffusivities is illustrated in Figures 3.6b and 3.6c. Predictably, as D is increased from 10^{-17} to 10^{-14} m^2 s^{-1}, the 'active' distributes further into the barrier and the profile becomes progressively less steep (Figure 3.6b). On the other hand, as D_s is increased from 10^{-20} to 10^{-17} m^2 s^{-1}, the total amount of 'active' in the stratum corneum increases progressively as its release from the microcapsules becomes faster (Figure 3.6c). Overall, therefore, diffusivity in the shell determines the absolute quantity of 'active' transferred into the stratum corneum, while its diffusivity in this membrane controls the depth of penetration into the barrier.

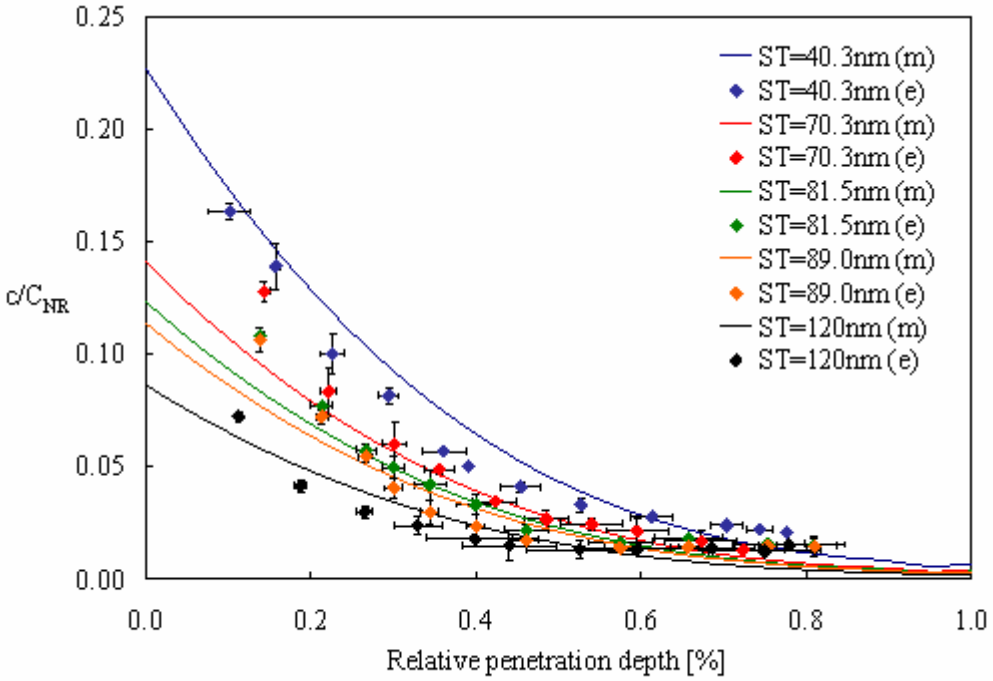
0.25
0.20
0.15
0.10
0.05
0.00
c/C_NR
0.0
0.2
0.4
0.6
0.8
1.0
Relative penetration depth [%]
ST=40.3nm (m)
ST=40.3nm (e)
ST=70.3nm (m)
ST=70.3nm (e)
ST=81.5nm (m)
ST=81.5nm (e)
ST=89.0nm (m)
ST=89.0nm (e)
ST=120nm (m)
ST=120nm (e)

(a)

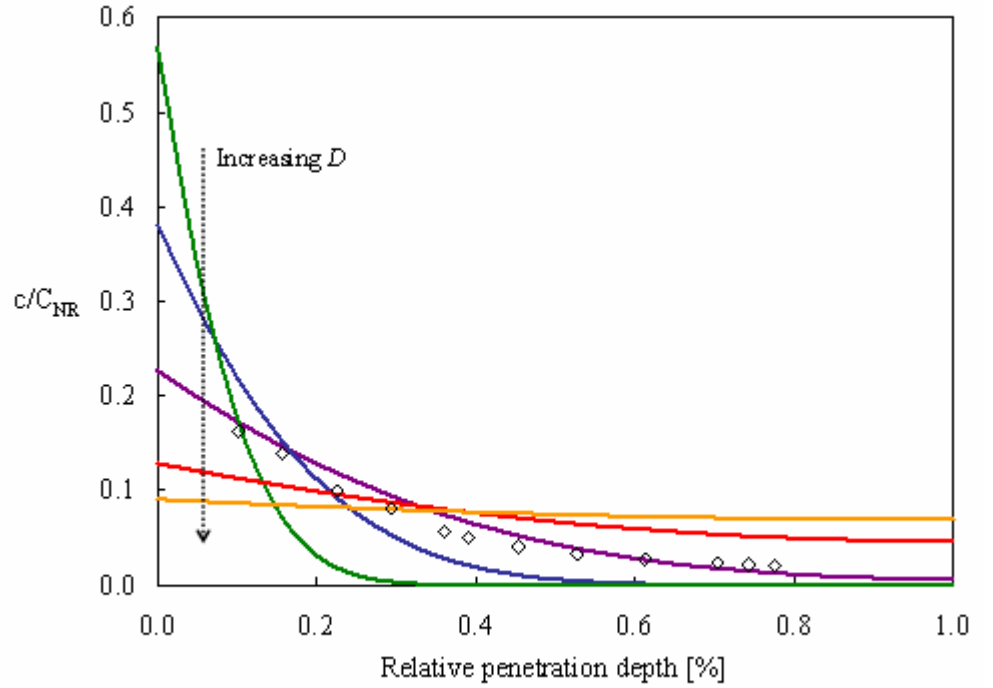
0.6
0.5
0.4
0.3
0.2
0.1
0.0
c/C_NR
Increasing D
0.0
0.2
0.4
0.6
0.8
1.0
Relative penetration depth [%]

(b) [1]

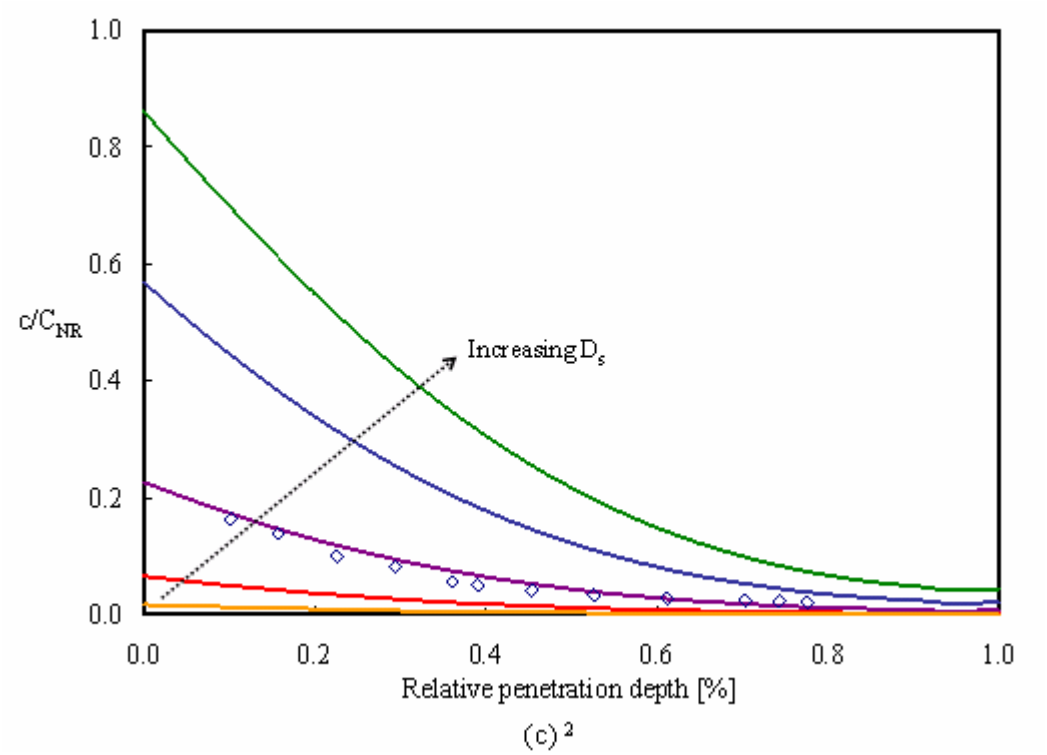

Figure 3.6: (a) Comparison of normalized Nile Red concentration (c/C_{NR}) profiles (mean ± SD; n=3) across the stratum corneum with the theoretical predictions (continuous lines) of the method for "active" delivery from microcapsules of different shell thickness (ST), with subsequent model predictions of the normalized Nile Red concentration (c/C_{NR}) profile for various values of diffusion coefficient of the "active" (b) across the stratum corneum, D, and (c) through the polymeric microcapsule shell, Ds.

[1] The data points shown are for Nile Red delivered from a formulation containing microcapsules of shell thickness 40 nm and having $D = 5 \times 10^{-16}$ m^2 s^{-1}.

[2] The data points shown are for Nile Red delivered from a formulation containing microcapsules of shell thickness 40 nm with $D_s = 1.5 \times 10^{-18}$ m^2 s^{-1}.

The Nile Red profiles in Figure 3.6a indicate that the concentration of 'active' in the oil core is much greater than that achieved in the stratum corneum. The approximate solution to the diffusion equation when $C_{NR} >> c$ can be applied, and the theoretical prediction that the behaviour of (c x L_s), as a function of penetration depth (x) into the stratum corneum, is independent of microcapsule shell thickness may be examined. This test is undertaken in Figure 3.7, and a collapse of the data on to a single profile is observed. Hence, this confirms that the dye diffusion process into the porcine skin is governed by Fickian diffusion.

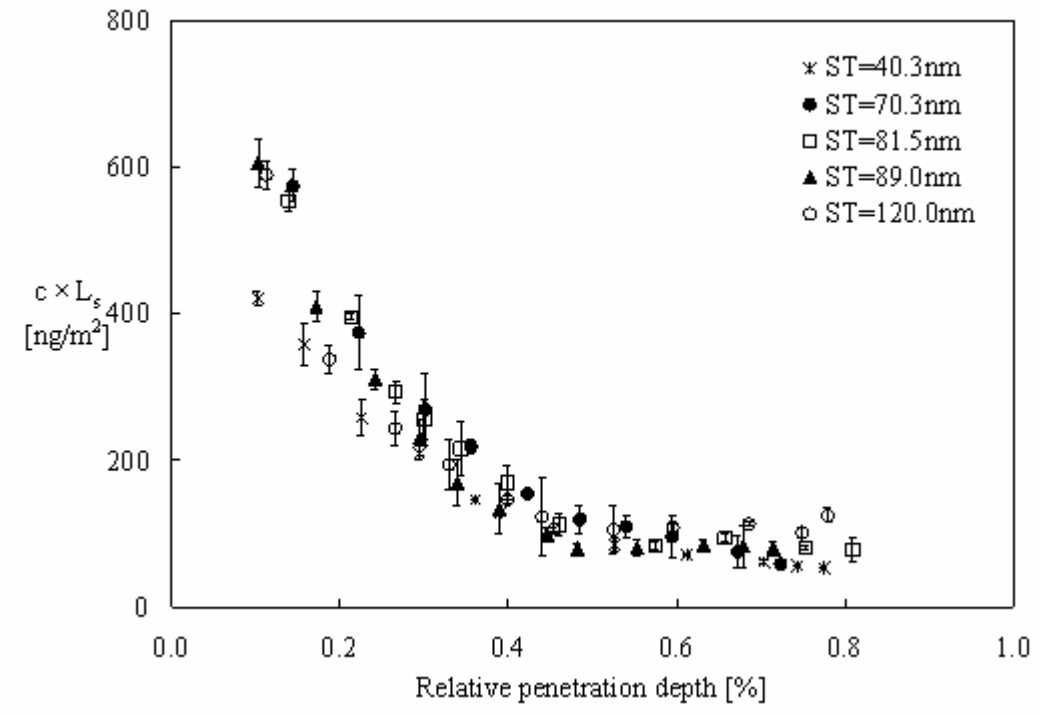

Figure 3.7: Predicted collapse of concentration profile data in Figure 3.5 to an essentially common profile when $C_{NR} >> c$ (the case for these experiments) (Data: mean ± SD; n = 3).

3.5 Conclusions

A range of polystyrene microcapsules, encapsulating Nile Red in a hexadecane core, were prepared and examined for their ability to deliver a model 'active' substance to the outer layers of mammalian skin. Increasing shell thickness reduced the rate and extent of 'active' transfer into

the outermost, and least permeable, layer of skin, the stratum corneum. The concentration profiles were successfully simulated with a diffusion model, which took into account the active's diffusivities in the stratum corneum and in the polymeric shell. The results suggested that the approach might be useful for the design and optimisation of consumer-health formulations for diverse applications.

Acknowledgements

This research was funded by the European Union, via an integrated project entitled NAPOLEON (NAnostructured waterborne POLymEr films with OutstaNding properties).

References

1. *Microencapsulated pharmaceuticals to thrive.* 2002 [cited 2007/12/10]; Available from: http://www.laboratorytalk.com/news/fro/fro128.html.
2. W. Meier, *Polymeric nanocapsules.* Chem Soc Rev, 2000. **29**(5): p. 295-303.
3. http://www.unilever.co.uk/ourvalues/sciandtech/science_behind_vitality/extra_protection.asp. *Extra protection when you need it.* 2008 [cited 2007/12/10].
4. Y. Ueda, A. Segawa, and M. Yoshioka, *The characteristics of a microcapsule with an entirely new wall material, `silicone-resin-polypeptide', and its application.* Int J Cosmet Sci, 2004. **26**(4): p. 215-215(1).
5. J. Franjione and N. Vasishtha, *The art and science of microencapsulation.* Technology Today 1995.
6. B.F. Gibbs, S. Kermasha, I. Alli, and C.N. Mulligan, *Encapsulation in the food industry: a review.* Int J Food Sci Nutr, 1999. **50**(3): p. 213-24.
7. M.S. Romero-Cano and B. Vincent, *Controlled release of 4-nitroanisole from poly(lactic acid) nanoparticles.* J Control Release, 2002. **82**(1): p. 127-35.
8. M. Sauer, D. Streich, and W. Meier, *pH-sensitive nanocontainers.* Adv Mater, 2001. **13**(21): p. 1649 - 1651.
9. G. Ibarz, L. Dähne, E. Donath, and H. Möhwald, *Smart micro- and nanocontainers for storage, transport, and release.* Adv Mater, 2001. **13**(17): p. 1324 - 1327.
10. A. Shulkin and H.D.H. Stover, *Photostimulated phase separation encapsulation.* Macromol, 2003. **36**(26): p. 9836-9839.
11. L.S. Zha, Y. Zhang, W.L. Yang, and S.K. Fu, *Monodisperse temperature-sensitive microcontainers.* Adv Mater, 2002. **14**(15): p. 1090-1092.
12. E. Strickland. *Nice nanostuff, but is it safe?* 2006 [cited 2007/12/10]; Available from: http://www.eastbayexpress.com/news/nice_nanostuff__but_is_it_safe_/.
13. A. Loxley and B. Vincent, *Preparation of poly(methylmethacrylate) microcapsules with liquid cores.* J Colloid and Interface Sci. , 1998. **208**(1): p. 49-62.
14. P.J. Dowding, R. Atkin, B. Vincent, and P. Bouillot, *Oil core-polymer shell microcapsules prepared by internal phase separation from emulsion droplets. I. Characterization and release rates for microcapsules with polystyrene shells.* Langmuir, 2004. **20**(26): p. 11374-11379.
15. P.J. Dowding, R. Arkin, B. Vincent, and P. Bouillot, *Oil core/polymer shell microcapsules by internal phase separation from emulsion droplets. II : Controlling the release profile of active molecules.* Langmuir, 2005. **21**(12): p. 5278-5284
16. N. Sekkat, Y.N. Kalia, and R.H. Guy, *Biophysical study of porcine ear skin in vitro and its comparison to human skin in vivo.* J Pharm Sci, 2002. **91**(11): p. 2376-81.

17. P.M. Elias, *Lipids and the epidermal permeability barrier* Arch Dermatol Res, 1981. **270**(1): p. 95-117.

18. H.N. Yow and A.F. Routh, *Formation of liquid core–polymer shell microcapsules.* Soft Matter, 2006. **2**: p. 940-949.

19. V.P. Shah, *Topical dermatological drug product NDAs and ANDAs - in vivo bioavailability, bioequivalence, in vitro release and associated studies*. 1998, US Depart. of Health and Human Services: Rockville. p. 1-9.

20. Y.N. Kalia, F. Pirot, and R.H. Guy, *Homogeneous transport in a heterogeneous membrane: water diffusion across human stratum corneum in vivo.* Biophys J, 1996. **71**(5): p. 2692-700.

21. R. Alvarez-Roman, A. Naik, Y.N. Kalia, R.H. Guy, and H. Fessi, *Skin penetration and distribution of polymeric nanoparticles.* J Control Release, 2004. **99**(1): p. 53-62.

22. K. Moser, K. Kriwet, A. Naik, Y.N. Kalia, and R.H. Guy, *Passive skin penetration enhancement and its quantification in vitro.* Eur J Pharm Biopharm, 2001. **52**(2): p. 103-12.

23. R.L. Anderson and J.M. Cassidy, *Variation in physical dimensions and chemical composition of human stratum corneum.* J Invest Dermatol, 1973. **61**(1): p. 30-2.

24. A. Rolland, N. Wagner, A. Chatelus, B. Shroot, and H. Schaefer, *Site-specific drug delivery to pilosebaceous structures using polymeric microspheres.* Pharm Res, 1993. **10**(12): p. 1738-1744.

25. C. Herkenne, A. Naik, Y.N. Kalia, J. Hadgraft, and R.H. Guy, *Ibuprofen transport into and through skin from topical formulations: in vitro-in vivo comparison.* J Invest Dermatol, 2007. **127**(1): p. 135-42.

26. K. Moser, K. Kriwet, C. Froehlich, Y.N. Kalia, and R.H. Guy, *Supersaturation: enhancement of skin penetration and permeation of a lipophilic drug.* Pharm Res, 2001. **18**(7): p. 1006-11.

27. A. Choucair, P.S. Lim, and A. Eisenberg, *Active loading and tunable release of doxorubicin from block copolymer vesicles.* Langmuir, 2005. **21**(20): p. 9308-9313

CHAPTER 4

DISPOSITION OF NANOPARTICLES AND AN ASSOCIATED LIPOPHILIC PERMEANT FOLLOWING TOPICAL APPLICATION TO THE SKIN

Disposition of nanoparticles and an associated lipophilic permeant following topical application to the skin

Xiao Wu[1], Gareth J. Price [2] and Richard H. Guy[1]

[1] Department of Pharmacy and Pharmacology, University of Bath, Claverton Down, Bath, BA2 7AY, UK

[2] Department of Chemistry, University of Bath, Claverton Down, Bath, BA2 7AY, UK

Abstract

Purpose: To determine the disposition of nanoparticles (NP) and an associated, lipophilic, model "active" on and within the skin following topical application. **Methods**: Fluorescein methacrylate and Nile Red-containing polystyrene and polymethylmethacrylate NP were prepared to differentiate the fate of the polymeric vehicle on and within the skin from that of the active ingredient. Fluorescein methacrylate was covalently introduced into the polymer, and NR was dispersed in the NP, which were characterized by dynamic light scattering, transmission electron microscopy and NMR. *In-vitro* skin permeation experiments were performed using dermatomed porcine skin. Post-treatment with NP formulations, the skin surface was either cleaned carefully with physiological buffer, or was simply dried with tissue, and then immediately visualized by confocal microscopy. **Results**: The mean NP diameters were less than 100 nm. Confocal images showed that NP were located post-treatment in skin "furrows" and around hair follicles. Surface cleaning with buffer removed the former but not all of the latter. At the skin surface, Nile Red remained in part associated with NP, but release of the "active" clearly occurred to some extent followed by its penetration into deeper layers of the stratum corneum (SC). **Conclusions**: The polymeric NP studied did not penetrate beyond the superficial SC but showed some affinity for hair follicles, and were able to release an associated "active" into the skin.

Keywords: Nanoparticles, skin, penetration, polystyrene, poly-(methyl methacrylate), confocal microscopy, stratum corneum.

4.1 Introduction

Recently, polymeric nanoparticles (NP) have been proposed as carriers for drugs and other active agents administered by topical administration. Examples include anti-inflammatory drugs [1, 2], anti-infective drugs [3], vitamins and sunscreens [4-6]. It has been claimed that drug-loaded NP achieve sustained release and consequently improve the therapeutic effect of dermatological formulations [2, 3]. More importantly, NP can increase the stability of sensitive actives by protecting the molecules in a polymeric shell. Based on this, NP have been incorporated into several commercially available cosmetic products to encapsulate various actives (e.g., vitamin A, Rose extract and wheat germ oil).

The development of topical formulations containing nano-sized materials has also been challenged by mechanistic and toxicity issues. Compared with larger particles, it has been suggested that nanostructures are more likely to penetrate the stratum corneum and gain access to the living cells within the epidermis and dermis. Should this be possible, then systemic exposure might occur (i.e., the nanoparticles being taken up into the blood and distributed to various tissues and organs), presenting thereby a potential toxicity risk for human health [7-10]. Therefore, understanding the topical disposition of both vehicle and active is essential for the use of nano-engineered topical formulations. Whether (and when) the active is released from the vehicle, and the fate of the vehicle itself, are very important questions concerning the safety of nanotechnology. To begin to address these issues, two series of polymeric NP have been prepared in which the polymer was covalently-labelled with fluorescein methacrylate (FMA, Figure 4.1a). A second fluorescent compound, Nile Red (NR, Figure 4.1b) was incorporated into the particles to simulate a hydrophobic active. Laser scanning confocal microscopy (LSCM) was used to track both fluorophores after topical application to porcine skin. Porcine skin is a good substitute for human skin having epidermal thickness, lipid composition, permeability, transepidermal water loss and low frequency impedance values which are very similar [11, 12].

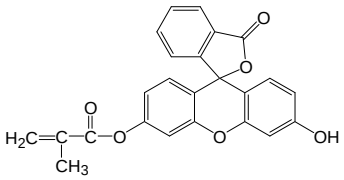

FMA

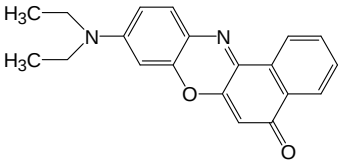

NR

Figure 4.1: Chemical structures of fluorescein methacrylate (FMA) and Nile Red (NR).

4.2 Materials

4.2.1 Tissue

Full thickness porcine skin was obtained from a local slaughterhouse. The skin was cleaned carefully under cold running water. The subcutaneous fat was removed with a scalpel. The remaining tissue was dermatomed to a thickness of ~750 µm. Finally, the dermatomed skin was stored frozen at -20°C for up to a maximum of one month before use.

4.2.2 Chemicals

Fluorescein O-Methacrylate (97% pure), Nile Red (analytical grade) and polystyrene (PS, MW: 44,000) were purchased from Sigma-Aldrich (St. Louis, MO, USA).

Styrene (99% GC), methyl methacrylate (99% GC) and potassium persulfate (KPS) were purchased from Sigma-Aldrich (Gillingham, Dorset, England). Other chemicals used were polymethylmethacrylate (PMMA, MW = 50,000 Fluka Analytical, Steinhelm, Germany), sodium dodecylsulphate (SDS, 99+% GC, Sigma-Aldrich, Japan), ruthenium tetroxide (Taab Laboratories, Aldermaston, England), phosphotungstic acid (Agar Scientific Ltd., Stansted, UK), and chloroform-d_1 (ISOTEC TM, Miamisburg, OH, USA).

4.3 Methods

4.3.1 Nanoparticle (NP) preparation

Before use, inhibitors were removed from the vinyl monomers by passage through an alumina column. The NP were prepared in an inert nitrogen atmosphere by free radical polymerization (see Figure 4.2). 200 cm^3 distilled water was placed in a round bottom flask, with 1 g of SDS added as an emulsifier. The aqueous surfactant solution was deoxygenated with N_2 to remove oxygen. 13 g of deoxygenated styrene were added into the aqueous phase. The mixture was vigorously stirred to form an emulsion and heated to 75°C. To start the polymerization, 0.1 g KPS dissolved in a small amount of water was added. The reaction was allowed to proceed under nitrogen for 3 hours. To prepare fluorescently labeled NP, 0.13 g of FMA and/or 0.13 g NR were mixed with the monomer before addition to the reaction. The same procedure was used for the preparation of PMMA NP.

Reaction A:

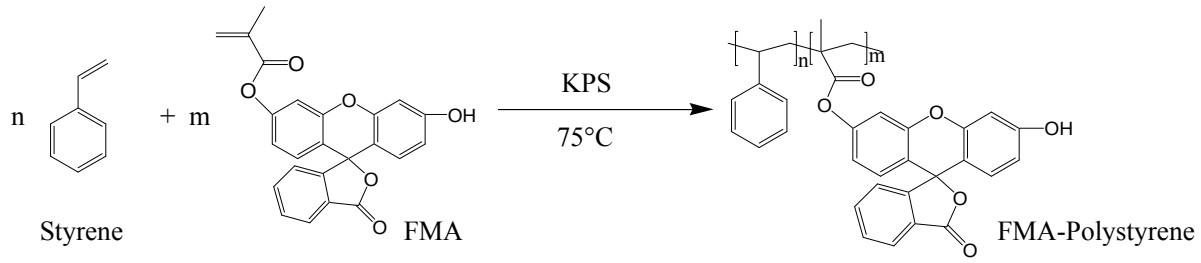

Reaction B:

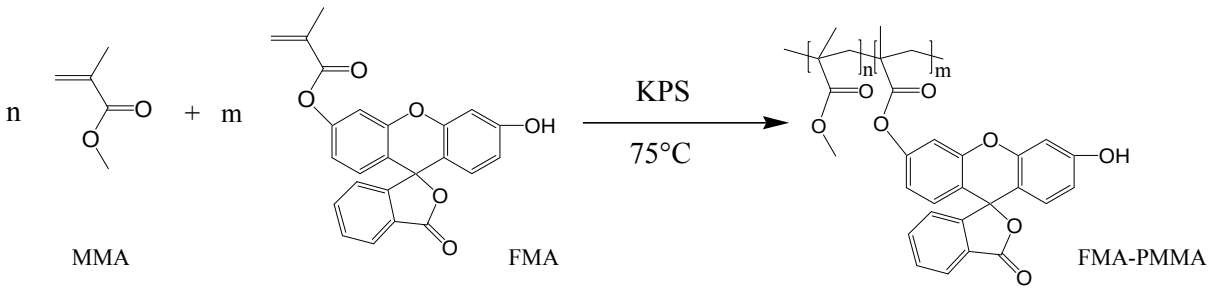

Figure 4.2: Polymerization of styrene (Reaction A) and methyl methacrylate (MMA) (Reaction B) with fluorescein methacrylate (FMA) using potassium persulfate (KPS) as an initiator at 75°C.

4.3.2 NP characterization

The mean size and polydispersity of the NP were measured with dynamic light scattering (DLS BI90Plus, Brookhaven Instruments Corporation, NY, USA). The morphology of the nanoparticles was observed on a JEOL JEM-2000 TEM at an accelerating voltage of 120kV. Each sample was prepared by casting a drop of NP dispersion onto a 300-mesh copper grid covered with carbon film. TEM images of PS NP were obtained as positively stained preparations by placing samples in ruthenium tetroxide vapour for 1 hr. TEM images of PMMA NP were obtained as negatively stained preparations by placing samples in phosphotungstic acid for 1 hour. ^{1}H NMR spectra were recorded in deuterated chloroform ($CDCl_3$) on a Bruker Avance™ III spectrometer (Billerica, MA, USA) operating at 400 MHz. Prior to analysis, the NP were washed with water and acetone to remove SDS and unreacted compounds, and freeze-dried (Heto PowerDry PL3000, Thermo Electron corporation, Waltham, MA, USA).

4.3.3 *In vitro* skin permeation

Before the experiment, the hairs were trimmed as close as possible to the skin surface. Skin permeation experiments were performed in vertical Franz diffusion cells thermostated at 37°C. The excised tissue was clamped between the donor and receptor compartments exposing a diffusion area of 3.8 cm^2. The receptor compartment was filled with physiological buffer (pH = 7.4); the donor compartment held 1 cm^3 of the NP formulation and was covered with Parafilm. After 6 hrs of exposure, the cell was dismantled, and the skin surface was either cleaned carefully with physiological buffer or was simply patted dry with tissue and then immediately visualized by confocal microscopy.

4.3.4 Laser scanning confocal microscopy (LSCM)

The skin was examined using a LSM 510 Invert Laser Scanning Microscope (Carl Zeiss, Jena, Germany). The system was equipped with an argon laser (excitation line at 488 nm) and a HeNe laser (excitation line at 543 nm). A Plan-Neofluar 10×/0.3 objective, an EC Plan-Neofluar 40×/1.30 oil DIC M27 objective and a Plan-Apochromat 63×/1.40 oil DIC M27 objective were used. Confocal

images were obtained in the plane parallel to the sample surface (xy-mode), or in the plane perpendicular (optical sectioning z-stack mode).

4.4 Results

4.4.1 NP characterization

Table 4.1 summarizes the properties of the NP formulations used in the *in vitro* permeation experiments.

Table 4.1: Properties of the PS and PMMA nanoparticulate (NP) formulations examined [a]

NP Formulation	Dyes included	Mean size (nm)	Polydispersity
PS	None	28.8	0.135
PS-FMA	FMA	28.0	0.141
PS-FMA-NR	FMA and NR	30.9	0.118
PMMA	None	79.0	0.171
PMMA-FMA	FMA	99.9	0.163
PMMA-FMA-NR	FMA and NR	68.5	0.133

[a.] PS = polystyrene; PMMA = polymethylmethacrylate; FMA = fluorescein methacrylate; NR = Nile Red

The individual NP were spherical and smooth as shown in Figure 4.3. The mean diameter of PS NP was less than 50 nm, while the PMMA NP were almost twice as large; these findings were confirmed by dynamic light scattering.

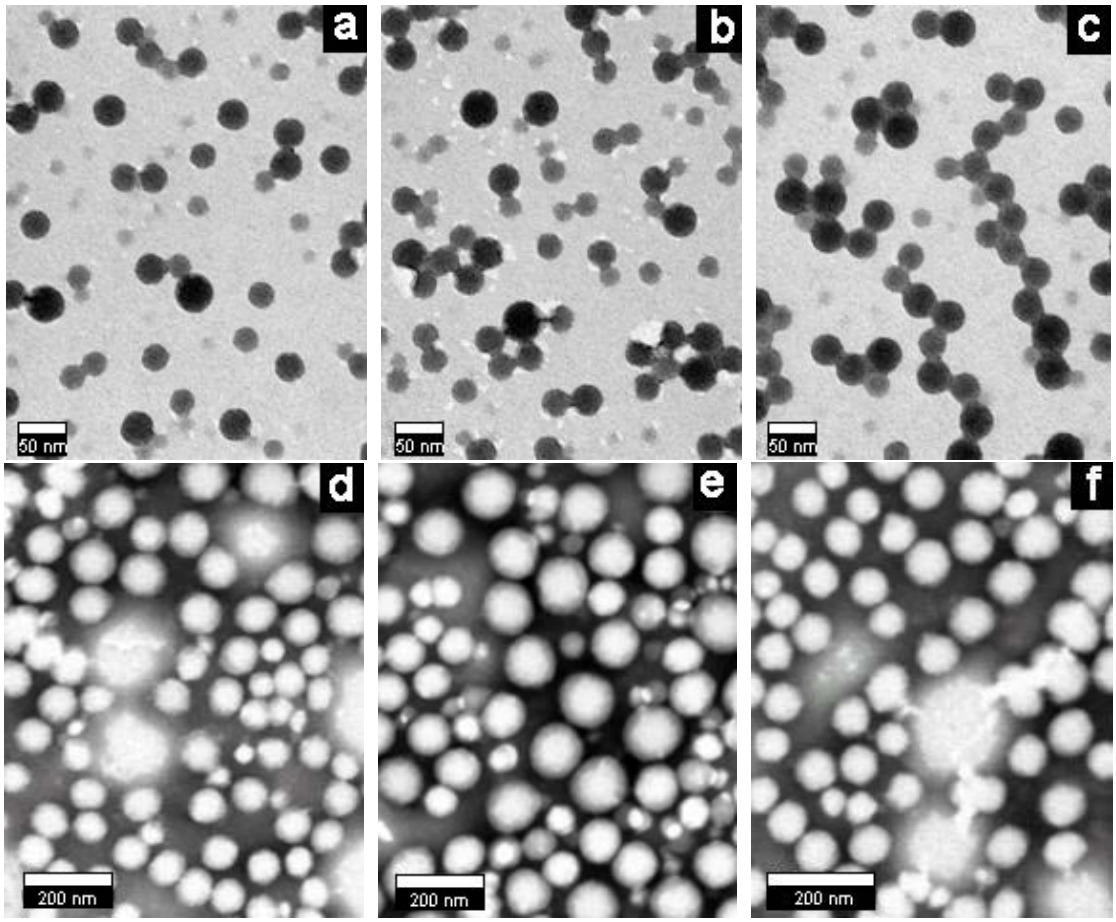

Figure 4.3: Transmission electron micrograph of PS and PMMA nanoparticles stained with ruthenium tetroxide (a, b and c, scale bar = 50 nm) or phosphotungstic acid (d, e, and f, scale bar = 200 nm). (a) Polystyrene NP alone, (b) polystyrene with fluorescein methacrylate (FMA) polymerized, (c) polystyrene with FMA polymerized and Nile Red (NR) absorbed, (d) polymethylmethacrylate (PMMA) NP alone, (e) PMMA with FMA polymerized, and (f) PMMA with FMA polymerized and NR absorbed.

Proton NMR spectra of polystyrene, FMA, PMMA and the two copolymers are shown in Figure 4.4. Those of the copolymers show signals from either PS or PMMA and FMA even after extensive dissolution/reprecipitation, indicating that FMA is covalently bound to the polymer.

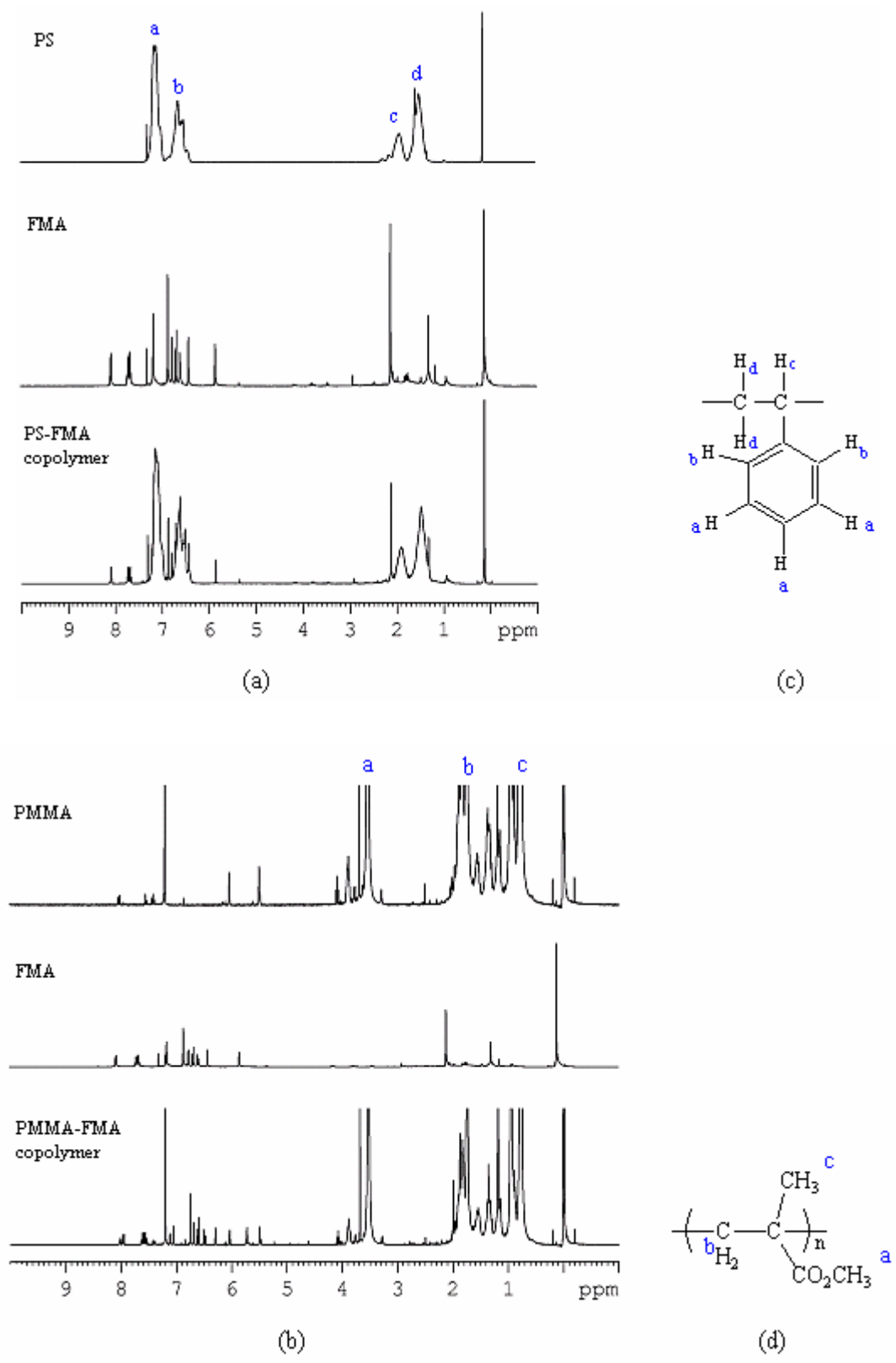

Figure 4.4: ^{1}H NMR spectra for (a) PS, FMA and PS-FMA copolymer, and (b) PMMA, FMA and PMMA-FMA copolymer, together with the structures and chemical shift assignments of (c) PS, and (d) PMMA.

4.4.2 LSCM images

Nile Red is commonly used to stain intracellular lipids, because it has an intense and stable red fluorescent emission under the excitation of HeNe laser at 543 nm. It is also a useful model for a topical/transdermal active because of its high lipophilicity (log $P_{o/w} > 3$) [13] and suitable molecular weight (318.4 $g.mol^{-1}$). FMA is a fluorescent monomer containing a polymerizable methyl acrylate functional group which can react with styrene and MMA. Under excitation at 488 nm, FMA generates a bright green fluorescence, which locates the NP as the dye is covalently bound to polymer. The use of NR and FMA allowed the fate of the NP and of the model lipophilic active to be monitored independently and simultaneously in the same experiment.

4.4.2.1 Control experiments

For each formulation, two control experiments were performed to validate the methodology used. Firstly, PS and PMMA nanoparticle formulations without FMA were separately applied to the skin surface. Figures 4.5a and 4.5d show the resulting confocal images, which manifest only very weak green fluorescence that is endogenous to the SC. When the fluorescently-labelled NP formulations were applied to the skin, distinctly different LSCM images were observed when the skin was either cleaned properly, or not cleaned at all. Figures 4.5b and 4.5e from the latter samples show that the NP were located in the skin furrows and around the hair follicles. In contrast, when the skin was cleaned (Figures 4.5c and 4.5f), there was almost no residual fluorescence, suggesting that the NP had remained at the surface and were then easily removed by the simple washing procedure.

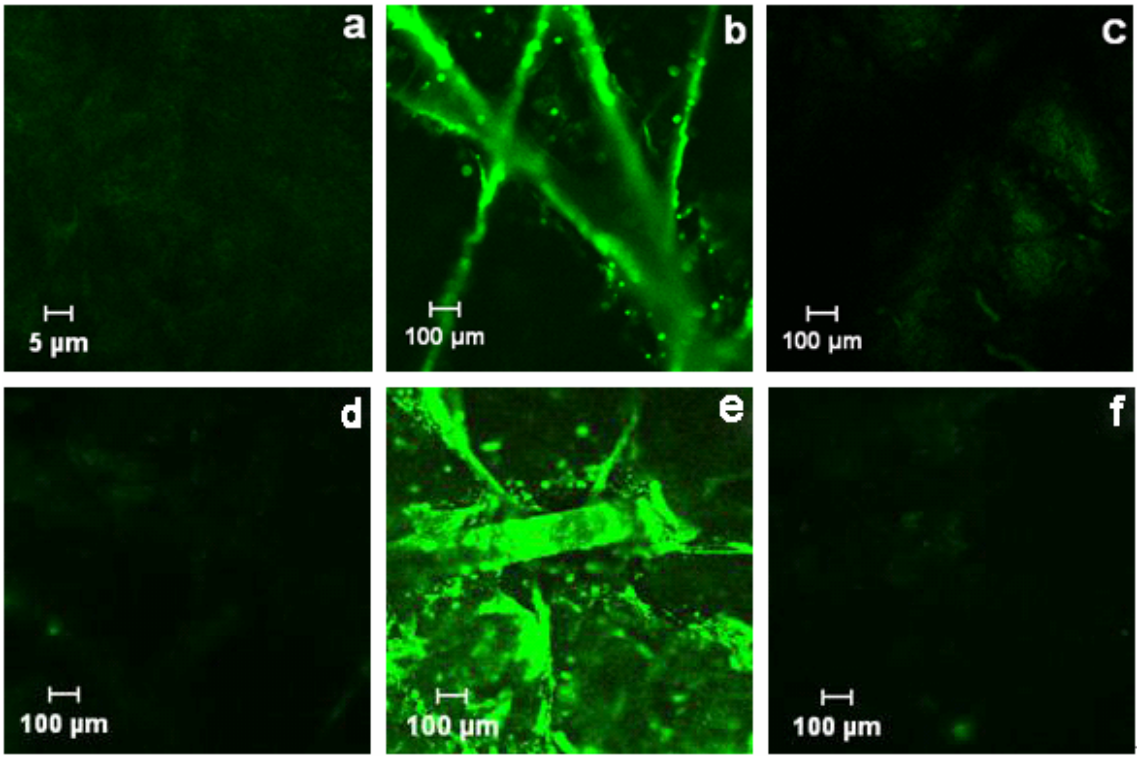

Figure 4.5: LSCM images of the skin surface following a 6-hour application of PS (panels a, b, c) or PMMA nanoparticles (panels d, e, f). In panels a and d, the NP were not fluorescently labelled with FMA and only a weak green fluorescence from the skin itself is seen. In panels b and e, the NP were fluorescently tagged and the skin surface was not cleaned before imaging; bright green fluorescence is apparent in the skin furrows and around the hair follicles. In panels c and f, the skin surface was cleaned before the confocal images were obtained; only the residual autofluorescence from the skin is observed suggesting that the NP had been effectively removed by the cleaning procedure.

4.4.2.2 LSCM images of skin treated with dual-labelled fluorescent NP without surface cleaning

For skin samples treated with dual fluorophore-labelled NP formulations, LSCM images were acquired using multitracking-mode with excitation wavelengths set at 488nm and 543nm. The fluorescence emission from the two dyes was captured separately and overlaid. Figure 4.6 and Figure 4.7 illustrate the disposition of the NP and of Nile Red on and within the skin, the surface of which was not cleaned at the end of the application period, of the polystyrene and

polymethylmethacrylate formulations, respectively. Location of the NP is shown by green fluorescence (from FMA covalently attached to the polymer), while the presence of Nile Red is highlighted in red. For the polystyrene formulation, NP and NR are seen on the skin surface and show clear residence in the skin furrows and around the follicular openings (Figures 4.6a and 4.6b). Overlay of green and red fluorescence in Figure 4.6c clearly emphasizes the co-localization of NP and active.

To examine the fate of the formulation as a function of depth into the skin, the tissue was mechanically sectioned post-treatment and then examined by LSCM at a plane beyond the mechanical section. The dispositions of NP and NR are shown in Figures 4.6d and 4.6e, respectively. Both images highlight a short, trimmed hair shaft on which NP and NR are co-localized. Again, NP are at the surface and NR is seen there too. However, separation of NR from the nanoparticles is apparent (Figure 4.6f, the overlay) with some permeation of the "active" to the deeper skin layers.

The corresponding images for the polymethylmethacrylate NP containing NR are in Figure 4.7. Co-localization of the fluorophores in skin furrows (Figures 4.7a and 4.7b) is again observed, although the overlay (Figure 4.7c) suggests that Nile Red has already been released to some extent at the skin surface. The cross-sectioned images (Figures 4.7d, 4.7e and 4.7f) reveal similar behaviour and again highlight an intensely labelled hair stub.

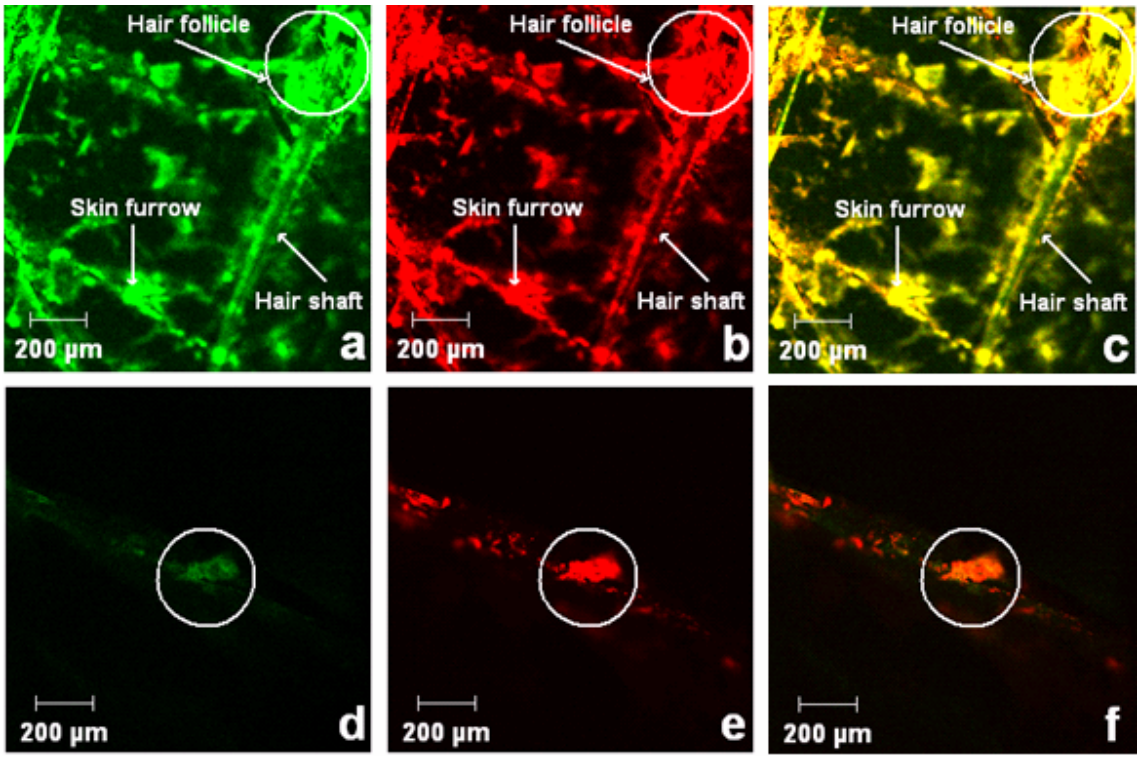

Figure 4.6: LSCM images (×10) from skin treated with fluorescently-labelled polystyrene NP (31 nm diameter) containing the model active NR. Panels a and b show fluorescence emission from the skin surface from the NP (panel a) and NR (panel b), respectively. Panel c shows the overlay of panels a and b and the co-localization of NP and "active" at the skin surface. Panels d and e illustrate cross-sectional images, respectively highlighting fluorescence from the NP and from NR. A distinctly labelled, short, trimmed hair is visible. Panel f is the overlay of panels d and e and suggests some permeation of released NR to the deeper skin layers.

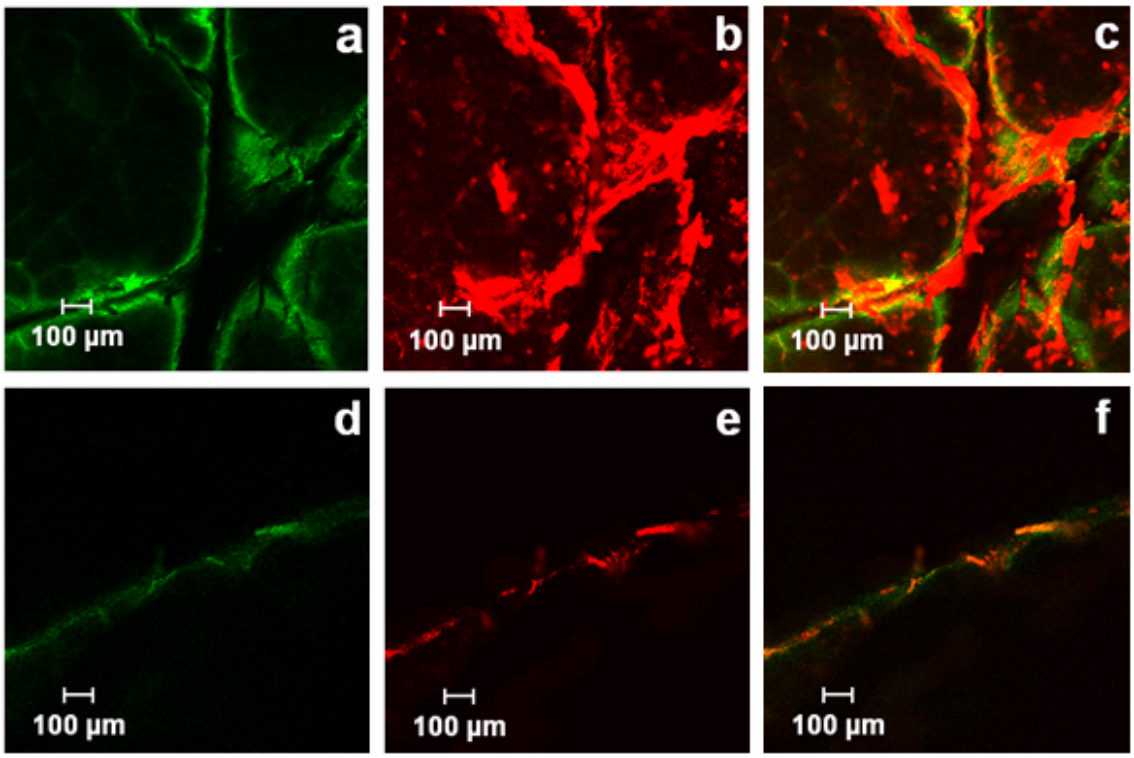

Figure 4.7: LSCM images (×10) from skin treated with fluorescently labelled polymethylmethacrylate NP (69 nm diameter) containing the model active NR. Panels a and b show fluorescence emission from the skin surface from the NP (panel a) and NR (panel b), respectively. Panel c shows the overlay of panels a and b, the presence of NP in the skin furrows and the release of NR from the NP at the skin surface. Panels d and e illustrate cross-sectional images, respectively highlighting fluorescence from the NP and from NR. Another short hair stub is visibly labelled. Panel f is the overlay of panels d and e and again reveals some degree of separation between NP and NR.

4.4.2.3 LCSM images of skin treated with dual-labelled fluorescent NP after surface cleaning

When the skin surface was properly cleaned by washing with buffer at the end of the 6-hour experiment (as opposed to simply drying off residual solution with a paper tissue), the LSCM images were significantly different. Using the dual-labelled polystyrene NP, post-cleaning there was very little green fluorescence visible (Figure 4.8a) other than that probably attributable to skin autofluorescence. In contrast, red fluorescence from NR was clearly visible around the

corneocytes, presumably reflecting the affinity of the lipophilic “active” for the SC intercellular lipid domains Figure 4.8b). Self-evidently, the overlay (Figure 4.8c) of Figures 4.8a and 4.8b reveals only the NR released from the NP prior to their removal by the surface cleaning procedure.

Further examination of the treated skin by optically sectioning the tissue in 1μm steps is shown in Figure 4.8d. The uptake of NR into the deeper SC is apparent. The appearance of green background autofluorescence can also be seen and demonstrates no greater intensity than that seen in control (untreated) samples, confirming that this signal is not due to the presence of the fluorescently-labelled polymer (data not shown).

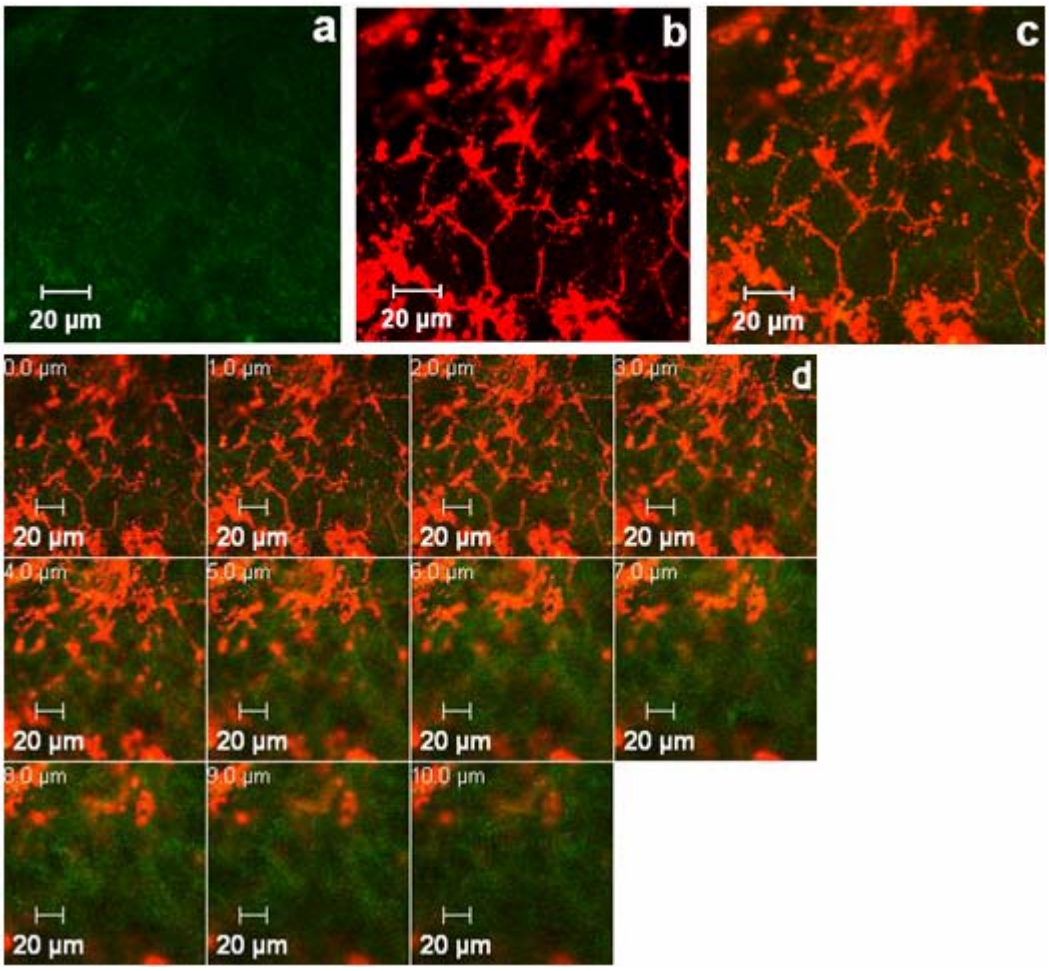

Figure 4.8: LSCM images (×63) from skin treated with fluorescently-labelled polystyrene NP (31 nm diameter) containing the model active. At the end of a 6-hour application, the skin surface was cleaned thoroughly with buffer and then dried. Panel a shows an almost complete absence of fluorescent NP at the surface suggesting that residual formulations had been effectively removed by washing. In contrast, panel b shows that NR had been released from the NP and had entered the lipid-rich intercellular space between the corneocytes. The overlay (panel c) and the 1 µm optical sections down to 10 µm confirm the uptake of "active" into the deeper SC; the weak autofluorescence of the skin itself becomes progressively apparent in the later sections.

The results from the poly-(methyl methacrylate) NP, when the skin surface is properly cleaned at the end of the application period, are similar. Figure 4.9a shows that no residual fluorescence from the NP is visible on the skin. On the other hand, NR has been released from the NP and has remained on/within the SC post-cleaning (Figure 4.9b and overlay Figure 4.9c). Only on hair follicles were the NP incompletely removed by skin washing (Figure 4.9d), and co-localization with the "active" was apparent (Figures 4.9e and 4.9f).

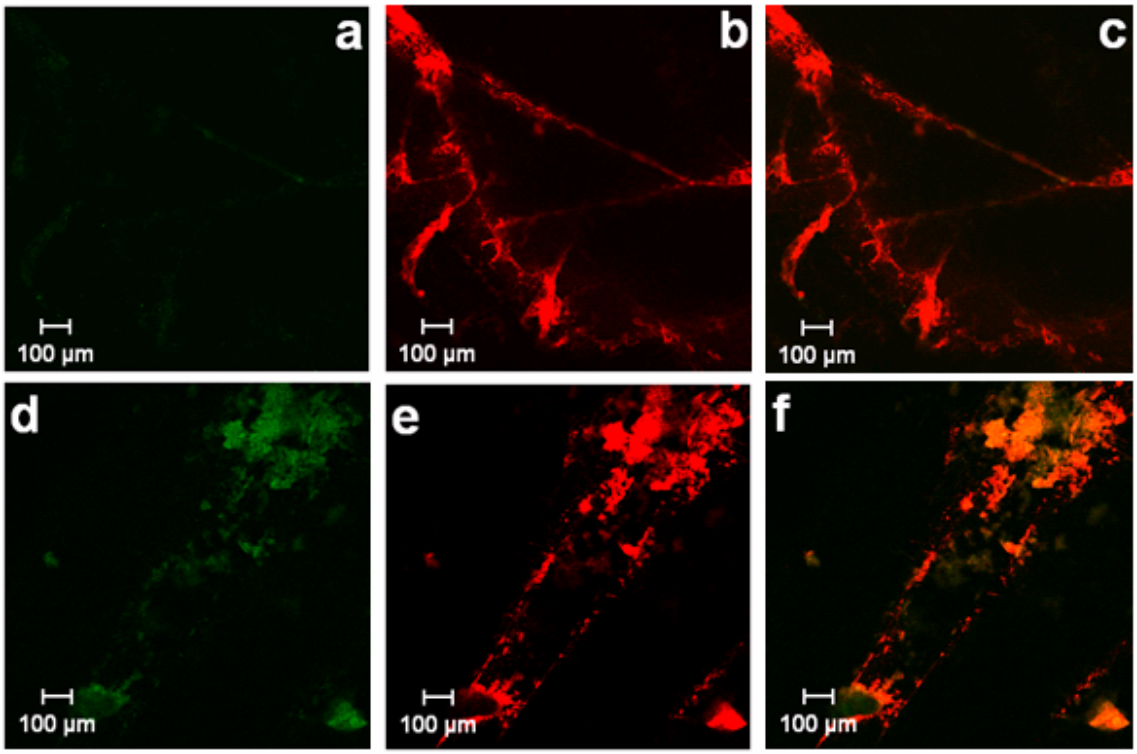

Figure 4.9: LSCM images from skin treated with fluorescently-labelled polymethylmethacrylate NP (69 nm diameter) containing NR. After a 6-hour application, the skin was thoroughly cleaned with buffer and dried. Panel a shows no residual presence of NP post-washing, while panel b (and overlay panel c) indicates that NR was released from the NP on/into the SC. Only on hair follicles were NP retained after cleaning (panel d) and co-localization of NR on these appendages was observed (panel e and overlay panel f).

4.5 Discussion

The confocal images presented in Figures 4.6 - 4.9 allow the following, principal conclusions to be drawn: (a) NP made of polystyrene or polymethylmethacrylate do not appear able to pass

beyond the most superficial layers of the SC following a topical application lasting 6 hours; (b) the NP show affinity for sequestration in skin furrows and on and around follicles; thorough cleaning can remove the former but not necessarily the latter; (c) the associated hydrophobic active (NR) is released from the NP and is able to diffuse into the deeper layers of the SC, from which it is not removed by surface cleaning.

The lack of penetration of NP across intact SC is perhaps not too surprising. It is difficult to envisage how a NP might traverse the SC transcellularly (which would involve uptake into corneocytes and translocalization through these cells). Equally, transport in the intercellular channels (100 nm width) of a ~50 nm diameter particle also seems unlikely given that the intercorneocyte space is filled with multiple lipid bilayers. The rigidity of the NP used in this study further undermines the possibility of their permeation across the barrier, as has been suggested in earlier work comparing the uptake of a lipophilic sunscreen from a nanoemulsion and from rigid NP made of cellulose acetate phthalate [5]. Parenthetically, from a practical standpoint, the fact that NP are retarded at the skin surface may be a distinct advantage for a sunscreen formulation, especially if they are able to create an occlusive film as well, from which the active may be slowly released over a prolonged period [14].

The issue of particle rigidity has also been addressed by comparing standard lipid-based vesicles with specially-designed elastic species [15, 16]. While the penetration of such elastic vesicles across the entire SC has not been equivocally demonstrated, evidence for enhanced “active” transport, and even for the presence of intact vesicles in deeper parts of the SC, has been reported [16].

Certainly, as has been observed here, it is clear that an “active” associated with topically applied NP can be released from the carrier and diffuse into the SC [4, 17, 18]. As reported elsewhere [3, 6, 19, 20], the delivery of the “active” will depend upon its physicochemical properties, its interaction with the nano-carrier, the manner of its association with the particle (surface adhesion, encapsulation, or a mixture of the two), as well as the dimensions and properties (hydrophobicity, hydrophilicity, charge, biodegradability) of the NP themselves.

Further work may be anticipated to explore in greater depth the potential of NP formulations to target “actives” to the hair follicles, for example, or to create a homogeneous and substantive surface film from which prolonged and controlled release may be achieved. Equally, while the penetration of NP across intact SC seems unlikely to pose a toxicological concern, the risk associated with contact to a damaged or diseased skin barrier merits considerable additional research.

Acknowledgements

Supported by the European Commission 6th Research and Technological Development Framework Programme (NAPOLEON: NAnostructured waterborne POLymEr films with OutstaNding properties) and a University Research Scholarship for Xiao Wu.

References

1. S. Miyazaki, A. Takahashi, W. Kubo, J. Bachynsky, and R. Loebenberg, *Poly n-butylcyanoacrylate (PNBCA) nanocapsules as a carrier for NSAIDs: in vitro release and in vivo skin penetration.* J Pharm Pharm Sci, 2003. **6**(2): p. 238-45.
2. J. Luengo, B. Weiss, M. Schneider, A. Ehlers, F. Stracke, K. Konig, K.H. Kostka, C.M. Lehr, and U.F. Schaefer, *Influence of nanoencapsulation on human skin transport of flufenamic acid.* Skin Pharmacol Physiol, 2006. **19**(4): p. 190-7.
3. H. Lboutounne, J.F. Chaulet, C. Ploton, F. Falson, and F. Pirot, *Sustained ex vivo skin antiseptic activity of chlorhexidine in poly(epsilon-caprolactone) nanocapsule encapsulated form and as a digluconate.* J Control Release, 2002. **82**(2-3): p. 319-34.
4. R. Alvarez-Roman, G. Barre, R.H. Guy, and H. Fessi, *Biodegradable polymer nanocapsules containing a sunscreen agent: preparation and photoprotection.* Eur J Pharm Biopharm, 2001. **52**(2): p. 191-5.
5. B.I. Olvera-Martinez, J. Cazares-Delgadillo, S.B. Calderilla-Fajardo, R. Villalobos-Garcia, A. Ganem-Quintanar, and D. Quintanar-Guerrero, *Preparation of polymeric nanocapsules containing octyl methoxycinnamate by the emulsification-diffusion technique: penetration across the stratum corneum.* J Pharm Sci, 2005. **94**(7): p. 1552-9.
6. B. Luppi, T. Cerchiara, F. Bigucci, R. Basile, and V. Zecchi, *Polymeric nanoparticles composed of fatty acids and polyvinylalcohol for topical application of sunscreens.* J Pharm Pharmacol, 2004. **56**(3): p. 407-11.
7. G. Oberdorster, E. Oberdorster, and J. Oberdorster, *Nanotoxicology: an emerging discipline evolving from studies of ultrafine particles.* Environ Health Perspect, 2005. **113**(7): p. 823-39.
8. G. Oberdorster, A. Maynard, K. Donaldson, V. Castranova, J. Fitzpatrick, K. Ausman, J. Carter, B. Karn, W. Kreyling, D. Lai, S. Olin, N. Monteiro-Riviere, D. Warheit, and H. Yang, *Principles for characterizing the potential human health effects from exposure to nanomaterials: elements of a screening strategy.* Part Fibre Toxicol, 2005. **2**: p. 8.
9. P.J. Borm, D. Robbins, S. Haubold, T. Kuhlbusch, H. Fissan, K. Donaldson, R. Schins, V. Stone, W. Kreyling, J. Lademann, J. Krutmann, D. Warheit, and E. Oberdorster, *The potential risks of nanomaterials: a review carried out for ECETOC.* Part Fibre Toxicol, 2006. **3**: p. 11.

10. P.H. Hoet, I. Bruske-Hohlfeld, and O.V. Salata, *Nanoparticles - known and unknown health risks.* J Nanobiotechnology, 2004. **2**(1): p. 12.

11. N. Sekkat, Y.N. Kalia, and R.H. Guy, *Biophysical study of porcine ear skin in vitro and its comparison to human skin in vivo.* J Pharm Sci, 2002. **91**(11): p. 2376-81.

12. G.A. Simon and H.I. Maibach, *The pig as an experimental animal model of percutaneous permeation in man: qualitative and quantitative observations--an overview.* Skin Pharmacol Appl Skin Physiol, 2000. **13**(5): p. 229-34.

13. S. Lombardi Borgia, M. Regehly, R. Sivaramakrishnan, W. Mehnert, H.C. Korting, K. Danker, B. Roder, K.D. Kramer, and M. Schafer-Korting, *Lipid nanoparticles for skin penetration enhancement-correlation to drug localization within the particle matrix as determined by fluorescence and parelectric spectroscopy.* J Control Release, 2005. **110**(1): p. 151-63.

14. S. Magdassi, *Delivery systems in cosmetics.* Colloids Surface A: Physicochem. Eng. Aspects, 1997. **123-124**: p. 671-679.

15. B.A. van den Bergh, J. Vroom, H. Gerritsen, H.E. Junginger, and J.A. Bouwstra, *Interactions of elastic and rigid vesicles with human skin in vitro: electron microscopy and two-photon excitation microscopy.* Biochim Biophys Acta, 1999. **1461**(1): p. 155-73.

16. P.L. Honeywell-Nguyen, G.S. Gooris, and J.A. Bouwstra, *Quantitative assessment of the transport of elastic and rigid vesicle components and a model drug from these vesicle formulations into human skin in vivo.* J Invest Dermatol, 2004. **123**(5): p. 902-10.

17. B. Muller and J. Kreuter, *Enhanced transport of nanoparticle associated drugs through natural and artificial membranes--a general phenomenon?* Int J Pharm, 1999. **178**(1): p. 23-32.

18. A.M. De Campos, A. Sanchez, and M.J. Alonso, *Chitosan nanoparticles: a new vehicle for the improvement of the delivery of drugs to the ocular surface. Application to cyclosporin A.* Int J Pharm, 2001. **224**(1-2): p. 159-68.

19. A. Rolland, N. Wagner, A. Chatelus, B. Shroot, and H. Schaefer, *Site-specific drug delivery to pilosebaceous structures using polymeric microspheres.* Pharm Res, 1993. **10**(12): p. 1738-1744.

20. P. Calvo, C. Remuñán-López, J.L. Vila-Jato, and M.J. Alonso, *Development of positively charged colloidal drug carriers: chitosan-coated polyester nanocapsules and submicron-emulsions.* Colloid Polym Sci, 1997. **275**(1): p. 46-53.

CHAPTER 5

PREPARATION AND *IN VITRO* EVALUATION OF TOPICAL FORMULATIONS BASED ON POLYSTYRENE-POLY-2-HYDROXYL METHACRYLATE NANOPARTICLES

Preparation and *in vitro* evaluation of topical formulations based on polystyrene-poly-2-hydroxyl methacrylate nanoparticles

Xiao Wu[1], Peter Griffin[2], Gareth J. Price[2] and Richard H. Guy[1]

[1] Department of Pharmacy and Pharmacology, University of Bath, Claverton Down, Bath, BA2 7AY, UK
[2] Department of Chemistry, University of Bath, Claverton Down, Bath, BA2 7AY, UK

Abstract

Purpose: To investigate *ex vivo*, the skin disposition of topically applied nanoparticles, composed of different proportions of polystyrene (PS) and poly-2-hydroxyethyl methacrylate (HEMA), and of an associated, model "active" (Nile Red). **Methods**: PS nanoparticles were prepared with 0, 5, 10 and 20% (w/w) HEMA, and were fluorescently labelled via the covalent incorporation of a small quantity of fluorescein methacrylate during the polymerization procedure. The fluorophore, Nile Red, acted as a model "active" and was associated with the nanoparticles during their preparation. The particles were characterised by dynamic light scattering, transmission electron microscopy and NMR. Nile Red loading was determined by ultracentrifugation. Skin uptake was assessed using porcine tissue in Franz diffusion cells following a 6-hour application of the nanoparticle formulation, and subsequent quantification by stratum corneum (SC) tape-stripping and confocal microscopy. **Results**: Nanoparticle diameters were less than 100 nm. Progressive introduction of HEMA into the particles decreased their hydrophobicity and reduced the extent to which Nile Red was associated with the nanocarriers (thereby lowering the effective applied dose). As a consequence, uptake of Nile Red into the skin, as assessed both by the amounts extracted from the SC tape-strips and by confocal microscopy, was less as the percentage HEMA increased. The confocal results also confirmed that the nanoparticles themselves were unable to move beyond the superficial SC layer, but did show

some affinity for hair follicle openings. **Conclusions**: The loading of a lipophilic "active" into nanoparticles, and its subsequent release when these formulations are applied topically, are sensitive to the composition and the relative hydrophobicity of the carrier.

Keywords: Nanoparticles, skin, stratum corneum, polystyrene, 2-hydroxyethyl methacrylate (HEMA), Nile Red, laser scanning confocal microscopy (LSCM), tape-stripping.

5.1 Introduction

The stratum corneum is the thin (~15 μm) outermost layer of the skin. It has been described as a "brick and mortar" structure [1] in which corneocytes are embedded in an intercellular lipid matrix. The corneocytes are arranged in parallel, overlapping, multicellular stacks perpendicular to the skin surface. The excellent permeability barrier of the skin protects the body against the loss of endogenous substances and from environmental insult [2].

Nanoparticles (NPs), incorporating drug or active ingredients have been employed in pharmaceutical and cosmetic formulations to increase transport into/across the skin, to improve the homogeneity of the vehicle's distribution on the skin, and to modulate flexibly the release of the active to the surface [3-9]. This has proved useful, for example, for those vehicles which are able to form thin, occlusive films which retain photoprotective actives. Increasingly, the physicochemical properties of the nanoparticles (size, charge, etc.) that determine their behaviour once applied to the skin, and the kinetics with which an "active" is released, are being understood, and have formed the basis of earlier research upon which the present study builds.

Here, four polystyrene (PS)-2-hydroxyethyl methacrylate (HEMA) NP formulations were prepared and tested on porcine skin. The influence of polymer hydrophobicity on the skin uptake of Nile Red (NR), a model "active" compound was investigated. As reported previously [10], a small amount of fluorescein methacrylate (FMA) was introduced into the polymerisation process to covalently label the nanoparticles and permit their disposition on and within the skin to be monitored as well. The structures of PS, FMA and HEMA are in Figure 5.1.

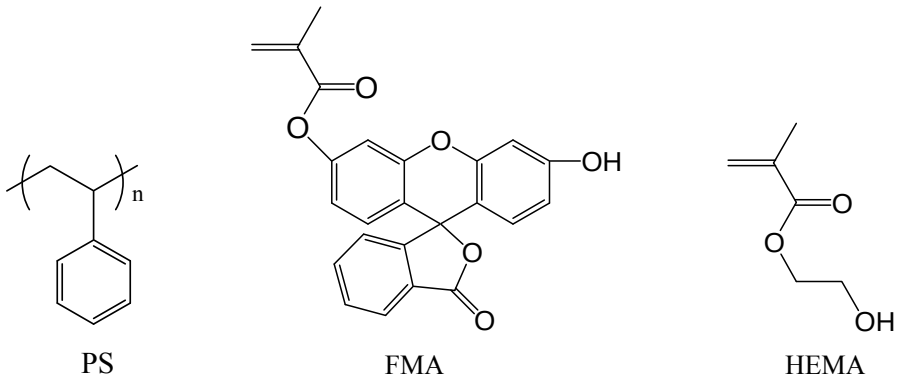

Figure 5.1: The chemical structures of polystyrene (PS), fluorescein methacrylate (FMA) and 2-hydroxyethyl methacrylate (HEMA).

5.2 Materials

5.2.1 Tissue

Full thickness porcine skin was obtained from a local slaughterhouse. The skin was cleaned carefully under cold running water. The subcutaneous fat was removed with a scalpel. The remaining tissue was dermatomed to a thickness of ~750 μm. Finally, the dermatomed skin was stored frozen at -20°C for up to a maximum of one month before use.

5.2.2 Chemicals

Fluorescein O-Methacrylate (FMA, 97% pure), Nile Red (NR, analytical grade) and polystyrene (MW = 44,000) were purchased from Sigma-Aldrich (St. Louis, MO, USA).

Styrene (99% GC), 2-hydroxyethyl methacrylate (HEMA, 98%) and potassium persulfate (KPS) were purchased from Sigma-Aldrich (Gillingham, Dorset, England). Other chemicals used were sodium dodecylsulphate (SDS, 99+% GC, Sigma-Aldrich, Japan), ruthenium tetroxide (Taab Labs, Aldermaston, England), chloroform-d_1 (ISOTEC TM, Miamisburg, OH, USA).

5.3 Methods

5.3.1 NP preparation

Styrene was first purified by passage through an alumina column to remove inhibitors. Nanoparticles were then prepared in an inert nitrogen atmosphere by free radical polymerisation (Figure 5.2). Fluorescein methacrylate (FMA, 0.13 g) and Nile Red (NR, 0.01 g) were dissolved in a 13 g of mixture of styrene and 2-hydroxylethyl methacrylate (HEMA) and deoxygenated under N_2. Four distinct compositions of the monomers were used containing, respectively, 0, 5, 10 and 20% w/w HEMA. Sodium dodecylsulphate (SDS, 1 g), an emulsifier, and potassium persulphate (KPS, 0.1 g), a free radical initiator, were dissolved in 200 ml of distilled water in a round-bottomed flask and degassed under N_2. This solution was then heated to ~75°C before the oil phase was added with vigorous stirring. Polymerisation and NP formation was carried out for 3 hours. The resulting particles contained FMA covalently and randomly incorporated into the PS-HEMA polymer. NR was absorbed on/in the NP.

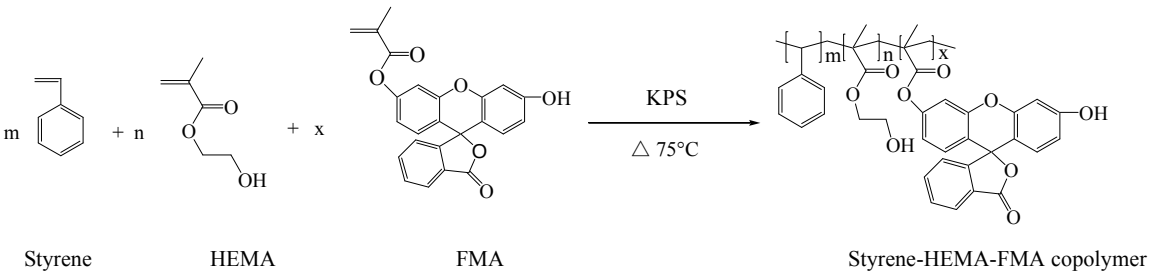

Figure 5.2: Preparation of styrene-2-hydroxyethyl methacrylate (HEMA)-fluorescein methacrylate (FMA) copolymers by emulsion radical copolymerization with potassium persulfate (KPS) at 75°C.

5.3.2 NP characterization

The mean size and polydispersity of the NP were measured by dynamic light scattering (DLS BI90Plus spectrophotometer, Brookhaven Instruments Corporation, NY, USA). NP morphology was observed on a JEOL (JEM-2000) transmission electron microscope (TEM) at an accelerating voltage of 120kV. Each sample was prepared by casting a drop of NP dispersion onto a 300-mesh copper grid covered with carbon film. TEM images of the NP were obtained as positively stained

preparations by placing samples in ruthenium tetroxide vapour for 1 hr [11].

To determine the degree of Nile red incorporation into the nanoparticles, the formulations were filtered (0.45 μm nylon filters, Whatman, Japan) and then subjected to ultracentrifugation at 17000 g for 3 h at 20°C. The supernatant was kept for analysis of Nile Red. The sediment was washed with distilled water to remove surfactant and again centrifuged 17000 g for 3 h. The resulting pellet was freeze-dried, and then dissolved in dichloromethane. Finally, Nile Red in this organic solvent was measured by HPLC (Dionex, Sunnyvale, CA, USA) with fluorescence detection at 559 nm and 630 nm for excitation and emission wavelengths, respectively. A Hypersil BDS C18 (5 μm) 250×4.6 mm column, was used and the mobile phase was dichloromethane pumped at a flow rate of 1 ml/min at 25°C. Each injection was 200 μl. The Nile Red retention time was 5.6 minutes. Nile Red in the supernatant was also measured by HPLC using a mobile phase comprising acetonitrile-water (80:20). The column, injection volume, and temperature were as above. The retention time in this case was 12.1 minutes. ^{1}H-NMR spectra were recorded in deuterated chloroform ($CDCl_3$) on a Bruker Avance™ III spectrometer (Billerica, MA, USA) operating at 400 MHz. Prior to analysis in $CDCl_3$, the NP were washed with water and acetone to remove SDS and unreacted compounds, and freeze-dried (Heto PowerDry PL3000, Thermo Electron Corporation, Waltham, MA, USA).

5.3.3 *In vitro* skin permeation

Visible hairs on the skin were first trimmed as close as possible to the surface. Skin permeation experiments were performed in vertical Franz diffusion cells thermostated at 37°C. The excised tissue was clamped between the donor and receptor compartments exposing a diffusion area of 3.8 cm^2. The receptor phase was physiological buffer (pH = 7.4); the donor compartment held 1 ml of the NP formulation and was covered with Parafilm. After an application lasting 6 hrs, the cell was dismantled, and the skin was immediately either examined by confocal microscopy or tape-stripped to determine the NR concentration profile across the SC.

5.3.4 Laser scanning confocal microscopy (LSCM)

The treated skin was first cleaned with physiological buffer and dried with tissue. The skin was then examined using a LSM 510 Invert Laser Scanning Microscope (Carl Zeiss, Jena, Germany). The system was equipped with both an argon laser (excitation line at 488 nm) and a HeNe laser (excitation line at 543 nm). A Plan-Neofluar 10×/0.3 objective, an EC Plan-Neofluar 40×/1.30 oil DIC M27 objective and a Plan-Apochromat 63×/1.40 oil DIC M27 objective were used. Confocal images were obtained in the plane parallel to the sample surface (xy-mode), or in the plane perpendicular (optical sectioning z-stack mode).

5.3.5 Tape-stripping

A validated tape-stripping procedure was used to assess the depth of NR penetration into the SC and to recover NR from the treated skin [12]. About 20 2.7×2.7 cm^2 tapes were prepared (Scotch® No.845 Book Tape, 3M Media, Broken, Germany). To delimit a fixed area for tape stripping, a 5×5 cm square mask was prepared with a central aperture of 2 cm diameter. A strip of adhesive tape was pressed firmly onto the skin surface, and then removed in a single movement. The direction of stripping was changed with each tape to ensure a more uniform removal of the SC with fewer tape-strips. Before and after each tape-strip, transepidermal water loss (TEWL) across the skin was measured (Aquaflux, Biox Systems Ltd., London, UK) to provide an idea of when most of the SC had been removed and to signal the end of the tape-stripping process. This was considered appropriate when TEWL reached 80 $g^{-1}m^{-2}h$. The tapes were weighed before and after stripping to determine the mass of SC removed. As the density of the tissue is ~1 g/cm^3 [13], the volume of SC removed by each strip is known (assuming uniform coverage of SC on the tape-strip [14]). Then, given that the area stripped is fixed, the thickness of SC removed as tape-stripping proceeds can be found.

5.4 Results and discussion

For each polymerisation, the measured conversions were > 90%. The individual NP were spherical and smooth, as shown by TEM (Figure 5.3). The mean diameter of the NP was less than 100 nm, an observation confirmed by dynamic light scattering (DSC) (Table 5.1).

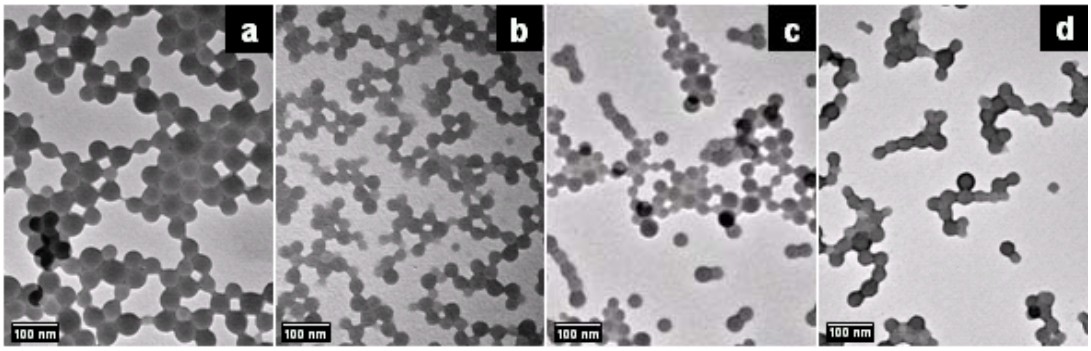

Figure 5.3: Transmission electron microscopy of nanoparticles stained with ruthenium tetroxide. (a) PS; (b) PS-HEMA (95/5); (c) PS-HEMA (90/10); (d) PS-HEMA (80/20). Scale bar = 100 nm.

NR encapsulation varies inversely with the percentage of HEMA co-polymerized into the nanoparticles (Table 5.1). That is, as the hydrophobicity of the particles was reduced (by increasing the amount of HEMA relative to PS), the affinity of the lipophilic dye, Nile Red, for the polymer decreased proportionally. A relatively constant amount of Nile Red was recovered in the supernatant for all nanoparticles, and it is inferred that the remaining fraction of the dye was associated with surfactant micelles.

Table 5.1: Properties of nanoparticle formulations

Nanoparticle formulation	Average diameter (nm)	Polydispersity index	% Nile Red associated	% Nile Red in supernatant
Polystyrene (PS)	73.8	0.092	73.15 ± 1.14	6.43 ± 0.48
PS - 5% HEMA	45.8	0.120	59.42 ± 2.07	6.21 ± 0.35
PS - 10% HEMA	43.2	0.130	41.06 ± 1.85	6.20 ± 0.33
PS - 20% HEMA	36.7	0.165	17.66 ± 1.20	6.20 ± 0.35

Proton NMR spectra of HEMA, polystyrene, and the copolymer are shown in Figure 5.4. The copolymer shows signals from polystyrene and HEMA even after extensive dissolution/reprecipitation. However, because of the polymerization reaction, the copolymers do not have signals at 5.6 and 6.1 ppm, which are present in HEMA's spectrum. While we did not investigate the polymer microstructure in detail, the spectra revealed no evidence of formation of blocks of the two monomers.

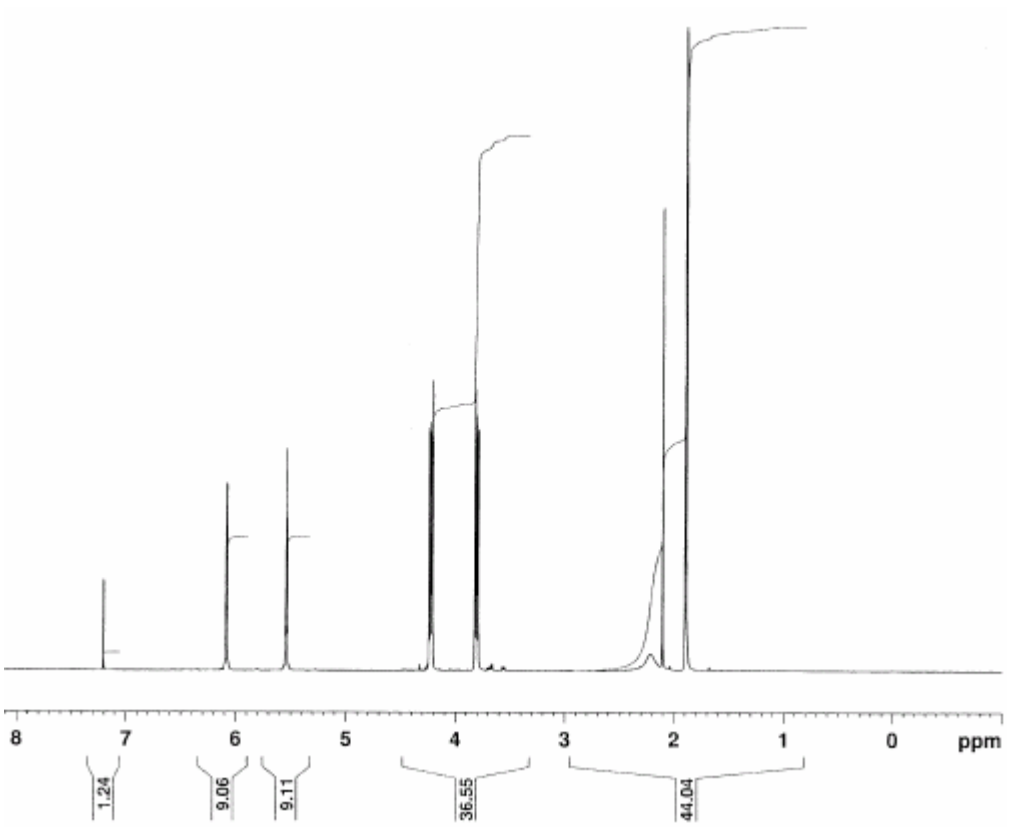
8
7
6
5
4
3
2
1
0
ppm
1.24
9.06
9.11
36.55
44.04

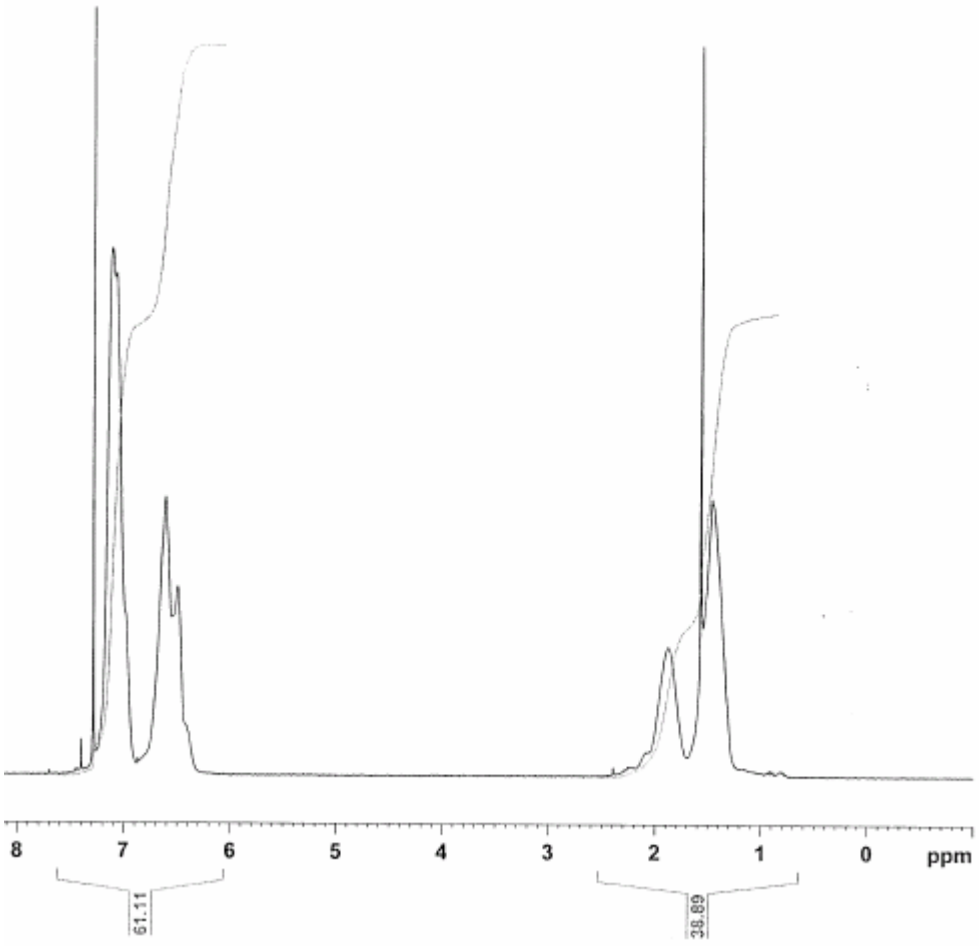
8
7
6
5
4
3
2
1
0
ppm
61.11
38.89

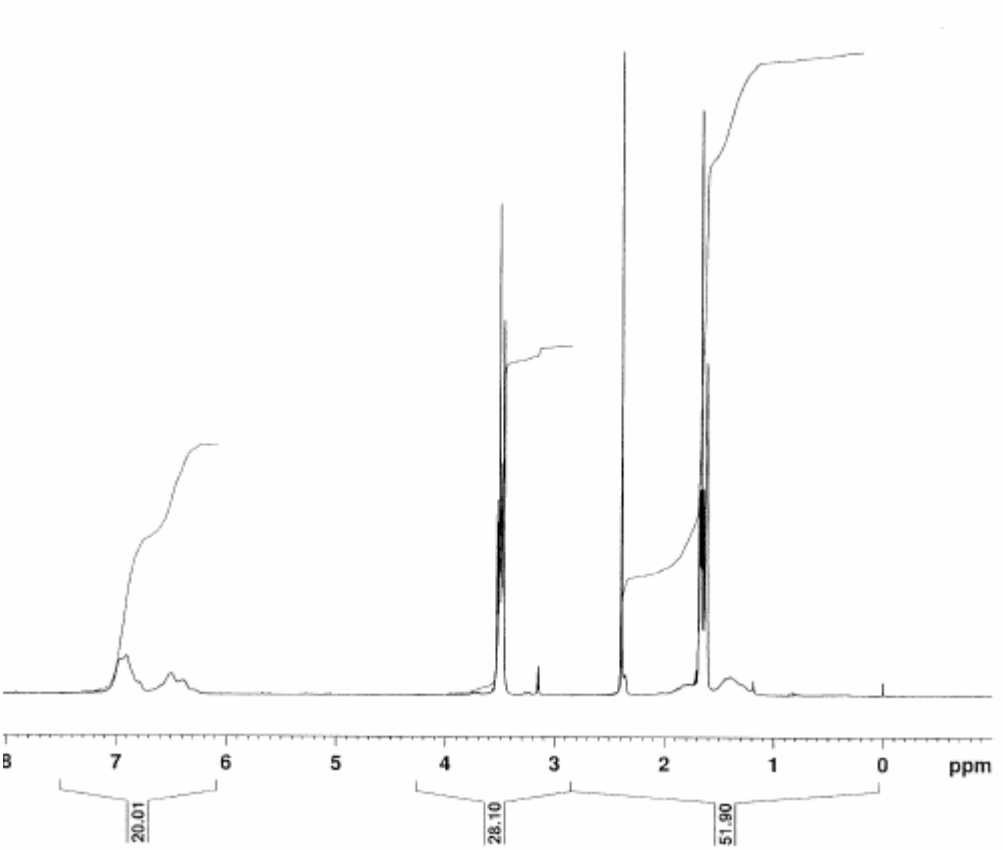

Figure 5.4: ^{1}H NMR spectra of HEMA (top), polystyrene (middle) and their copolymer (bottom).

5.4.1 LSCM results

The dual-fluorescently labeled nanoparticles permitted the simultaneous visualization of the disposition/penetration of the carriers and of the model active (Nile Red) on and within the superficial skin. Moreover, the treated skin could be mechanically cross-sectioned as well, enabling the distribution of the fluorescent probes to be visualized as a function of depth. In this case, the confocality of the microscope used permitted artifacts from the sectioning to be avoided [15, 16].

Figure 5.5 shows LSCM images of skin treated with PS nanoparticles. Localisation and release of Nile Red in skin "furrows" is apparent in the images from the skin surface. However, the green fluorescence from the polymer itself is very weak, suggesting that the cleaning procedure efficiently removed the particles post-treatment. The cross-sectional images confirm

these observations and show that Nile Red is released and penetrates into the deeper SC, in agreement with the results from previous studies [17, 18]. The overlay images of green and red fluorescence reveal only the presence of the latter. The behaviour of PS nanoparticles containing 5% HEMA is shown in Figure 5.6. It is apparent that less Nile Red uptake into the SC has taken place. Once again, the persistence of the particles themselves post-treatment and surface cleaning is poor although there is evidence in Figure 5.6d that the carriers have been noticeably retained on a hair stub, and that the Nile Red has remained largely associated with the polymer here. Again, this observation is consistent with earlier reports in the literature [17]. Figure 5.7 continues the trend seen in Figure 5.6 and illustrates the disposition of PS nanoparticles with 10% HEMA. Affinity of the particles for follicular structures is clearly observed, with the Nile Red co-localised with the polymer. On the skin surface, in contrast, the model active has separated from the carrier. Finally, when the HEMA content in the PS nanoparticles is raised to 20%, the images post-treatment and surface cleaning reveal only very faint red fluorescence, with no sign of retained polymer as shown in Figure 5.8. In this case, the Nile Red loading is very low, such that the driving force for permeation (even supposing an efficient release from the nanoparticle) is low. Overall, the confocal experiments reveal that (i) introducing hydrophilicity into the nanoparticles alters their behaviour on skin; (ii) the disposition of an associated lipophilic “active” (Nile Red) is influenced by nanoparticle properties; (iii) increasing the percentage of HEMA in PS nanoparticles significantly reduces the uptake of Nile Red into the SC; and (iv) there is no evidence that nanoparticles can penetrate beyond superficial SC. The latter conclusion agrees completely with recent findings from multiphoton microscopy experiments tracking the fate of poly-(lactide-co-glycolide) nanoparticles in the SC [19].

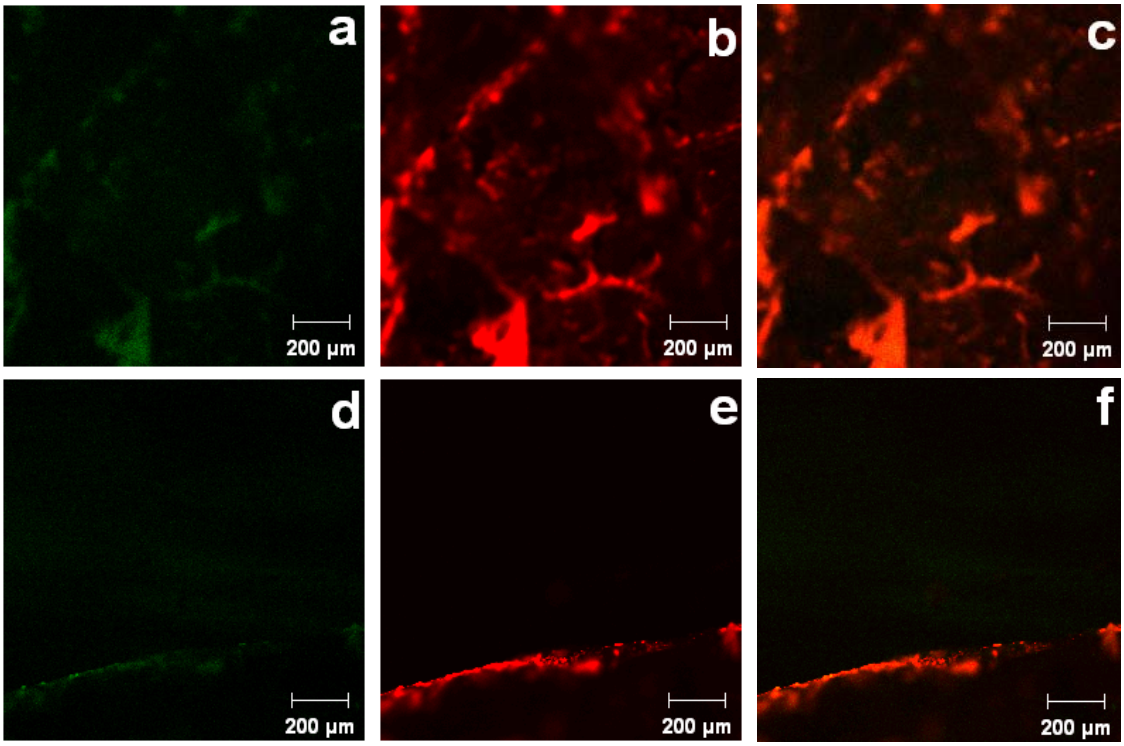

Figure 5.5: PS nanoparticle-treated skin surface (top) and cross-sectional images (below). (a) (d) Green fluorescence from the FMA, indicating the location of the polymer. (b) (e) Red fluorescence from Nile Red. (c) (f) Overlaid images of green and red fluorescence.

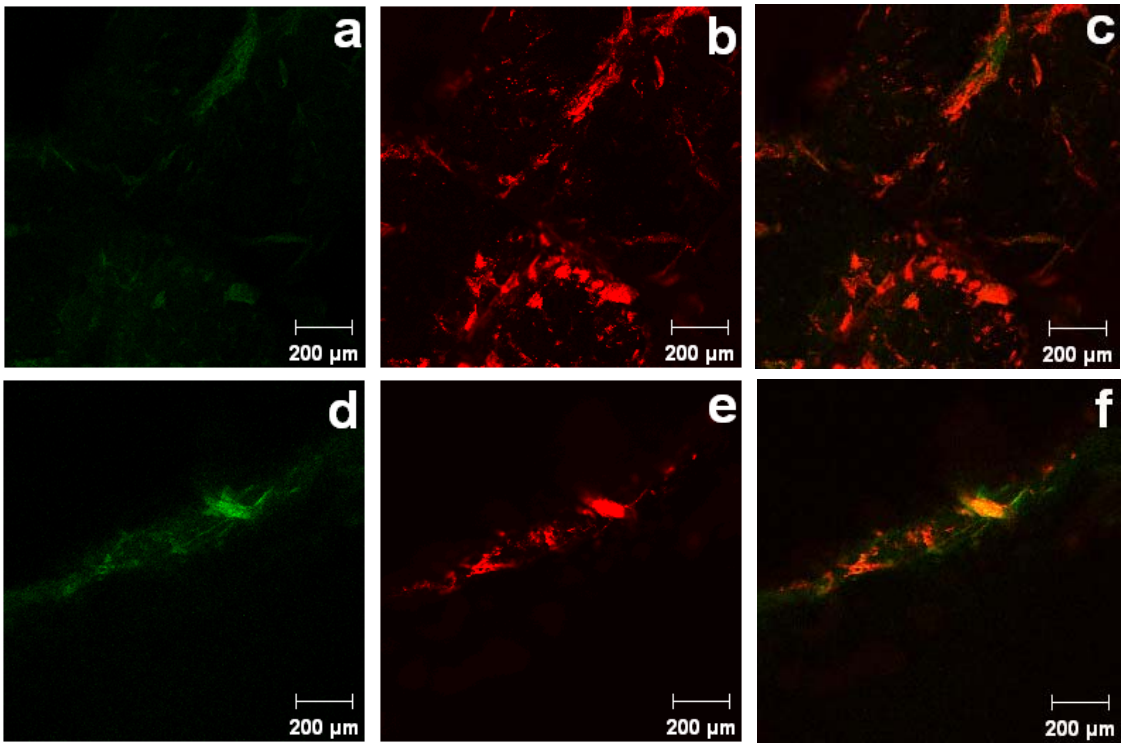

Figure 5.6: PS-5%HEMA nanoparticle-treated skin surface (top) and cross section images (below). (a) (d) Green fluorescence from the FMA, indicating the location of the polymer. (b) (e) Red fluorescence from Nile Red. (c) (f) Overlaid images of green and red fluorescence.

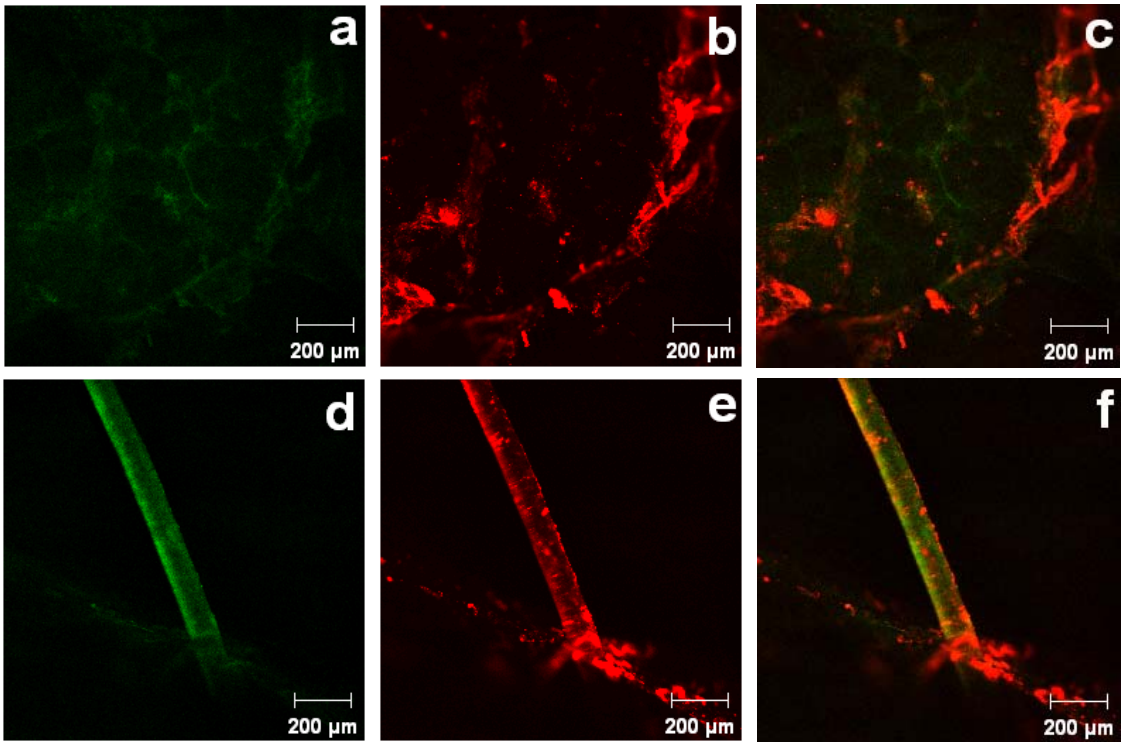

Figure 5.7: PS-10%HEMA nanoparticle-treated skin surface (top) and cross section images (below). (a) (d) Green fluorescence from the FMA, indicating the location of the polymer. (b) (e) Red fluorescence from Nile Red. (c) (f) Overlaid images of green and red fluorescence.

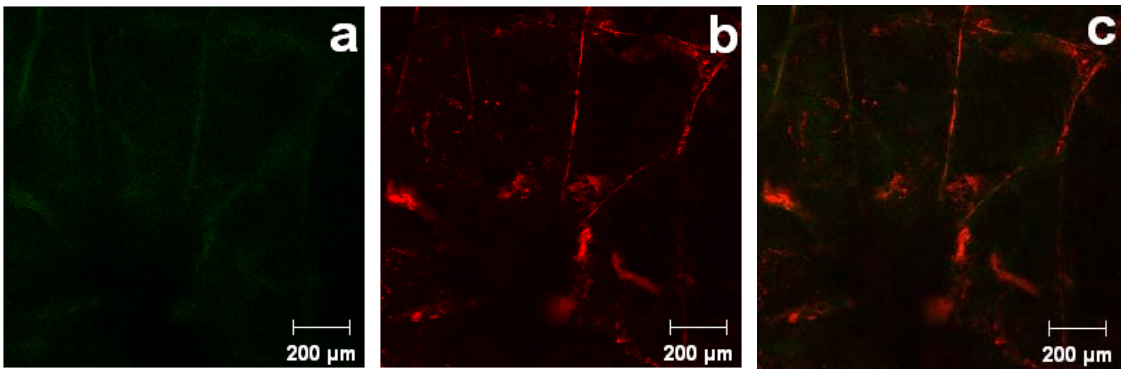

Figure 5.8: PS-20%HEMA nanoparticle-treated skin surface (top). (a) Green fluorescence from the FMA, indicating the location of the polymer. (b) Red fluorescence from NR. (c) Overlaid image of green and red fluorescence. Red fluorescence was not observed in cross section skin samples, due to inefficient Nile Red penetration in the SC.

5.4.2 *In vitro* skin permeation experiments

In all experiments, irrespective of the nanoparticle composition used, no fluorescence (red or green) was ever detected in the receptor phase, confirming the LSCM observations that the disposition of the various formulation compounds was constrained to the SC.

The SC concentration profiles of Nile Red delivered from the four different nanoparticle carriers are in Figure 5.9. From the concomitant measurements of TEWL and of the mass of SC removed on each tape, it was possible (as previously published [14]) to express the concentrations as a function of relative position within the SC, thereby correcting for differences in absolute SC thickness from one porcine skin sample to another. This approach is reflected in the good reproducibility in the obtained results, and the clear separation, in terms of Nile Red uptake, between the nanoparticle formulations.

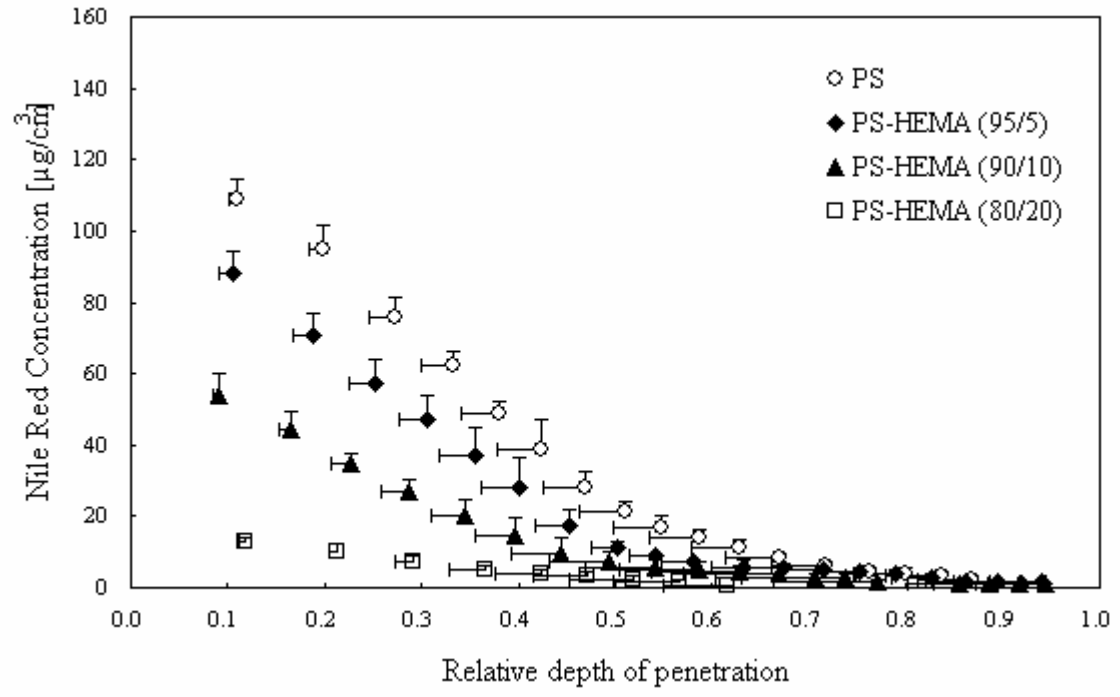

Figure 5.9: Concentration profiles of Nile Red across the SC as a function of relative depth into the membrane (n = 5, mean ± SD). Please note that 0 indicates the SC surface and 1 reflects the SC-stratum granulosum interface).

The integrated amounts of active taken up from each PS-HEMA polymer are displayed in

Figure 5.10 and reinforce the fact that Nile Red penetration into the SC was significantly reduced with each increment in the percentage HEMA incorporated into the polymer. The diminishing load of Nile Red in the nanoparticles as the percentage HEMA was increased (Table 5.1) almost certainly underlies the trend in Figure 5.10. Indeed, if the average amounts of the dye taken up into the SC are divided by the fraction of the active eventually associated with the particles, the ratios are remarkably consistent: 0.17, 0.16, 0.15 and 0.07 for PS, PS–5% HEMA, PS–10% HEMA and PS–20% HEMA, respectively. The apparent divergence for the nanoparticles containing the greatest level of HEMA is probably due, at least in part, to the fact that detection of Nile Red in many of the SC tape-strips following treatment with this formulation was close to or below the limits of quantitation/detection.

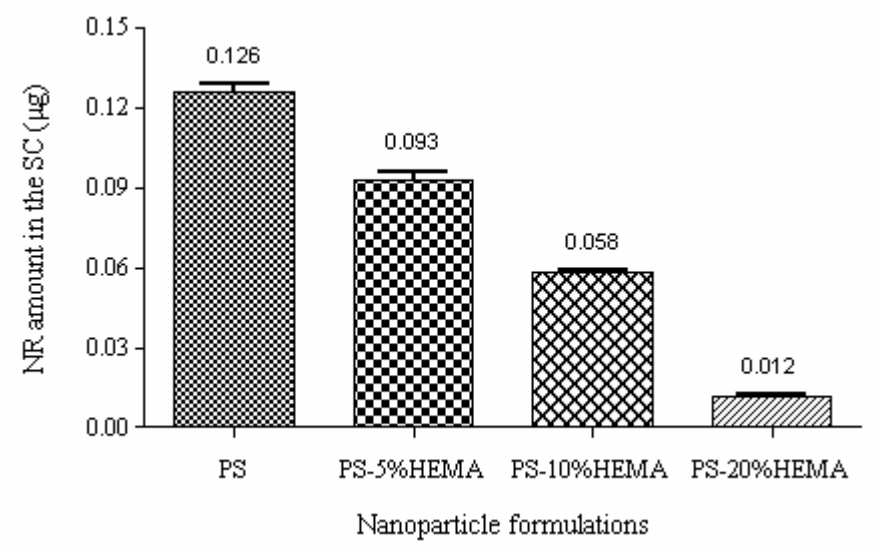

Figure 5.10: Total quantities (in µg) of Nile Red in the SC after a 6-hour application of four NP formulations.

It is appropriate to point out that these findings concur with earlier work from our laboratory [20] in which the SC uptake of Nile Red was observed to decrease as the nanoparticle polymer was changed from PS to poly-caprolactone to cellulose acetate butyrate; in other words, as the polymer became progressively more hydrophilic. As has been seen here, despite employing the same amount of Nile Red in the nanoparticle preparation procedure, the quantity eventually associated with the carrier depends upon polymer properties, and becomes less and less as the

hydrophilicity is increased.

5.5 Conclusions

The incorporation of a lipophilic active into a series of PS nanoparticles was sensitive to the percentage of the hydrophilic co-polymer (HEMA) present. As a result, the uptake of the active into the skin, following topical application of the nanoparticle formulations, was less efficient as the hydrophobicity of the carriers decreased. Results from confocal microscopy and SC tape-stripping experiments underpin these conclusions and provide valuable tools, therefore, for the development and optimisation of future nanoparticle formulations.

Acknowledgements

Supported by the European Commission 6th Research and Technological Development Framework Programme (NAPOLEON: NAnostructured waterborne POLymEr films with OutstaNding properties) and a University Research Scholarship for Xiao Wu.

References

1. P.W. Wertz and D.T. Downing, *Stratum corneum: biological and biochemical considerations*, in *Transdermal drug delivery*, J. Hadgraft and R.H. Guy, Editors. 1989, Marcel Dekker, Inc.: New York. p. 1-22.
2. J.A. Bouwstra, P.L. Honeywell-Nguyen, G.S. Gooris, and M. Ponec, *Structure of the skin barrier and its modulation by vesicular formulations.* Prog Lipid Res, 2003. **42**(1): p. 1-36.
3. I.P. Kaur and R. Agrawal, *Nanotechnology: a new paradigm in cosmeceuticals.* Recent Pat. Drug Delivery Formulation, 2007. **1**(2): p. 171-182.
4. R. Alvarez-Roman, G. Barre, R.H. Guy, and H. Fessi, *Biodegradable polymer nanocapsules containing a sunscreen agent: preparation and photoprotection.* Eur J Pharm Biopharm, 2001. **52**(2): p. 191-5.
5. B. Luppi, T. Cerchiara, F. Bigucci, R. Basile, and V. Zecchi, *Polymeric nanoparticles composed of fatty acids and polyvinylalcohol for topical application of sunscreens.* J Pharm Pharmacol, 2004. **56**(3): p. 407-11.
6. J. Luengo, B. Weiss, M. Schneider, A. Ehlers, F. Stracke, K. Konig, K.H. Kostka, C.M. Lehr, and U.F. Schaefer, *Influence of nanoencapsulation on human skin transport of flufenamic acid.* Skin Pharmacol Physiol, 2006. **19**(4): p. 190-7.
7. H. Lboutounne, J.F. Chaulet, C. Ploton, F. Falson, and F. Pirot, *Sustained ex vivo skin antiseptic activity of chlorhexidine in poly(epsilon-caprolactone) nanocapsule encapsulated form and as a digluconate.* J Control Release, 2002. **82**(2-3): p. 319-34.
8. J. Shim, H. Seok Kang, W.S. Park, S.H. Han, J. Kim, and I.S. Chang, *Transdermal delivery of mixnoxidil with block copolymer nanoparticles.* J Control Release, 2004. **97**(3): p. 477-84.
9. S. Miyazaki, A. Takahashi, W. Kubo, J. Bachynsky, and R. Loebenberg, *Poly n-butylcyanoacrylate (PNBCA) nanocapsules as a carrier for NSAIDs: in vitro release and in vivo skin penetration.* J Pharm Pharm Sci, 2003. **6**(2): p. 238-45.
10. X. Wu, G.J. Price, and R.H. Guy, *Preparation and in vitro evaluation of topical formulations based on polystyrene-poly-2-hydroxyl methacrylate nanoparticles.* J Control Release, 2008. Submitted.
11. J.S. Trent, J.I. Scheinbeim, and P.R. Couchman, *Ruthenium tetraoxide staining of polymers for electron microscopy.* Macromolecules, 1983. **16**(4): p. 589-598.
12. V.P. Shah, *Topical dermatological drug product NDAs and ANDAs - in vivo bioavailability, bioequivalence, in vitro release and associated studies*. 1998, US Depart. of Health and Human Services: Rockville. p. 1-9.
13. R.L. Anderson and J.M. Cassidy, *Variation in physical dimensions and chemical composition of human stratum corneum.* J Invest Dermatol, 1973. **61**(1): p. 30-2.

14. Y.N. Kalia, F. Pirot, and R.H. Guy, *Homogeneous transport in a heterogeneous membrane: water diffusion across human stratum corneum in vivo.* Biophys J, 1996. **71**(5): p. 2692-700.

15. D.M. Shotton, *Confocal scanning optical microscopy and its application for biological specimens.* J Cell Sci, 1989. **94**: p. 175-206.

16. R. Alvarez-Roman, A. Naik, Y.N. Kalia, H. Fessi, and R.H. Guy, *Visualization of skin penetration using confocal laser scanning microscopy.* Eur J Pharm Biopharm, 2004. **58**(2): p. 301-16.

17. R. Alvarez-Roman, A. Naik, Y.N. Kalia, R.H. Guy, and H. Fessi, *Skin penetration and distribution of polymeric nanoparticles.* J Control Release, 2004. **99**(1): p. 53-62.

18. J.A. Bouwstra, F.E.R. Dubbelaar, G.S. Gooris, and M. Ponec, *The lipid organisation in the skin barrier.* Acta Derm Venereol Suppl (Stockh), 2000. **208**: p. 23-30.

19. F. Stracke, B. Weiss, C.M. Lehr, K. Konig, U.F. Schaefer, and M. Schneider, *Multiphoton microscopy for the investigation of dermal penetration of nanoparticle-borne drugs.* J Invest Dermatol, 2006. **126**(10): p. 2224-33.

20. X. Wu, B. Biatry, C. Cazeneuve, and R.H. Guy, *The influence of polymeric materials and particle size on the disposition of a lipophilic chemical in the stratum corneum from nanoparticulate/mesoparticulate formulations*. 2008, University of Bath: Bath.

CHAPTER 6

TOPICAL FORMULATIONS CONTAINING CHARGED NANOPARTICLES: LOCAL DISPOSITION AND POTENTIAL FOR DRUG DELIVERY

Topical formulations containing charged nanoparticles: local disposition and potential for drug delivery

Xiao Wu[1], Katharina Landfester[2], Anna Musyanovych[2] and Richard H. Guy[1]

[1] Department of Pharmacy and Pharmacology, University of Bath, Claverton Down, Bath, BA2 7AY, UK

[2] Department of Organic Chemistry III, University of Ulm, Albert-Einstein-Allee 11, 89081, Germany

Abstract

The objective of this preliminary investigation was to examine the disposition of charged nanoparticles on and within the skin following their topical application and to explore whether the formulations have potential utility for the local delivery of an associated "active" substance. Three nanoparticles (~100 nm in diameter) were investigated: cationic amino-functionalized polystyrene, an anionic carboxy-functionalized polystyrene and anionic poly-(L-lactide). To track the fate of the particles, each was associated with the fluorophore, N-(2,6-diisopropylphenyl)-perylene-3,4-dicarboximine (PMI). Formulations were applied to excised skin for 6-hours. After cleaning the skin surface post-treatment, the skin was either examined by laser scanning confocal microscopy or subjected to repeated tape-stripping and subsequent analysis of the stratum corneum (SC) removed for the presence of PMI. The cationic nanoparticles showed clear affinity for the negatively-charged skin surface (in contrast to the anionic carriers) and delivered a significantly greater amount of the model "active" (PMI) into the SC.

Keywords: Charged nanoparticles, skin, stratum corneum, confocal microscopy, tape-stripping.

6.1 Introduction

The use of nanoparticles as constituents of topical formulations of drug and cosmetics is receiving significant attention [1-9]. It is clear that the nature of the particle, such as its size and composition, will influence the manner in which it interacts with the skin and the rate and extent with which it releases an associated "active" species into the stratum corneum (SC), the outermost, and principal barrier layer of the membrane [10, 11].

As part of a wider-ranging investigation into the disposition of nanoparticles on the skin, this preliminary study considers the impact of using charged polymers to prepare the carriers. Given that an important perceived benefits of nanoparticles in topical formulations is their ability to persist on, or in close proximity to, the skin surface, and given that (under normal physiological conditions), the skin carries a net negative charge [12, 13], it seems logical to anticipate that nanoparticles supporting different overall charges would likely interact with the barrier in clearly distinctive manners.

Here, the fates of those nanoparticle formulations (one cationic, two anionic), containing a fluorescent dye as a model "active" compound, are evaluated by confocal microscopy and by SC tape stripping following their application to the porcine skin *in vitro* (an accepted surrogate for the human barrier) [14, 15].

6.2 Materials

6.2.1 Tissue

Full thickness porcine skin was obtained from a local slaughterhouse. The skin was cleaned carefully under cold running water. The subcutaneous fat was removed with a scalpel. The remaining tissue was dermatomed to a thickness of ~ 750 μm. Finally, the dermatomed skin was stored frozen at -20°C for up to a maximum of one month before use.

6.2.2 Chemicals

N-(2,6-diisopropylphenyl)-perylene-3,4-dicarboximine (PMI) (BASF, Germany), ruthenium tetroxide (Taab Laboratories, Aldermaston, England), phosphotungstic acid (Agar Scientific Ltd., Stansted, UK).

6.2.3 Nanoparticle formulations

The three nanoparticle formulations considered were prepared from the following polymers: (a) positively-charged, amino-functionalized polystyrene (PS-NH_3^+), (b) negatively-charged, caroboxy-functionalized polystyrene (PS-CO_2^-), and (c) negatively charged, biodegradable poly-(L-lactide) (PLL^-). The miniemulsion preparation method and subsequent characterization of the particles are reported in detail elsewhere [16]. The fluorophore PMI (structure in Figure 6.1) was associated with each of the nanoparticles and provided a means with which to track the performance of the carriers once applied to the skin. Table 6.1 summarizes the key characteristics of the nanoparticles examined.

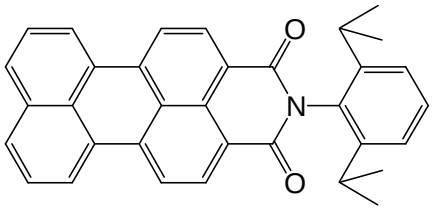

Figure 6.1: Chemical structure of N-(2,6-diisopropylphenyl)-perylene-3,4-dicarboximine (PMI).

Table 6.1: Key characteristics of nanoparticle formulations examined.

NP formulations	Particle size (nm)	Solid content (wt %)	Zeta-potential (mV)	Incorporated PMI (mg/g polymer)
PS-NH_3^+	115	2.5	48	0.51
PS-CO_2^-	87	5.7	-21	0.29
PLL^-	138	2.6	-34	0.57

6.3 Methods

6.3.1 Nanoparticle morphology

Nanoparticles were observed on a JEOL JEM-2000 TEM at an accelerating voltage of 120kV. Each sample was prepared by casting a drop of the nanoparticle dispersion onto a 300-mesh copper grid covered with carbon film. TEM images were obtained either as positively stained preparations by placing samples in ruthenium tetroxide vapour for 1 hr or as negatively stained preparations by placing samples in phosphotungstic acid vapour for 1 hr.

6.3.2 *In vitro* skin permeation experiments

First, any visible hairs were trimmed as close as possible to the skin surface. Experiments were performed in vertical Franz diffusion cells thermostated at 37°C. The excised skin was clamped between the donor and receptor compartments exposing a diffusion area of 3.8 cm^2. The receptor medium was physiological buffer (pH = 7.4); the donor solution was 1 ml of a nanoparticle dispersion formulation. After a 6-hour application under occlusive conditions, the cell was dismantled, and the skin surface was cleaned with buffer. The skin surface was either examined by confocal microscopy or subjected to repeated adhesive tape-stripping to determine the distribution of PMI across the SC [17].

6.3.3 Laser scanning confocal microscopy (LSCM)

Confocal microscopy was performed with a LSM 510 Invert Laser Scanning Microscope (Carl Zeiss, Jena, Germany). The system was equipped with an argon laser at 488 nm. A Plan-Neofluar 10×/0.3 objective was used. Confocal images were obtained in the plane parallel to the sample surface (xy-mode), or in the plane perpendicular (optical sectioning z-stack mode).

6.3.4 Tape-stripping

A validated SC tape-stripping procedure was used to recover PMI form the treated skin and to assess its spatial distribution in the barrier [18].

6.3.5 High performance liquid chromatography (HPLC)

PMI on the tape strips was extracted into acetonitrile via their immersion in the solvent at least 12 hrs. These extracts were then filtered (Whatman PTFE filter, 0.45μm) into HPLC vials and assayed chromatographically (Dionex, Sunnyvale, CA, USA) with fluorescence detection at 479 nm and 539 nm for excitation and emission wavelengths, respectively. A Hypersil BDS C18 (5 μm) 250×4.6 mm column, was used and the mobile phase was tetrohydrofuran pumped at a flow rate of 1 ml/min at 25°C. Each injection was 200 μl. The PMI retention time was 8.5 minutes.

6.4 Results and discussion

The individual NP were round and smooth, (Figure 6.2) and their mean diameters were less than 150 nm.

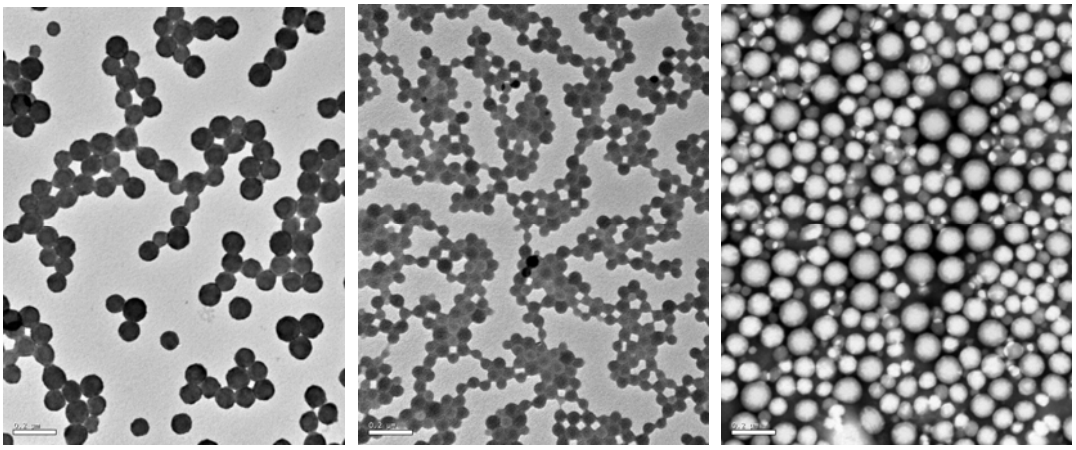

Figure 6.2: Transmission electron microscopy images of functionalized fluorescent nanoparticles. Left panel: Amino-functionalized polystyrene latex particles ($PS\text{-}NH_3^+$); Middle panel: Carboxyl-functionalized polystyrene latex particles ($PS\text{-}CO_2^-$); Right panel: Biodegradable poly (L-lactide) particles (PLL^-).

Immediately after dismantling the diffusion cells, and removing the remaining formulation (but before properly washing the surface), a macroscopic inspection of the skin revealed a striking difference between $PS\text{-}NH_3^+$ and $PS\text{-}CO_2^-$ nanoparticles (Figure 6.3). A clear affinity for

the skin of the cationic formulation could be discerned, consistent of course with the net negative charge on the skin membrane.

Figure 6.3: Illustrative photographs of skin treated with either cationic PS-NH_3^+ (left) or anionic PS-CO_2^- (right) prior to surface cleaning.

Confocal images were observed either in the usual way by optically sectioning the tissue at progressively increasing depth, or following a mechanical cross section and examination of the sample beyond the cut plane to avoid any physical artifacts caused by the sectioning procedure [19].

Figure 6.4 shows representative image from skin treated with PS-NH_3^+. Bright green fluorescence from PMI is seen at the surface, where the nanoparticles are likely to be concentrated, and across the SC (the much weaker signals from the deeper epidermis is due to the skin autofluorescence – control image not shown). These results contrast dramatically with those in Figure 6.5 and Figure 6.6 from skin treated with the anionic PS-CO_2^- and PLL^-, respectively. For these nanoparticles, little evidences of either their retention on the skin surface or that they have significantly released PMI into the SC can be seen.

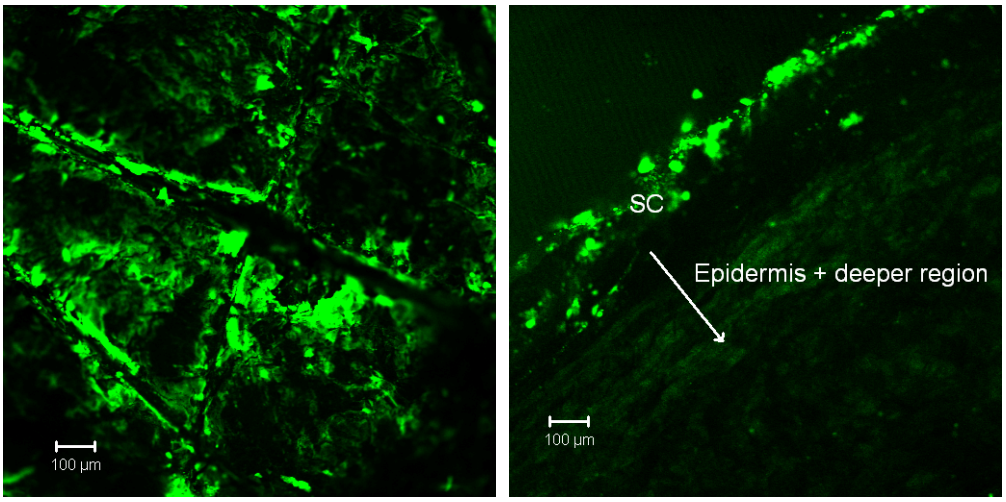

Figure 6.4: LSCM images (×10) of porcine skin following a 6-hour application of PS-NH_3^+ nanoparticles. Left panel: Skin surface image showing bright green fluorescence from PMI. Right panel: Image of a mechanical cross-section. PMI fluorescence is visualized only in the SC.

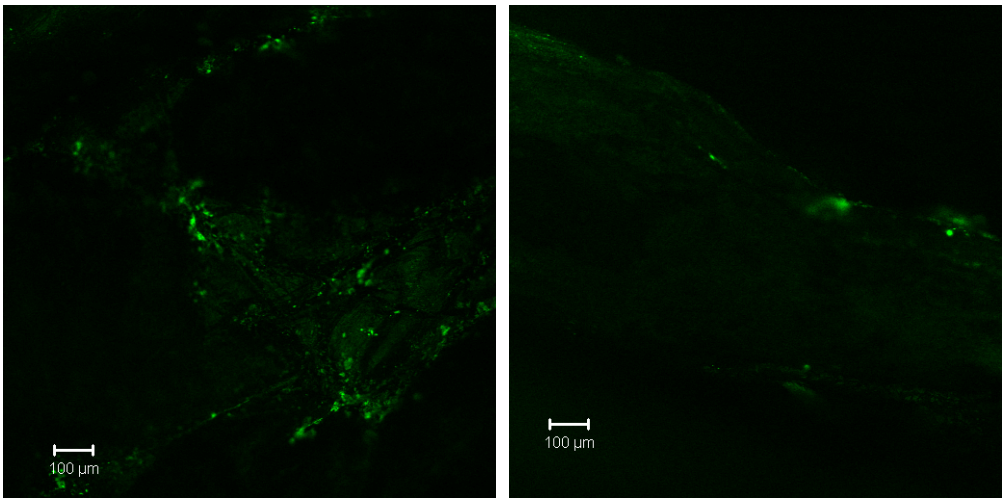

Figure 6.5: LSCM images (×10) of porcine skin following a 6-hour application of PS-CO_2^- nanoparticles. Left panel: Skin surface image showing minimal fluorescence. Right panel: Image of a mechanical cross-section. PMI fluorescence is barely visible.

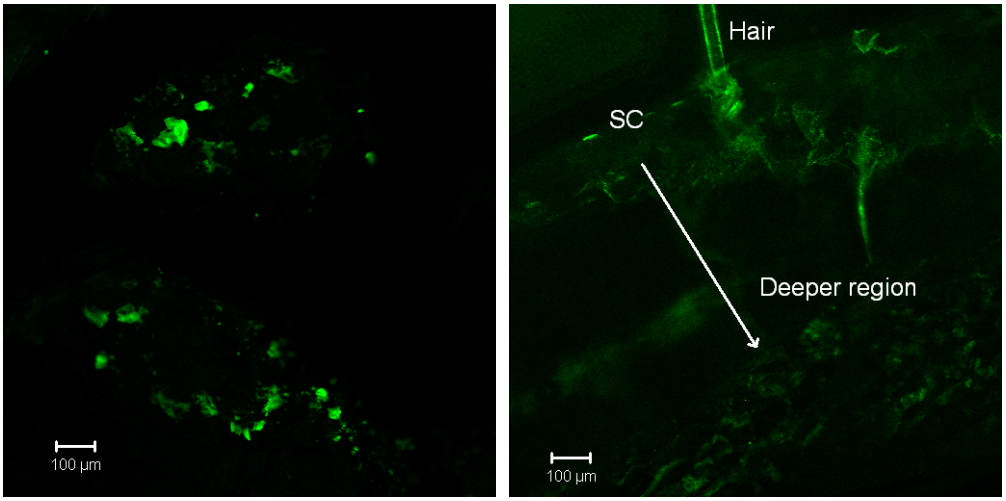

Figure 6.6: LSCM images (×10) of porcine skin following a 6-hour application of PLL⁻ nanoparticles for 6-hour. Left panel: Skin surface image showing negligible fluorescence. Right panel: Image of a mechanical cross-section. The fluorescence is very weak in all skin layers.

In the *in vitro* skin permeation experiments, independent of the nanoparticle formulation used, no PMI was ever detected in the receptor compartment; that is, PMI did not penetrate beyond the superficial SC, an observation consistent with the LSCM results.

The SC tape-strips were extracted and the PMI in each layer was determined by HPLC. Before extraction, the pre-weighed tapes were weighed again to assess the mass of SC removed on each strip and hence the relative depth of PMI penetration into the membrane [20]. The SC concentration profiles of the fluorophore after a 6-hour application of the different nanoparticle formulations are shown in Figure 6.7, and the integrated, total uptakes of PMI into the SC are in Figure 6.8. There is a statistically significant difference observed with "delivery" of the active being clearly better from the cationic nanoparticles, as compared to those of opposite charge. The results concur with the LSCM observations and suggest that an electrostatic attraction between positively charged nanoparticles and the negatively-charged skin may offer an advantageous attribute to improve the transfer of an active from the formulations into the SC.

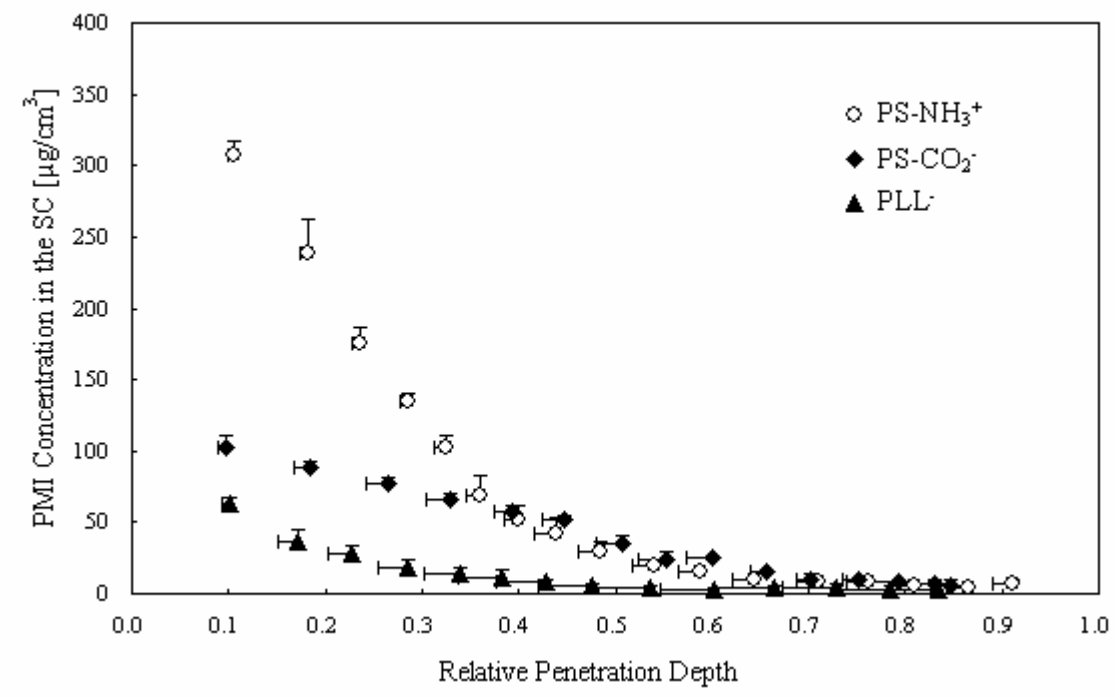

Figure 6.7: Concentration profiles of PMI across the SC (n = 5, mean ± SD). The relative depth of penetration is zero at the skin surface, and has a value of 1 at the SC-stratum granulosum interface.

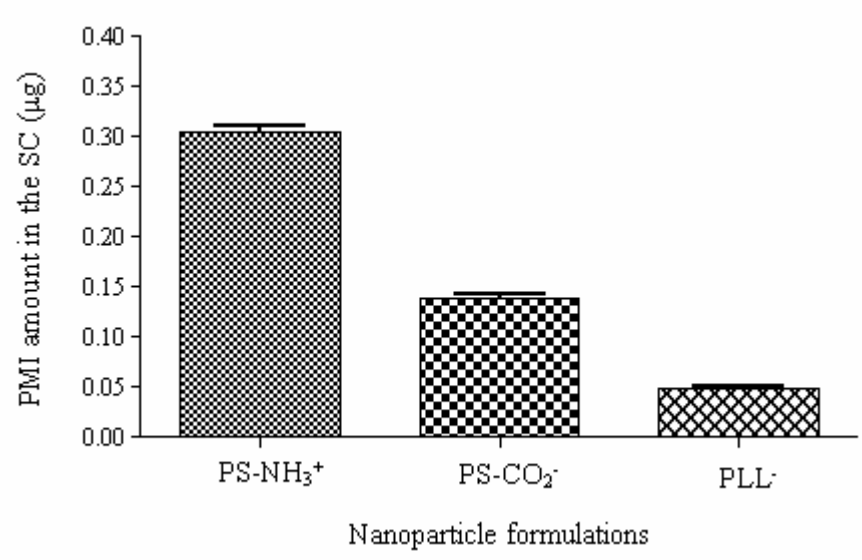

Figure 6.8: Uptake of PMI into the SC following a 6-hour application of three nanoparticle formulations. A one-way ANOVA shows that there is a significant difference (alpha < 0.05) between all the nanoparticle formulations considered.

6.5 Conclusions

The isoelectric point of mammalian skin falls in the range of 4 to 5, conferring a net negative charge on the membrane under normal physiological conditions. Positively-charged nanoparticles, not unexpectedly, show a greater attraction to the skin than those of opposite charge, and offer a better opportunity for the delivery of an associated “active” compound into the stratum corneum.

Acknowledgements

Supported by the European Commission 6th Research and Technological Development Framework Programme (NAPOLEON: NAnostructured waterborne POLymEr films with OutstaNding properties) and a University Research Scholarship for Xiao Wu.

References

1. R. Alvarez-Roman, G. Barre, R.H. Guy, and H. Fessi, *Biodegradable polymer nanocapsules containing a sunscreen agent: preparation and photoprotection.* Eur J Pharm Biopharm, 2001. **52**(2): p. 191-5.
2. J. Luengo, B. Weiss, M. Schneider, A. Ehlers, F. Stracke, K. Konig, K.H. Kostka, C.M. Lehr, and U.F. Schaefer, *Influence of nanoencapsulation on human skin transport of flufenamic acid.* Skin Pharmacol Physiol, 2006. **19**(4): p. 190-7.
3. M. Simeonova, R. Velichkova, G. Ivanova, V. Enchev, and I. Abrahams, *Poly(butylcyanoacrylate) nanoparticles for topical delivery of 5-fluorouracil.* Int J Pharm, 2003. **263**(1-2): p. 133-40.
4. S. Miyazaki, A. Takahashi, W. Kubo, J. Bachynsky, and R. Loebenberg, *Poly n-butylcyanoacrylate (PNBCA) nanocapsules as a carrier for NSAIDs: in vitro release and in vivo skin penetration.* J Pharm Pharm Sci, 2003. **6**(2): p. 238-45.
5. B. Luppi, T. Cerchiara, F. Bigucci, R. Basile, and V. Zecchi, *Polymeric nanoparticles composed of fatty acids and polyvinylalcohol for topical application of sunscreens.* J Pharm Pharmacol, 2004. **56**(3): p. 407-11.
6. B.I. Olvera-Martinez, J. Cazares-Delgadillo, S.B. Calderilla-Fajardo, R. Villalobos-Garcia, A. Ganem-Quintanar, and D. Quintanar-Guerrero, *Preparation of polymeric nanocapsules containing octyl methoxycinnamate by the emulsification-diffusion technique: penetration across the stratum corneum.* J Pharm Sci, 2005. **94**(7): p. 1552-9.
7. J. Shim, H. Seok Kang, W.S. Park, S.H. Han, J. Kim, and I.S. Chang, *Transdermal delivery of mixnoxidil with block copolymer nanoparticles.* J Control Release, 2004. **97**(3): p. 477-84.
8. G. Lambert, E. Fattal, H. Pinto-Alphandary, A. Gulik, and P. Couvreur, *Polyisobutylcyanoacrylate nanocapsules containing an aqueous core as a novel colloidal carrier for the delivery of oligonucleotides.* Pharm Res, 2000. **17**(6): p. 707-14.
9. H. Lboutounne, J.F. Chaulet, C. Ploton, F. Falson, and F. Pirot, *Sustained ex vivo skin antiseptic activity of chlorhexidine in poly(epsilon-caprolactone) nanocapsule encapsulated form and as a digluconate.* J Control Release, 2002. **82**(2-3): p. 319-34.
10. X. Wu, B. Biatry, C. Cazeneuve, and R.H. Guy, *The influence of polymeric materials and particle size on the disposition of a lipophilic chemical in the stratum corneum from nanoparticulate/mesoparticulate formulations*. 2008, University of Bath: Bath.
11. X. Wu, P. Griffin, G.J. Price, and R.H. Guy, *Preparation and in vitro evaluation of topical formulations based on polystyrene-poly-2-hydroxyl methacrylate nanoparticles*. 2008, University of Bath: Bath.
12. A. Luzardo-Alvarez, M. Rodriguez-Fernandez, J. Blanco-Mendez, R.H. Guy, and M.B. Delgado-Charro, *Iontophoretic permselectivity of mammalian skin: characterization of hairless*

mouse and porcine membrane models. Pharm Res, 1998. **15**(7): p. 984-7.

13. D. Marro, R.H. Guy, and M.B. Delgado-Charro, *Characterization of the iontophoretic permselectivity properties of human and pig skin.* J Control Release, 2001. **70**(1-2): p. 213-7.
14. N. Sekkat, Y.N. Kalia, and R.H. Guy, *Biophysical study of porcine ear skin in vitro and its comparison to human skin in vivo.* J Pharm Sci, 2002. **91**(11): p. 2376-81.
15. G.A. Simon and H.I. Maibach, *The pig as an experimental animal model of percutaneous permeation in man: qualitative and quantitative observations--an overview.* Skin Pharmacol Appl Skin Physiol, 2000. **13**(5): p. 229-34.
16. V. Holzapfel, A. Musyanovych, K. Landfester, M.R. Lorenz, and V. Mailander, *Preparation of fluorescent carboxyl and amino functionalized polystyrene particles by miniemulsion polymerization as markers for cells.* Macromol Chem Phys, 2005. **206**(24): p. 2440-2449.
17. C. Herkenne, A. Naik, Y.N. Kalia, J. Hadgraft, and R.H. Guy, *Dermatopharmacokinetic prediction of topical drug bioavailability in vivo.* J Invest Dermatol, 2007. **127**(4): p. 887-94.
18. V.P. Shah, *Topical dermatological drug product NDAs and ANDAs - in vivo bioavailability, bioequivalence, in vitro release and associated studies*. 1998, US Depart. of Health and Human Services: Rockville. p. 1-9.
19. M.E. Meuwissen, J. Janssen, C. Cullander, H.E. Junginger, and J.A. Bouwstra, *A cross-section device to improve visualization of fluorescent probe penetration into the skin by confocal laser scanning microscopy.* Pharm Res, 1998. **15**(2): p. 352-6.
20. C. Herkenne, I. Alberti, A. Naik, Y.N. Kalia, F.X. Mathy, V. Preat, and R.H. Guy, *In vivo methods for the assessment of topical drug bioavailability.* Pharm Res, 2008. **25**(1): p. 87-103.

CHAPTER 7

CONCLUSIONS AND PERSPECTIVES

Conclusions and perspectives

7.1 Conclusions

Nanoparticles (NP) are interesting and advantageous components to be incorporated into topical preparations, based on their unique physiochemical properties, such as transparency in solution, occlusive film formation, and small size. They can protect a sensitive “active” from degradation by the environment. Some specially designed NP can also modulate the release of the active into the skin.

It is very important to understand the mechanism with which the active is delivered to the desired skin site after topical application of active-loaded NP formulation. In detail, the following basic questions have been addressed in this thesis: (i) What happens to the NP when they come into contact with the skin? Do they remain at the surface or penetrate at all into the different strata of the skin? Do they have a particular affinity for any specific structures (e.g., hair follicles)? (ii) What happens to the “active” encapsulated or associated with the NP? Does it remain with the particles, or is it released? If the latter, with what kinetics and at what location does this release take place? (iii) In what manner is the fate of the NP, and release of the “active” influenced by the size, hydrophobicity and charge of NP, and physicochemical properties of the “active”?

To begin this project, methods for the preparation of polymeric nano/meso-particles were designed to meet the objectives of the work. The prepared NP were characterized by dynamic light scattering (DLS), transmission electron microscope (TEM) and NMR to guarantee the quality of formulations used in subsequent skin permeation experiments. Ultracentrifugation was utilized to assess the active associated with nanoparticles. Following skin permeation experiments on porcine skin, the tape-stripping technique was used to measure stratum corneum (SC) thickness and to determine the distribution profile and penetration depth of “active” in the skin. Laser scanning confocal microscopy (LSCM) observations confirmed the results obtained by tape-stripping. Importantly, LSCM distinguished the “fates” of the NP vehicle and of the

"active" on and within the skin.

This chapter summarizes the conclusions obtained from different aspects of this research, including NP preparation and characterization, tape-stripping, LSCM, influence of particle size, hydrophobicity, and surface charge on NP topical application, and the "fates" of both the NP vehicle and the active.

7.1.1 Nanoparticle preparation and characterization

Basically, the NP used in this study were prepared by two techniques: free radical polymerization from monomers and miniemulsion solvent evaporation from preformed polymers.

The advantage of free radical polymerization is that functional monomer, for example, fluorescent dye and charged surface groups, can react and covalently bind with the nanoparticle polymer, thus enabling the application of NP for different experimental purposes. In one part of this work, a fluorophore, fluorescein methacrylate (FMA), was reacted with styrene and methyl methacrylate to produce fluorescent nanoparticle vehicles. The preparation procedure is straightforward. Figure 7.1 shows the LSCM image of a thin layer of NP fluorescently labeled with FMA. A number of green fluorescent clusters of NP are seen spreading homogeneously in the observed sample area. As the magnification capability of LSCM is not high enough to see individual nanoparticles, only clusters of NP are recorded. A second fluorophore, Nile Red, was associated with NP as a lipophilic model "active". With the two fluorescent probes, the "fates" of NP vehicle and of the active were successfully distinguished.

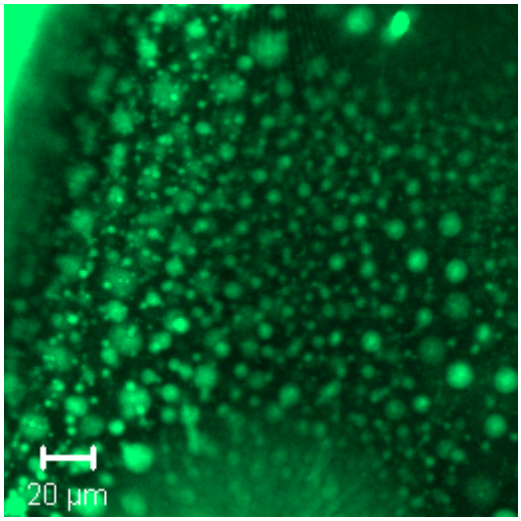

Figure 7.1: Laser scanning confocal microscopy (LSCM) image of NP fluorescently labeled with fluorescein methacrylate (FMA).

The advantage of the classic miniemulsion solvent evaporation method is that the molecular weight of polymers forming the nanoparticles is precisely controlled, and consequently the particle size of nanoparticles falls in a narrow range. However, the disadvantage of this technique is the introduction of organic solvent in the fabrication process. The removal of the organic solvent is an essential step, but relatively difficult to perform, as the surfactant used in the formulation results in foams in the rotary evaporation system sometimes causing the formulation to reflux. To avoid this problem, the pressure of the system has to be reduced very slowly and regularly.

Dynamic light scattering is a popular technique to determine the size distribution profile of small particles in solution. However, any particles present, including polymer residues, dust and even air bubbles, can bias the results. Therefore, transmission electron microscopy (TEM) was employed to confirm nanoparticle size. Prior to observation, TEM samples have to be appropriately stained. It was demonstrated here that polystyrene and poly-(methyl methacrylate) NP could be stained by ruthenium tetroxide and phosphotungstic acid, respectively. Poly-(L-lactide) NP could be stained by phosphotungstic acid, uranyl acetate and ruthenium tetroxide. TEM images of poly-(L-lactide) NP stained by these three compounds are shown in Figure 7.2. The results show that negative staining (staining the background) by phosphotungstic

acid is the best choice for poly-(L-lactide) NP. Thus, the importance of choosing an appropriate staining agent is emphasized for TEM examination of polymeric NP.

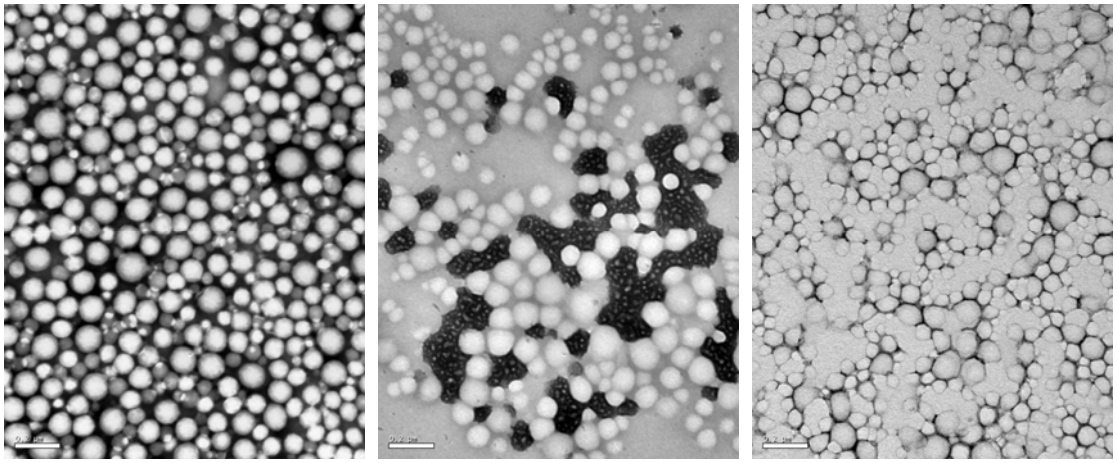

Figure 7.2: Transmission electron microscopy (TEM) images of poly-(L-lactide) nanoparticles after staining in (a) phosphotungstic acid, (b) uranyl acetate, and (c) ruthenium tetroxide vapours. Scale bars in all three images represent 0.2 μm.

7.1.2 Tape-stripping

Tape-stripping was used to assess the depth of "active" penetration into the SC and to recover "active" from the treated skin. The thickness of SC removed as tape-stripping proceeds was also determined. The variability of SC thickness between different skins is clear, and therefore emphasizes the value of the determination of SC thickness when the disposition of "active" across the barrier is to be evaluated, as it means that all concentrations can be expressed on a common scale of SC penetration depth normalized by the total membrane depth.

The concentration profiles of the active in porcine SC following delivery from different kinds of NP formulations show good reproducibility, indicating the validity of the tape stripping method.

7.1.3 Laser scanning confocal microscopy (LSCM)

LSCM is a valuable tool to visualize fluorescently-labeled biological samples. It provides in-depth information of skin without perturbation or destruction of the sample. Additionally, in this work, skin samples were sometimes mechanically sectioned and then examined by LSCM at a plane beyond the cut surface (thereby avoiding artifacts associated with the sectioning procedure). The results obtained from cross-sectioned samples are in agreement with those obtained from the optical sections.

7.1.4 Influence of particle size on Nile Red disposition in the SC

Three NP formulations with average diameters of 90 nm, 260 nm, and 630 nm were used to elucidate the influence of particle size on Nile Red (NR) disposition in the SC. The results demonstrated NR was more efficiently transferred into the SC from the nano/meso-carriers as the particle size increased. The total amounts of NR delivered into the SC from 90 nm, 260 nm, and 630 nm formulations were 0.023, 0.033, and 0.058 μg, respectively. As the precise localization of NR in the nano/mesoparticles is not known, an unambiguous explanation for the observations is not possible. However, if as suspected, NR is predominantly absorbed onto the particle surface, then the larger carriers obviously offer a smaller surface area and the "leaving tendency" of NR from the vehicle would be enhanced.

7.1.5 Influence of hydrophobicity on Nile Red disposition in the SC

Two groups of nanoparticle formulations, (i) polystyrene, poly-(ε-caprolactone), and cellulose acetate butyrate (CAB) nanoparticles, and (ii) polystyrene nanoparticles co-polymerized with 0, 5, 10, and 20% 2-hydroxyethyl methacrylate (HEMA), were prepared to investigate the influence of hydrophobicity of NP on Nile Red disposition in the SC. The results from both experiments demonstrated that uptake of NR was greatest from the most hydrophobic polymer (PS) and least from the most hydrophilic polymers (CAB and PS-20%HEMA). These differences are dependent upon the different loadings of Nile Red in the different NP. The incorporation efficacy of lipophilic Nile Red decreases with decreasing hydrophobicity of the NP. Nile Red incorporation efficacy, uptake into the SC, and uptake normalized by different fractional loadings are

summarized in Table 1. The results show that, as expected, Nile Red release from the least hydrophobic nanoparticle into the lipophilic SC is favoured relative to that from the more hydrophobic polymers.

Table 7.1: Nile Red incorporation efficacy, uptake into the SC, and uptake normalized by different fractional loadings.

Formulations	Nile Red incorporation efficacy (%)	Nile Red uptake in the SC (μg)	NR uptake in the SC normalized by its loading
PS-NR-NP	77	0.053	0.69
CAPA-NR-NP	49	0.038	0.78
CAB-NR-NP	24	0.029	1.20
PS NP	73	0.126	0.17
PS-5% HEMA NP	59	0.093	0.16
PS-10% HEMA NP	41	0.058	0.15
PS-20% HEMA NP	18	0.012	0.07

7.1.6 Influence of surface charge on Nile Red disposition into the SC

Cationic amino-functionalized polystyrene, an anionic carboxy-functionalized polystyrene and anionic poly-(L-lactide) NP were used to investigate the influence of surface charge of NP on N-(2,6-diisopropylphenyl)-perylene-3,4-dicarboximine (PMI) disposition into the SC. The results demonstrated a statistically significant difference with the "delivery" of PMI being greater from the cationic nanoparticles, as compared to those of opposite charge. As the isoelectric point of mammalian skin falls in the range of 4 to 5, conferring a net negative charge on the membrane under normal physiological conditions, positively-charged nanoparticles, not unexpectedly, show a greater attraction to the skin than negatively-charged nanoparticles, and offer a better opportunity for the delivery of an associated "active" compound into the stratum corneum.

7.1.7 The "fates" of the nanoparticle vehicle and associated "active"

The polymeric NP studied in all of our experiments did not penetrate beyond the superficial SC but showed some affinity for hair follicles. Dual fluorescently labeled polystyrene and

poly-(methyl methacrylate) NP enabled the distributions of the vehicle and associated "active" in the SC to be tracked independently. LSCM images showed that the NP vehicle and "active" were principally co-localized in the skin furrows and around the hair follicles. Surface cleaning with buffer mostly removed the NP vehicle but the "active" was able to diffuse into the SC. At the skin surface, Nile Red remained in part associated with NP, but release of the "active" clearly occurred to some extent followed by its penetration into deeper layers of the SC.

7.2 Perspectives

7.2.1 Assess toxicity of nanoparticles by topical application

The skin penetration studies performed have enhanced the understanding of how nanoparticles interact with skin and have improved the design of studies to measure these interactions. A number of variables, which influence the skin disposition of NP and an associated "active" have been clarified. Suggestions for future work include:

(a) The experiments described here and most previous studies have employed particles of ~100 nm in diameter [1-3]. There remains a need to further evaluate smaller particles, such as quantum dots (< 20 nm).

(b) Investigation of a range of formulation bases that could influence skin uptake of NP by altering skin structure or increasing the solubility of the NP in the skin [4]. This is important because ingredients that act as "penetration enhancers" are commonly incorporated in cosmetic preparations.

(c) Investigation of NP penetration across compromised or diseased skin (e.g., in acne or eczema, post-shaving, or severe sunburn).

7.2.2 Improve product homogeneity and persistence after topical application

The evaluation objectives would include:

(a) Characterization of surface properties for skin-care applications, specifically to improve film product homogeneity after application. (i.e., control of spreading)

(b) Improve product persistence (effect durability) after application (Figure 7.3 and 7.4), especially to enhance waterproof properties for suncare products, to optimize anti-penetration properties for preservatives and perfumes, and to explore methods for the co-formulation of particles as additives.

Figure 7.3: Example of a good oil-in-water emulsion film structure post-application.

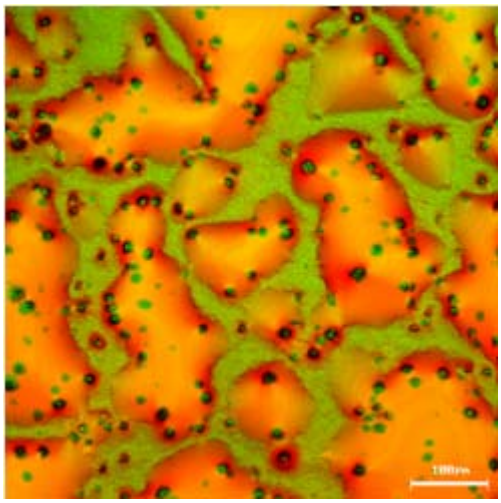

Figure 7.4: Example of a poor oil-in-water emulsion film structure post-application.

7.2.3 Enhance topical bioavailability

Techniques for active encapsulation need to be improved to enhance active skin bioavailability. The entrapment of actives during particle formation is a significant challenge involving a compromise between particle formation and active stability. The technological difficulties are such that efforts should be initially focussed upon the entrapment of actives after particle formation, especially concentrating upon: adsorption (hydrophobic)/complexation (ionic), and swelling with a common solvent. Evaluation of entrapment could use fluorescence probes (Nile Red, cationic dyes…) and confocal microscopy to assess encapsulation yields and release profiles (effects of solvent, pH, ionic strength).

References

1. A.S. Dussert, E. Gooris, and J. Hemmerle, *Characterization of the mineral content of a physical sunscreen emulsion and its distribution onto human stratum corneum.* Int J Cosmet Sci, 1997. **19**(3): p. 119-29.
2. F. Pflucker, V. Wendel, H. Hohenberg, E. Gartner, T. Will, S. Pfeiffer, R. Wepf, and H. Gers-Barlag, *The human stratum corneum layer: an effective barrier against dermal uptake of different forms of topically applied micronised titanium dioxide.* Skin Pharmacol Appl Skin Physiol, 2001. **14 Suppl 1**: p. 92-7.
3. J. Schulz, H. Hohenberg, F. Pflucker, E. Gartner, T. Will, S. Pfeiffer, R. Wepf, V. Wendel, H. Gers-Barlag, and K.P. Wittern, *Distribution of sunscreens on skin.* Adv Drug Deliv Rev, 2002. **54 Suppl 1**: p. S157-63.
4. M. Kreilgaard, *Influence of microemulsions on cutaneous drug delivery.* Adv Drug Deliv Rev, 2002. **54 Suppl 1**: p. S77-98.